REPUBLIC OF CAMEROON

REPUBLIQUE DU CAMEROUN

MINISTRY OF HIGHER EDUCATION

MINISTERE DE L'ENSEIGNEMENT SUPERIEUR

Ecole Nationale Supérieure des Travaux Publics

UNIVERSITÀ DEGLI STUDI DI PADOVA

DEPARTMENT OF CIVIL ENGINEERING

DEPARTEMENT DE GENIE CIVIL

DEPARTMENT OF CIVIL, ARCHITECTURAL AND ENVIRONMENTAL ENGINEERING

DYNAMIC ANALYSIS OF CABLE-STAYED BRIDGES AFTER AN ACCIDENTAL CABLE FAILURE MECHANISM

CASE STUDY: MARSASSOUM BRIDGE IN SENEGAL

A thesis submitted in partial fulfilment of the requirements for the degree Of Master of Engineering (MEng) in Civil Engineering

Curriculum: **Structural Engineering**

Presented by:

NOTOUOM DEMGNE Rose Ornella

Student number: **15TP20988**

Supervised by:

Prof. Carlo Pellegrino

Co-supervised by:

Dr. Paolo ZAMPIERI

Dr. Cyrille TETOUGUENI

Academic year: 2019/2020

REPUBLIC OF CAMEROON

REPUBLIQUE DU CAMEROUN

MINISTRY OF HIGHER EDUCATION

MINISTERE DE L'ENSEIGNEMENT SUPERIEUR

Ecole Nationale Supérieure des Travaux Publics

UNIVERSITÀ DEGLI STUDI DI PADOVA

DEPARTMENT OF CIVIL ENGINEERING

DEPARTEMENT DE GENIE CIVIL

DEPARTMENT OF CIVIL, ARCHITECTURAL AND ENVIRONMENTAL ENGINEERING

DYNAMIC ANALYSIS OF CABLE-STAYED BRIDGES AFTER AN ACCIDENTAL CABLE FAILURE MECHANISM

CASE STUDY: MARSASSOUM BRIDGE IN SENEGAL

A thesis submitted in partial fulfilment of the requirements for the degree Of Master of Engineering (MEng) in Civil Engineering

Curriculum: **Structural Engineering**

Presented by:

NOTOUOM DEMGNE Rose Ornella

Student number: **15TP20988**

Supervised by:

Prof. Carlo Pellegrino

Co-supervised by:

Dr. Paolo ZAMPIERI

Dr. Cyrille TETOUGUENI

Academic year: 2019/2020

DEDICATION

To my family

Especially to my beloved parents

ACKNOWLEDGMENTS

This work would not have been completed without the combined efforts of individuals who contributed directly and/or indirectly to its realisation. I wish to express my sincere thanks and gratitude to:

- Prof, **Simonetta COLA**, who makes us the great honor to chair this jury;
- Prof. **MBESSA Michel**, for agreeing to review this work. Thank you also for the answers to my many concerns;
- My supervisors Prof. **Carlo PELLEGRINO**, Dr. **Paolo ZAMPIERI,** Dr. **Cyrille TETOUGUENI** and Eng. **Landry FOSSOUO** for all the guidance and advices they provide me with, during this thesis work;
- Professors **George NKENG** and **Carmelo MAJORANA** for all their academic and administrative support during these five years spent at ENSTP in the MEng program in partnership with University of Padua in Italy;
- The Vice-director of ENSTP, Dr. **BWEMBA Charles Loïc** for his perpetual help and advices during our sojourn in this school;
- Prof. **MBESSA Michel**, the Head of Department of Civil Engineering for his tutoring and valuable advices;
- All the **teaching staff** of NASPW and University of Padua for their good quality teaching and the motivation they developed in us to continue our studies;
- My family and more specially my father **NOTOUOM Jean** and my mother **MBAKAM TAMO Ruth Sylvie**, for the education and financial support during all these years;
- Eng. **Armel MBIA** for his advises which helped me during this work;
- All my **classmate**s and all my **friends** who were a source of motivation and tenacity. As a team, together we have been able to achieve more;
- My **siblings** Junior, Hilaria, Aurelle and Anderson for their love and affection since my childhood.

LIST OF NOTATIONS

Pi	Preliminary pretension in cable
Ri	Reaction at ith cable anchorage
α_i	Angle between girder and stay i
Ai	Area of ith cable
σ_a	Allowable unit stress for the cable
w_{DL}	Uniform dead load
w_{LL}	Uniform live load
s	Distance between stays
Po	Force acting on the back-stay cable
Fh	Horizontal force at the top of the pylon
α_0	Angle between girder and back-stay
σ_{stay}	Computed axial tensile stress in stay
σ_{all}	Allowable stress in stay
f_{uc}	Ultimate tensile strength of cable
N_{ed}	Computed axial force in stay
A_{eff}	Effective area
Po	Ambient pressure
P_{so}	Peak over-pressure
t_A	Arrival time of blast
t_o	Positive phase duration
P_{so}^-	Minimum pressure
t_o^-	Negative phase duration
i_s	Positive impulse
Z	Scaled distance
R	Standoff distance
W	Explosive weight
[M]	Mass matrix
[C]	Damping matrix
[K]	Stiffness matrix

p(t)	Dynamic load
u(t)	System displacement
ü(t)	System acceleration
$\dot{u}(t)$	System velocity
$G_{k,j}$	Permanent loads
P	Pretension loads
$Q_{k,i}$	Variable loads
A_d	Accidental load
$\gamma_{G,j}$	Partial factors of permanent loads
$\gamma_{Q,i}$	Partial factors of variable loads
ψ	Multipliers for the characteristic values of variable loads
α_{Qik}	Values of adjustment factors
TS_k	Tandem Load
UDL_k	Uniform distributed load
q^*_{fk}	Traffic load on footways
T_k	Temperature load
A_c	Slab section area
ε	Thermal coefficient
E_{cm}	Concrete elastic modulus
T_{beam}	Temperature load per beam
n_L	Steel-concrete homogenization coefficient at long-term
n_0	Steel-concrete homogenization coefficient at short-term
$\varepsilon_{ca}(\infty)$	Autogeneous shrinkage
$\varepsilon_{cd}(\infty)$	Dry shrinkage at infinite
$N_{c,r\infty}$	Shrinkage load
$E_{c,eff}$	Reduced modulus of elasticity for concrete
N_{beam}	Shrinkage load per beam
F_{wa}	Hydrostatic force
ρ_{wa}	Water density
h	Water depth
b	Obstacle width
v_{wa}	Average water velocity

α	Angle of incidence of blast load
b_{eff}	Mixed section effective width
Le	Length of influence
y_{id}	Coordinate y of gravity centre of ideal mixed section
A_{steel}	Area of main beam
A_{slab}	Effective area of slab
A_{id}	Area of ideal mixed section
J_{id}	Moment of inertia of ideal mixed section
$W_{up,slab}$	Resistance modulus relative to slab upper section
$W_{low,slab}$	Resistance modulus relative to slab lower section
$W_{up,steel}$	Resistance modulus relative to steel upper section
$W_{low,steel}$	Resistance modulus relative to steel lower section
$\sigma_{up,slab}$	Stress at slab upper section
$\sigma_{low,slab}$	Stress at slab lower section
$\sigma_{up,steel}$	Stress at steel upper section
$\sigma_{low,steel}$	Stress at steel lower section
V_{Ed}	Design shear value
$V_{pl,Rd}$	Design plastic shear resistance
A_v	Resisting shear area
$V_{b,Rd}$	Shear buckling resistance
P_{Rd}	Design shear resistance of a stud
d	Stud diameter
hs	Stud height
τ_b	Shear stress per meter
n_s	Number of studs per meter
N_{Ed}	Design axial value
$N_{b,Rd}$	Axial buckling resistance
χ	Reduction factor
$\bar{\lambda}$	Slenderness
σ_c	stress in concrete at SLS
σ_s	stress in steel reinforcement at SLS
y	Neutral axis position
J	Moment of inertia of the section

E_r	Reduced modulus of elasticity of cables
E_c	elastic modulus of cable material
A	Cable cross section
T	Cable tension
Lh	Horizontal component of the cable chord
g	Weigth per unit length of the cable

ABSTRACT

The principal objective of this thesis is to evaluate robustness of cable-stayed bridge after cable failure due to blast loads. To achieve this aim, a literature review was done in order to have a view on cable-stayed bridge, on accidental failures mechanisms. The case study used for different analyses was a cable-stayed bridge based on Marsassoum bridge project in Senegal. Secondly pretension forces in cables were computed using MIDAS/civil software. Afterwards, the static loads acting on the bridge have been evaluated in order to perform static analysis. Verifications have been done according to Eurocodes norms. In the next point, we computed blast pressure loads with software RCBlast and performed a nonlinear time-history with SAP2000 software. Two different explosive weights of TNT (250 kg and 500 kg), at the three following locations i.e., bridge start, tower location and mid-span, were considered for blast occurring above the deck level. Then, the influence of those parameters on local response of bridge structural components have been determined. From the results obtained, cables that have crossed strain limit imposed were removed in order to investigate types of progressive collapse that the bridge can undergo. Results of dynamic analysis revealed that, location of blast influences considerably local response of bridge elements. Analyses have also outcome that low stand-off distance increases the amount of damage on bridge elements. For explosive weight of blast, as it is increased, the displacement of joint or stresses in girders also increase. Considering cable loss, mixed-type collapse was identified. For robustness of this cable-stayed bridge, it cannot be certified because we have formation of plastic zones in girders on a side and a series of structural elements failures on the other side.

Keywords: Cable-stayed bridge, blast, explosive weight, standoff distance, time-history analysis, progressive collapse, robustness.

RESUME

L'objectif principal de cette thèse était d'évaluer la robustesse d'un pont à haubans sous une charge explosive suite à la rupture de certains câbles. Pour atteindre cet objectif, une revue de la littérature a été réalisée afin d'avoir une idée sur les ponts à haubans et sur les différents mécanismes de défaillances accidentelles. L'étude de cas utilisée pour les différentes analyses était un pont à haubans basé sur le projet de pont de Marsassoum au Sénégal. Deuxièmement, les forces de prétension dans les câbles ont été calculées à l'aide du logiciel MIDAS/civil. Ensuite, les charges statiques agissant sur le pont ont été évaluées afin d'effectuer une analyse statique. Les vérifications ont été effectuées conformément aux normes des Eurocodes. Au point suivant, nous avons calculé les pressions dues à l'explosion à l'aide du logiciel RCBlast et procédé à une analyse dynamique non linéaire avec le concours du logiciel SAP2000. Deux masses différentes d'explosifs de TNT (250 kg et 500 kg), aux trois emplacements suivants, c'est-à-dire au début du pont, à l'emplacement de la tour et à mi-portée, ont été pris en compte pour une détonation se produisant au-dessus du niveau du pont. Ensuite, l'influence de ces paramètres sur la réponse locale des éléments structurels du pont a été déterminée. A partir des résultats obtenus, les câbles ayant franchi la limite de déformation imposée ont été retirés afin d'étudier les types d'effondrement progressif que peut subir le pont. Les résultats de l'analyse dynamique ont révélé que l'emplacement de l'explosion influence considérablement la réponse locale des éléments du pont. Des analyses ont également révélé qu'une faible distance de séparation augmente la quantité de dommages sur les éléments de pont. Pour la masse d'explosif, à mesure qu'elle augmente, le déplacement d'un joint ou les contraintes dans les poutres augmentent également. Compte tenu de la perte de câble, un effondrement de type mixte a été identifié. Pour la robustesse de ce pont à haubans, il ne peut pas être certifié car nous avons la formation de zones plastiques dans les poutres d'un côté et une série de ruptures d'éléments structurels de l'autre côté.

Mots clés : Pont à haubans, explosion, masse d'explosif, distance de séparation, analyse dynamique non-linéaire, effondrement, robustesse.

LIST OF FIGURES

LIST OF TABLES

TABLE OF CONTENTS

GENERAL INTRODUCTION

Numerous terrorist events during the last few decades, including the 2001 attack on the World Trade Centre, have heightened building owners, governments and design professionals of concern about the safety of bridges during intentional/unintentional blast load effects. Many researchers have carried out experimental and numerical investigations to examine building structure's response to explosive loads; studies on bridges subjected to blast loads are limited. Cable-stayed bridges construction has tremendously increased in the world. Because of their strong presence, they are potential to car bomb attacks. For better performance, cable-stayed bridge behaviour under blast load has to be study.

With this in mind, structural engineers and other professionals are continuously researching and developing cost-effective methodologies in order to have a better comprehension of bridges behaviour especially cable-stayed bridges under blast loads and also to protect lives.

The key objective of this thesis is to investigate robustness of cable-stayed bridge after cable failure due to blast loads by using softwares SAP2000 and MIDAS/civil.

In order to achieve this objective, this thesis is divided in four main axes hereafter outlined. The first chapter is focused on a general overview of cable-stayed bridge, presentation of its main components, design procedures and some advantages and disadvantages have been mentioned. The second chapter is devoted to literature review of accidental failures mechanisms on cable-stayed bridge, an overview of blast load and a summary of some works that have been done on blast against bridges. The third chapter carries on methodology. Here, the approach used in loads determination and static verifications shall be discussed. Next, a presentation of dynamic analysis procedure will be done, as well as method used to model blast load acting on cable-stayed bridge for numerical analysis. At the end, in the fourth chapter which is the presentation of our results and their interpretations, the study case will be detailed first. Secondly, static analysis and corresponding verifications will follow. The third point concerns the effects of blast loads on cable-stayed bridge, and a comparative analysis will be done for different loading scenarios considered. Finally, progressive collapse scenarios will be checked and robustness of cable-stayed bridge will be evaluated.

CHAPTER 1: LITERATURE REVIEW

Introduction

A cable-stayed bridge is a structural system with a continuous girder (or bridge deck) supported by inclined stay cables from the towers (or pylons). From the mechanical point of view, the cable-stayed bridge is a continuous girder bridge supported by elastic supports. Cable-stayed bridges are used worldwide nowadays. To understand how it works, it is necessary to have a view of everything which is around the concept of cable-stayed bridge. It will begin by a short history about evolution of cable-stayed bridge, followed by the description of bridge components and different bridges configurations. Next, will be the presentation of design procedures. Some advantages and disadvantages will be given before ending with some examples of cable-stayed bridge in the world.

1.1 Evolution of cable-stayed bridge

The idea for the cable-stayed system was perhaps inspired by the drawbridges of medieval castles and the rope-braced masts of tall ships. The very first documented image of a cable-stayed bridge appears in the *Machinae Novae*, a book by Fausto Veranzio published in 1615. Many cable-stayed bridges were built in the early part of 19th century, but it was not until the 1950s they started becoming prevalent like other bridge types, such as truss bridges, arch bridges, and suspension bridges. Several cable-stayed bridges collapsed due to lack of understanding of such a system, particularly due to inadequate resistance since it was not possible to tension the stays, and they became slack under various load conditions(Weiwei Lin, 2017). These ideas were not well adapted and improved until the construction of the Brooklyn Bridge (Figure 1.1), completed in 1883, by the American bridge engineer John Roebling (Parke & Hewson, n.d.).

Figure 1.1. Brooklyn bridge (Wikipédia)

Even though cable-stayed systems had been adopted in bridge construction earlier in history, none of these early examples set a precedent and the Strömsund Bridge (Figure 1.2) in Sweden is usually considered the first modern cable-stayed bridge. The Strömsund Bridge (1955) constructed by the firm Demag, with the assistance of the German engineer Dischinger, has one main span and two side spans—a global arrangement that has often been used for suspension bridges. The main span of 182.6 m is supported by two sets of stay cables radiating from the top of each pylon. The pylons are of the portal type and the stay cables are anchored on either side of the bridge deck, thus providing both vertical and torsional support to the deck. Stiffening girders and pylons are in steel, whereas the deck consists of a concrete slab(Chen & Duan, 2014).

In the following years, the system was developed further to replace many of the bridges destroyed in Germany during World War II. Cable stayed bridges proved more economic, for moderate spans, than either the suspension or arch bridge forms. The first cable-stayed bridge in Germany is the Theodor Heuss Bridge (completed in 1957) across the Rhine River in Düsseldorf. The bridge is a three-span structure with a main span of 260 m (Figure 1.3). The stiffening girder and pylons are in steel. The pylons are of the freestanding post (or mast) type with the posts located at the edge of the girder providing two vertical cable planes. The stay cables are arranged in a harp configuration with three sets of stay cables from each post, for terminology refer to Section 1.3— Stay cable arrangement (Chen & Duan, 2014).

Figure 1.2. Strömsund Bridge, Sweden, completed in 1955

Figure 1.3. The Theodor Heuss Bridge in Düsseldorf (Niels J. Gimsing, 2012)

Initially, cable-stayed structures were used for bridge spans of 60 to 250 m but today they span much longer distances and are the only system that challenges suspension bridges in super-long spans. Their spans grew to 302 m in 1959 with the Severin Bridge (Germany), to 404 m in 1974 with the Saint Nazaire Bridge (France), and 856 m in 1995 with Michel Virlogeux's Normandy Bridge (France).

Today, the Russky Island Bridge (Russia) has the longest span of this system, 1.104 m achieved in 2012 (Figure 1.4*)*.

Figure 1.4. Russky Island Bridge (Sputnik, 2018)

1.2 Components of cable-stayed bridge

Cable-stayed bridges are extremely elegant and very effective structures and they are also architectural landmarks. They consist of one or more towers (or pylons), from which cables support the bridge deck at many points along the spans. The combination of multiple simple systems allows for a structure where the role of each of its components is well defined.

1.2.1 Cables

Cables, also known as stays, are made up of one or more strands and are the key load carrying and transferring members in cable stayed bridges. They serve as support and provide vertical stiffness to the deck girders (Bernardo, 1998). The choice of cable depends on its properties, essentially its mechanical strength.

1.2.1.1 The seven-wire strand

It is the simplest, cheapest and most common type of strand to be found within cable supported bridge. Commonly used as tendons in pre-stressed concrete, its tensile strength lies between 1770 and 1860 MPa. Typically, the nominal modulus of elasticity for the seven-wire strand will be only 6–8% lower than for the wires themselves, i.e., a typical modulus of elasticity of E=195GPa.

Figure 1.5. Seven-wire strand (Niels J. Gimsing, 2012)

1.2.1.2 Locked-coil strands

Locked coil stays have been incorporated into many of the earliest cable-stay bridges. The stays are factory produced on planetary stranding machines, each layer being applied in a single pass through the machine and contra-laid between each layer. The core of the stay is composed of conventional round steel wires while the final layers comprise Z-shaped steel wires which lock together creating an extremely compact stay cross-section. A typical example of a locked coil stay is illustrated in Figure 1.6. Modern locked coil stays provide all the wires in a finally galvanised condition and will achieve a tensile strength of up to 1770 MPa. The stays are commonly anchored by zinc- filled sockets although sometimes stays that are sheathed with a polyethylene protection have their sockets filled with epoxy resin. The largest locked coil stays manufactured to date are the 167 mm diameter stays supplied for the Rama IX Bridge over the Chao Phraya River, Bangkok (Parke & Hewson, 2008).

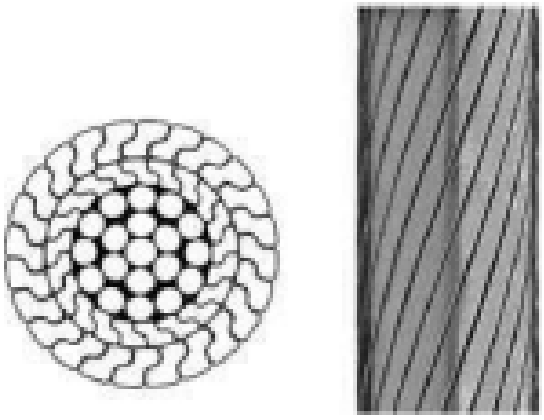

Figure 1.6. Locked coil cable (courtesy Bridon International Ltd)

1.2.1.3 Parallel wire strand

- Parallel wire strand (PWS) most commonly comprises 7mm diameter finally galvanised round steel wires with a tensile strength of 1570 MPa. PWS stays may either be prefabricated or assembled on site, the wires being installed without a lay or helix within a polythene tube and injected with cement grout or wax. Cables were arranged with truly parallel wires of equal length and consequently some difficulties were experienced in coiling the cables on reels for transportation.

- The new PWS system (Figure 1.7) was developed with a tensile strength up to 1770 MPa. The stay is prefabricated and with a long lay helix to improve coiling on to the reel. The

individual wires within these anchorages incorporate button heads transferring the full load to the anchor. The socket is then filled with a proprietary epoxy compound that is claimed to enhance the fatigue resistance of the stay. Other manufacturers provide these stays with conventional socketed anchorages filled with zinc or epoxy resin (Parke & Hewson, n.d.).

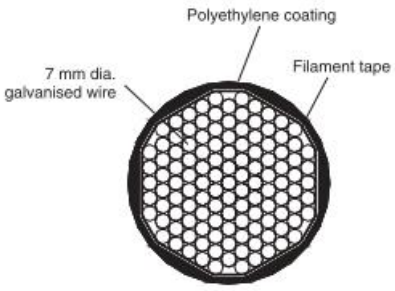

Figure 1.7. New parallel wire strand (PWS) (ICE, 2008)

1.2.1.4 Helical cables

Helical or spiral strand stays, which are illustrated in Figure 1.8, are also factory fabricated on a planetary stranding machine similar to the locked coil stay but are entirely manufactured from finally galvanised round steel wires. The wires are usually of 5mm diameter with a tensile strength of either 1570 MPa or 1770 Mpa.

Their nominal modulus of elasticity is generally 15–25% below the value for straight wires. A typical value for the nominal modulus of elasticity of the helical strand then becomes E=170 GPa. Spiral strands show low fatigue strength (Bernardo, 1998).

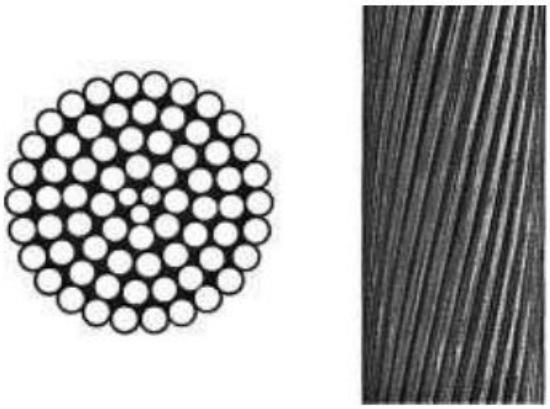

Figure 1.8. Spiral strand cable (courtesy Bridon International Ltd)

1.2.1.5 Parallel strand stays

Parallel-strand cables are in principle composed in the same way as parallel-wire cables, with the exception that the individual 7mm wires are replaced by seven-wire strands and have a tensile strength of 1770 MPa. The most common arrangements of parallel-strand cables are shown in Figure 1.9. It is, however, easy to apply intermediate sizes by leaving out some of the seven-wire strands, and it is also indicated by some of the suppliers that parallel-strand cables can be made with up to 127 seven-wire strands.

The seven-wire strands are generally made of galvanized wires and in the present standard version the seven wires are furthermore protected by an extruded high density polyethylene (HDPE) sheath (Figure 1.10). With an individual HDPE protection of each seven-wire strand the completed stay cable might be made as a parallel-strand bundle without further protection. It will, however, be necessary to add binders around the bundle at intervals of approximately 40 m to ensure integrity and avoid individual oscillations of the single wires (Niels J. Gimsing, 2012).

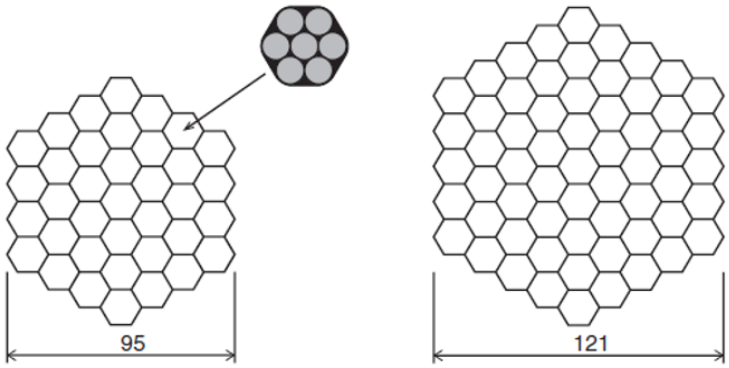

Figure 1.9. Parallel-strand cables comprising seven-wire strands (Niels J. Gimsing, 2012)

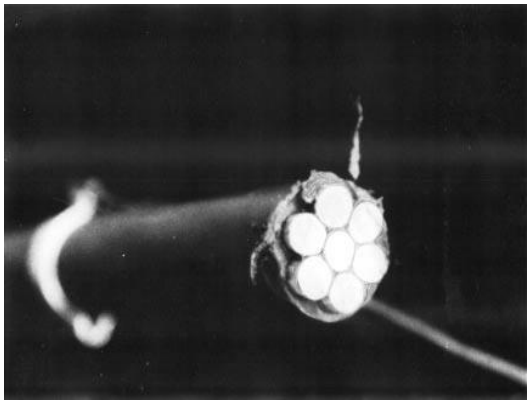

Figure 1.10. Seven-wire strand with an extruded high density polyethylene (HDPE) sheath (Niels J. Gimsing, 2012)

1.2.1.6 Bar stays

Bar bundles contain up to ten threaded steel bars with a tensile strength of 1230 MPa coupled together in 12 m lengths. The bars have been conventionally placed within a steel tube and protected with a cement grout (Figure 1.11). The use of couplers connecting the bars will give a much reduced fatigue resistance when compared with the equivalent wire or strand systems. Coupled bar systems are thus rarely used where significant variations in the stay load are likely to occur. Tests have also been undertaken to assess the effective- ness of cement grout as a protective medium. These tests concluded that transverse and longitudinal cracking of the grout rapidly develops due to temperature effects, live load strains and wind vibration. It may be assumed that the cement grout provides little protection against corrosion (Parke & Hewson, n.d.).

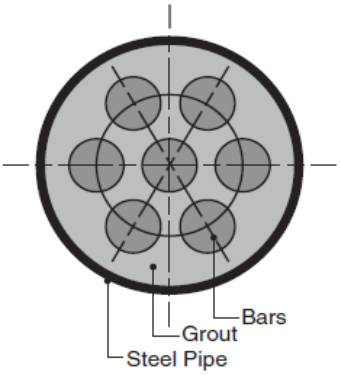

Figure 1.11. Bar cable (Niels J. Gimsing, 2012)

1.2.1.7 Advanced composite stays

Advanced composite stays also known as Carbon Fibre Reinforced Polymers (CFRP) ropes have exceptional strength to weight ratio. The modulus of elasticity of the carbon fibre is about 160 GPa lower than that of steel (210 GPa). They are difficult to anchor and are more expensive than the traditional steel wires or bars, not quite in common use and are very sensitive to lateral pressure (Parke & Hewson, 2008)

1.2.2 Deck

Rather than being merely supported by the cable, as in the suspension bridge form, the deck of the cable-stayed bridge is an integral part of the structure resisting both bending and an axial force derived from the horizontal component of the stay force. As such, cable-stayed bridge deck forms have been developed as steel section incorporating an orthotropic road deck, concrete section and composite section.

1.2.2.1 Steel deck section

For early cable-stayed bridges, the steel deck was used due to its high load- capacity to weight ratio and larger span capacity between cable stays. In addition, the reduction in deck weight can result in an economic design for large span bridges, as in the Tatara Bridge. For steel bridges, the box girder type with an orthotropic deck appears to be the most efficient not only because this integral action system offers substantial strength for resisting compressive forces but also because it has better torsional stiffness to counter unsymmetrical loading and wind force (Bhatti et al., 1985). The orthotropic road deck generally consists of a thin surfacing material laid on steel plate stiffened longitudinally. The stiffeners are supported by transverse floor beams.

The design of the deck cross-section is dominated by the arrangement of the stays. Where a single central plane of stays is adopted the torsional resistance of the deck section is the only means of carrying any eccentric loading and therefore a strong torsion box must be provided.

A common arrangement, originated by German designers, is to divide the cross-section of the torsion box into three or five cells. The central cell is the same width as the pylon such that the cable stays may be readily anchored within it. Examples of this arrangement are the Rama IX Bridge, Bangkok, divided into three cells (figure 1.12).

With highway structures of moderate span and where two planes of stay cable are used, the rigidity of the torsion box deck cross-section is unnecessary and it is possible to simplify the section to that of twin longitudinal girders. Early designs, such as the Knie Bridge (figure 1.13) over the River Rhine at Dusseldorf, Germany with a main span of 320 m, combined longitudinal steel plate girders with an orthotropic deck (Weiwei Lin, 2017).

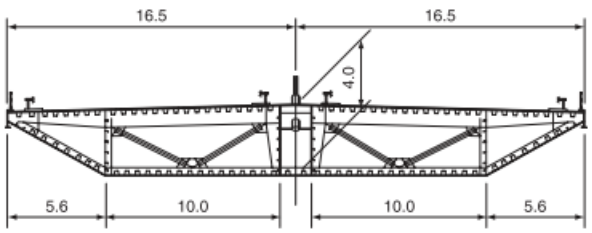

Figure 1.12. Multi-cell box deck (Weiwei Lin, 2017)

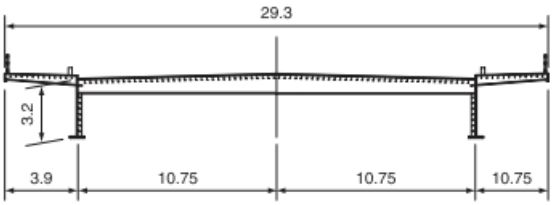

Figure 1.13. Twin girder steel deck (Weiwei Lin, 2017)

When two planes of stays are connected to each edge of the deck, eccentric loading of the deck can be carried by the cable system. However, the strong torsion box can still be beneficial when a highly eccentric loading is carried, such as where both road and rail are running on the deck and the heavy rail loading has to be located eccentric to the deck section. Such a deck will improve the distribution of the loads between the two cable planes. The torsion box can also be more easily adapted into a streamlined shape, essential for reducing wind drag and for improving aerodynamic stability in very long spans (Parke & Hewson, n.d.).

1.2.2.2 Concrete deck section

Reinforced or prestressed concrete decks can be made of precast elements or they can be cast in place. The concrete deck is suitable for medium spans because the cost of concrete is relatively low but its weight increases the dead load of the bridge thus requiring larger dimensions for cables, pylons, piers, and anchorage structures. For a cable-stayed bridge with single central plane of stays, a strong torsion box-section is needed to provide the torsional resistance, as shown in Fig 1.14. While for a cable-stayed bridge with multicable system, the deck will be an open girder cross section bridges with very long spans should use cross sections with high torsional stiffness. The twin beam concrete deck used in Dames Point Bridge over St Johns River in Florida (Figure 1.15), USA, provided as an example of a simplified deck form (Weiwei Lin, 2017).

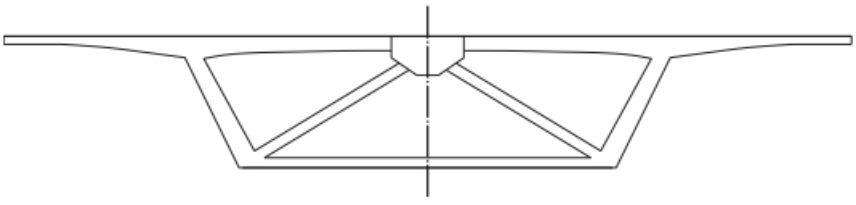

Figure 1.14. Concrete torsion box deck (Weiwei Lin, 2017)

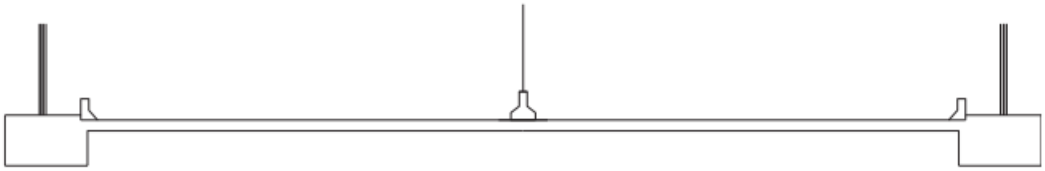

Figure 1.15. Twin beam concrete deck (Weiwei Lin, 2017)

1.2.2.3 Composite deck

The deck in cable-stayed bridges can also be built as steel-concrete composite section. Composite construction of steel and concrete is a popular structural method due to its numerous advantages against conventional solutions. The optimal combination of the properties of the two most popular construction materials, i.e., steel and concrete, results in structures that are both safe and economic (Vasdravellis et al., 2012). In cable-stayed bridges, the composite concrete slab over the steel orthotropic deck provides a new option. In composite bridges the anchors can be aligned with the stiffening girder or placed in an exterior position (under or in the slab plan). To minimise the displacement in the middle span, a combination of deck types such as steel deck, concrete deck, and composite deck can be used for the mid-span and side spans. In such a case, heavier section (i.e., concrete section or composite section) should be used in side span, while lighter section (i.e., steel section or composite section) should be used in midspan to reduce the downward deflection in midspans and avoid the upward defection in side spans (Weiwei Lin, 2017).

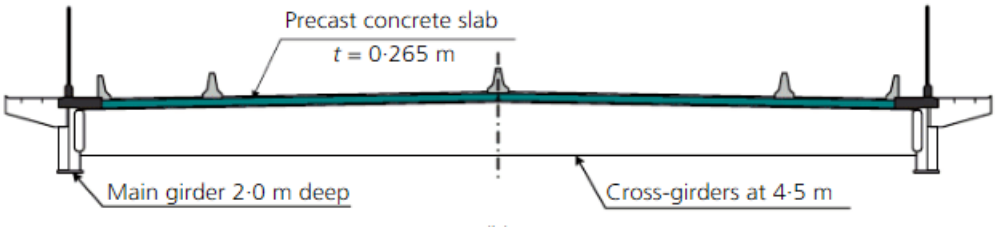

Figure 1.16. Alex Fraser Bridge, Canada, composite deck cross-section (Weiwei Lin, 2017)

1.2.3 Pylons

The pylon is the main feature that expresses the visual form of any cable-stayed bridge, giving an opportunity to impart a distinctive style to the design. The primary function of the pylon is to transmit the forces arising from anchoring the stays and these forces will dominate the design of the pylon. The pylon should ideally carry these forces by axial compression where possible, such that any eccentricity of loading is minimised.

1.2.3.1 Pylon shape and arrangement

The optimum form of a pylon depends on whether the pylon supports one or more cable planes and on the foundation conditions.

The H-shape pylons are the most common for cable-stayed bridges with two vertical cable planes. It is similar to the double arrangement, but has a lateral member connecting the two columns.

Central mono-column pylons, A-shaped and inverted Y-shaped pylons may be used with one or more cable planes. The diamond shaped pylon can be considered a variation of the A- and inverted Y-shaped pylons where the pylon legs are kinked at the level of the girder to allow them to be supported on a single foundation of minimum dimensions (Chen & Duan, 2014).

To be specific, bridge towers can be designed as H frame, A frame, and inverted Y frame pylons, diamond pylon, and twin-diamond pylon, as illustrated in Figure 1.17.

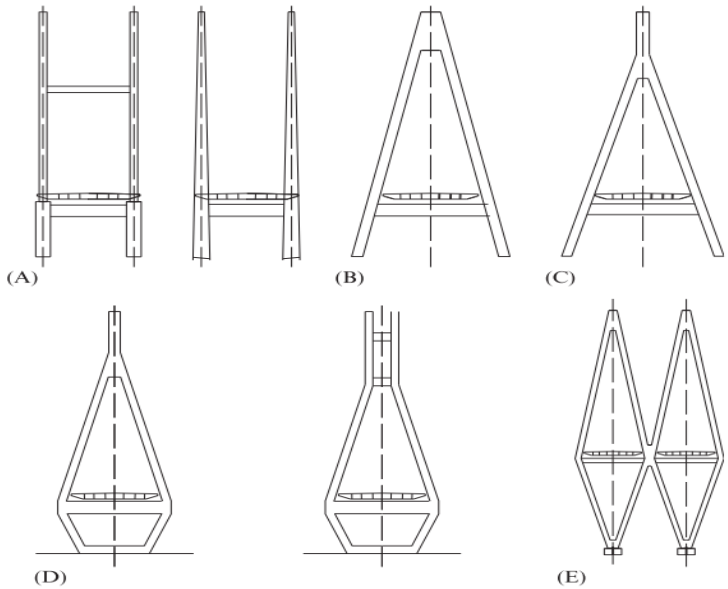

Figure 1.17. Pylons in cable-stayed bridges. (A) H-frame. (B) A-frame. (C) Inverted Y-frame pylons. (D) Diamond pylon. (E) Double diamond pylon (Weiwei Lin, 2017).

1.2.3.2 Pylon materials

Although the early cable-stayed bridges were with a few exceptions constructed with steel pylons, concrete has turned out to be an economical alternative as the pylons are compression members. Concrete is now generally the preferred material in pylons for large

cable-stayed bridges and are usually constructed by climb forming. However, steel pylons may be a better option in areas exposed to large earthquakes.

a) Steel pylons

Early cable-stayed pylon designs were predominantly constructed as steel boxes with thick steel plates joined together by either welding or riveting. The advantage of metal pylons lies in their quicker fabrication and erection, but the buckling of the tower is a concern.

b) Concrete pylons

Concrete is very efficient when supporting loads in axial compression. Pylons, especially large cable-stayed bridges, can also be built more economically with reinforced or prestressed concrete. Advances in concrete construction and modern formwork technology have made the use of concrete increasingly competitive for pylon construction, despite the much greater self-weight when compared with a steel alternative. Concrete has proved particularly adaptable to the more complex forms of pylon. Many varied types of pylon have been developed to support both the vertical and inclined stay layouts (Parke & Hewson, n.d.).

1.2.4 Stay cable anchorage

The stay cables may be anchored in the pylon or pass through the pylon supported on a cable saddle. Cable saddles have been used on smaller and medium range projects and simplifies geometry in the otherwise congested area in the anchorage zone. However, cost and additional stresses in the stay cables due to contact pressure on the saddle limit the use.

In pylons with limited external dimensions the stay cables may be taken through the pylon and anchored on the opposite face. This is sometimes referred to as a “crisscrossing” arrangement. In order to avoid creating a torsional moment in the pylon it is desirable to arrange the stay cables in a symmetrical pattern. This can be achieved by arranging two cable planes in at least one of the spans (main span, side span or in both main span and side span).

If the pylon is composed of a box section in the anchorage zone the stay cables can be anchored behind the front and back wall of the pylon. In case of a concrete pylon, which is the most common, the stay cables can either be anchored directly on concrete corbels in which case horizontal prestressing is often introduced in the pylon walls. Alternatively, the stay cables can be anchored inside a steel anchor box that is connected to the concrete walls with shear studs. In this case the side walls of the anchor box transfer the tensile component of the stay force in the direction of the bridge axis.

1.3 Stay cable arrangement

The versatile cable-stayed-bridge concept lends itself to a large variety of geometrical configurations. The arrangement of the cables can be easily adjusted to suit the numerous requirements of site conditions and aesthetics for highway and pedestrian bridges.

1.3.1 Transversal arrangement

In the transverse direction to the longitudinal axis of the bridge, the cables may lie in either a single or a double plane and may be symmetrically or asymmetrically placed, and may lie in oblique or vertical planes.

1.3.1.1 Single-plane system

The single-plane cable arrangement is generally used with a divided roadway deck with the cables passing through the median strip and anchored below the roadway (Figure 1.18). This arrangement is not only economical but aesthetically pleasing as well. For conventional roadways very little additional width is required in the deck to accommodate the cables. However, for narrow median strips additional deck width may be required in order to allow sufficient space for the single towers.

Figure 1.18. Single-plane configuration (Hodariyat bridge)

In a single-plane cable arrangement, the cables support vertical and gravity loads only. The torsional forces that develop because of the asymmetrical vehicular loading and/or wind forces must be resisted by a torsionally stiff box girder in order to transmit the unbalanced forces to the piers (Podolny & Scalzi, 1986).

1.3.1.2 Double-plane system

The two principle double-planar cable systems are: one system consisting of a vertical plane located at each edge of the superstructure and another system in which the cable planes

are oblique, sloping toward each other from the edges of the roadway and anchored at the towers along the longitudinal centreline of the deck (Figure1.19).

Figure 1.19. Double-plane configuration (Mohammed VI Bridge)

Using the double-plane cable system, the anchorage may be located either on the outside of the deck structure or within the limits of the deck roadway. With the cable anchorages on the outside of the deck an advantage is gained, since no portion of the roadway is required for the connection fittings (Podolny & Scalzi, 1986).

1.3.1.3 Triple-plane system

The deck of a bridge provided with multiple-stay lateral suspension and with very wide roadway is generally subjected to transverse bending forces which are greatly in excess of the longitudinal bending. It can be avoided by using a three-plane system of suspension (Walther et al., 1999).

The concept is appropriate for use in urban areas, where it may be necessary to include mass transit centre lanes or special bus lanes as well as three or four vehicular lanes in each direction.

1.3.2 Longitudinal layout

According to the longitudinal cable layout, the cable-stayed bridges can be classified into four types: mono, fan, modified fan, and harp, as. All these cable configurations have been used in practice, but the cable configuration generally does not have a major effect on the behaviour of the bridge except in very long span structures (Tang, 1999).

1.3.2.1 Mono cable system

The mono design uses a single cable from its towers, and is one of the lesser- used cable-stayed bridge type and is rarely built. The Neckar River Bridge in Germany is a typical mono cable-stayed bridge. Cable-stayed bridges with a smaller number of cable stays are occasionally used, like the Toyosato-Ohashi Bridge in Osaka (Figure 1.20).

Early cable-stayed bridges were designed with very few stay cables, but this involves substantial erection costs. Modern cable-stayed bridges tend to use many more cables to ensure greater economy (Weiwei Lin, 2017).

Figure 1.20. The Toyosato-Ohashi Bridge in Osaka. (Photo by Lin,2017)

1.3.2.2 Fan cable system

In the fan design, all stay cables connect to or pass over the top of the towers. The fan design is structurally superior with minimum moment applied to the towers. In addition, due to the steeper cable slopes, the fan design is structurally efficient with maximum vertical component for sustaining the vertical loads, but smallest axial force applied to the main girders. The fan system was adopted for several of the early designs of the modern cable-stay bridges, including the Strömsund Bridge (Parke & Hewson, n.d.). However, there are also obvious difficulties in practical application due to the possible corrosion and fatigue problems at the pylon head caused by the large amount of cable forces. In addition, the anchorages are generally very heavy and complicated and the tower is needed to be further strengthened at the termination point. An example can be seen in Figure 1.21, which illustrates Edgar Cardoso bridge in Portugal.

Figure 1.21. Edgar Cardoso bridge in Portugal (Robert Cortright, 2007)

1.3.2.3 Modified fan system

To avoid the difficulties in a fan cable system due to the "fixation together" of cable stays, the modified fan cable system is developed. In this system, the cables connect near the top of the tower but is spaced sufficiently from each other for the benefits of better fixation like improved force transmission, and easy access to individual cables for inspection and maintenance (Weiwei Lin, 2017). In order to give sufficient room for anchoring, the cable anchor points are spaced vertically at 1.5–2.5 m.

The modified fan is particularly suitable for bridges with many cables. The modified fan cable system was used in the Neva-river bridge in St-Petersburg (Figure. 1.22).

Figure 1.22. Neva-river bridge in St-Petersburg (Gerashchenko, 2013)

1.3.2.4 Harp cable system

In the harp or parallel design, the cables are nearly parallel so that the height of their attachment to the tower is proportional to the distance from the tower to their mounting on the

deck. This arrangement provides a visual emphasis of the flow of forces from the back span to the main span and, in examples that are well proportioned, is aesthetically pleasing.

However, the arrangement is not as structurally efficient as the fan layout and relies on the bending stiffness of the pylon and/or deck for equilibrium under non-symmetrical live loading. When loading one end only of the stay system the load may be divided into symmetrical and antisymmetric components of loading. The symmetrical loading will be resisted by the triangle of forces formed by the stays, pylon and deck but the antisymmetric loading can only be resisted by bending of the deck, the pylon or a combination of both depending on their relative stiffness (Giovanni Tecchio, 2015).This disadvantage can be overcome by anchoring the back stay cable at approach pier locations so that any unbalanced load is resisted by the pier. An elegant example of this arrangement is the Knie Bridge over the River Rhine at Dusseldorf with its single pylon and 320m main span (Figure 1.23).

Figure 1.23. Knie Bridge (Nicolas Janberg, 2012)

1.4 Design Method of cable-stayed bridge

The design process for a cable-stayed bridge system with accepted geometrical layout may be divided into preliminary set of sectional properties, verification of assumed sections and change of sections if the previous assumed do not satisfy the specified requirements.

1.4.1 Preliminary design

The geometrical layout passes through the assumptions of span length, which is related to pylon height and deck cross section depth. Following that, stay area can be found after some preliminary calculation in order to have pretension forces in cables.

1.4.1.1 Span proportions

In any type of bridge structure, one of the first design considerations to be evaluated is the proportioning of the spans.

- For two-span asymmetrical structures, the longer span is in the range of 60 to 70% of the total length, or in another manner, a ratio of minor span to major span of 0.43 to 0.67.
- Span ratios for the conventional three-span cable-stayed structure vary according to use. For rail bridges, a back-span to main-span ratio of 0.40 to 0.42 results in a concentration of back stays (those connected to the rigid back-span pier) to counter the heavy uniform live load in the main span, which gives rise to main-span deflection and back-stay stress range. For highway bridges, back-span to main-span ratios of 0.45 to 0.48 have been used for contemporary composite bridges, and lesser ratios for more classical box girders with fewer stay cables. Wide box girders are mandatory as stayed girders for single-plane systems, to resist the torsion of eccentric loads. Box girders, even narrow ones, are also desirable for double-plane systems to enable cable connections to be made without eccentricity. Single-web girders, however, if properly braced, may be used (Brockenbrough & Merritt, 2011).
- In multiple-span structures, the spans are of equal length with the exception of flanking spans that connect to the approach spans or abutments.

1.4.1.2 Pylon height

The height of the pylon in relation to the span has a significant influence on cable forces, affecting in turn the amount of cable steel required. The pylon height of cable stayed bridge determines the overall stiffness of the structure, as the stay angle (α) increases, the required stay size will decrease and height of pylon will increase.

The ratio of the pylon height above the bridge deck to the centre span length for a three-span structure should be in the range of 0.16-0.2. For a two-span asymmetric structure, the longer span may be considered as one-half the span of a three span asymmetric structure (Bhatti et al., 1985).

1.4.1.3 Deck cross section

Depth of stayed girders range from 1/60 to 1/80 of the main span for box-girder designs. Composite-girder designs have more closely spaced stays, and are typically 1/150 to 1/200 of the main span in depth (Brockenbrough & Merritt, 2011).

1.4.2 Preliminary manual calculations

Following is a description of a method of manual calculation of reasonable initial values for use as input data for design of a cable-stayed bridge by computer. The manual procedure is not precise but does provide first-trial cable-stay areas. With the analogy of a continuous, elastically supported beam, influence lines for stay forces and bending moments in the stayed girder can be readily determined. From the results, stress variations in the stays and the girder resulting from concentrated loads can be estimated. If the dead-load cable forces reduce deformations in the girder and pylon at supports to zero, the girder acts as a beam continuous over rigid supports, and the reactions can be computed for the continuous beam. Inasmuch as the reactions at those supports equal the vertical components of the stays, the dead load forces in the stays can be readily calculated. If, in a first-trial approximation, live load is applied to the same system, the forces in the stays (Figure 1.24) under the total load can be computed from (1.1).

$$P_i = \frac{R_i}{\sin \alpha_i} \tag{1.1}$$

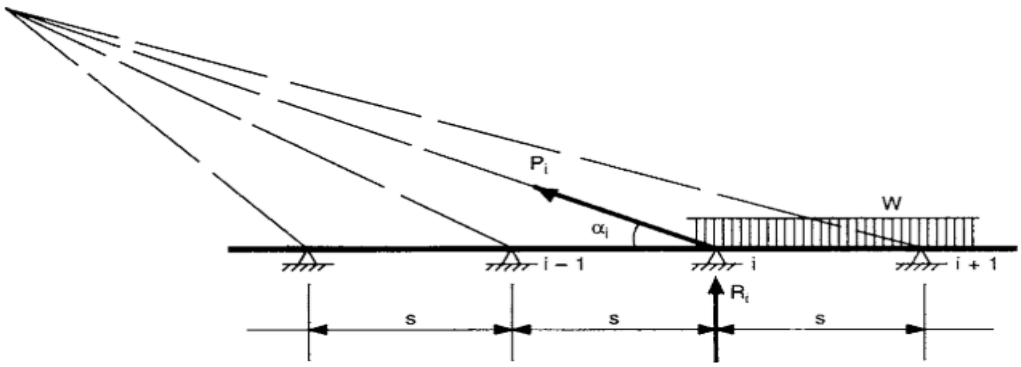

Figure 1.24. Cable-stayed girder continuous supported beam (Brockenbrough & Merritt, 2011)

Where

h_t sum of dead-load and live-load reactions at i

α_i angle between girder and stay i.

Since stay cables usually are designed for service loads, the cross-sectional area of stay i may be determined from equation (1.2):

$$A_i = \frac{R_i}{\sigma_a \sin \alpha_i} \tag{1.2}$$

where σ_a = allowable unit stress for the cable steel.

The allowable unit stress for service loads equals 0.45 f_u, where f_u = the specified tensile strength of the steel.

The reactions may be taken as R_i = ws, where w is the uniform load, kN/m, and s, the distance between stays. At the ends of the girder, however, R_i may have to be determined by other means.

Determination of the force P_o acting on the back-stay cable connected to the abutment (Figure 1.25) requires that the horizontal force Fh at the top of the pylon be computed first. Maximum force on that cable occurs with dead plus live loads on the centre span and dead load only on the side span. If the pylon top is assumed immovable, F_h (1.3) can be determined from the sum of the forces from all the stays, except the back stay:

$$F_h = \sum \frac{R_i}{\tan \alpha_i} \frac{R'_i}{\tan \alpha'_i} \tag{1.3}$$

Where

Ri — vertical component of force in the ith stay in the main span and side
Ri' — respectively

αi — angle between girder and the ith stay in the main span and side span,
αi' — respectively

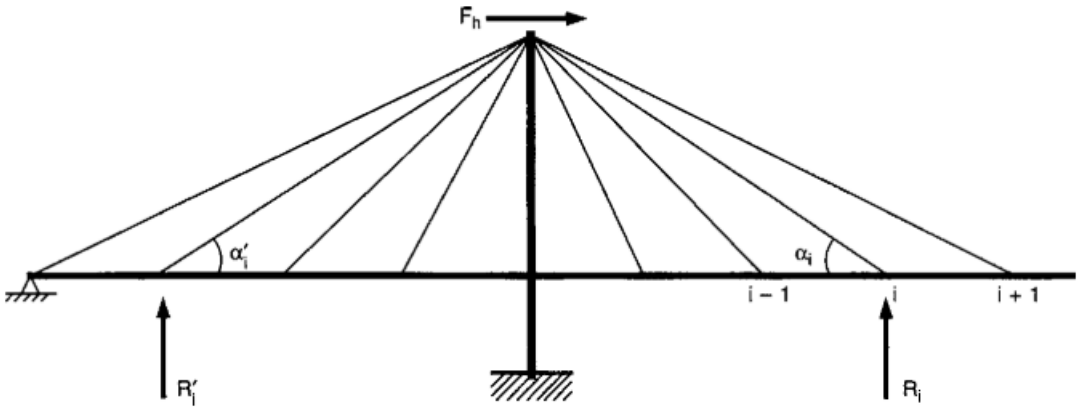

Figure 1.25. Horizontal force Fh at the top of a pylon (Brockenbrough & Merritt, 2011)

Figure 1.26 shows only the pylon and back-stay cable to the abutment. If, in Figure 1.25, the change in the angle α_0 is assumed to be negligible as F_h deflects the pylon top, the load in the back stay can be determined from equation (1.4):

$$P_o = \frac{F_h h_t^3 \cos \alpha_o}{3l_o(E_c I/E_s A_s) + h_t^3 \cos^2 \alpha_o} \tag{1.4}$$

If the bending stiffness E_cI of the pylon is neglected, then the back-stay force is given by :

$$P_o = \frac{F_h}{\cos \alpha_0} \tag{1.5}$$

where

h_t	height of pylon
l_o	modulus of elasticity of pylon material
E_c	moment of inertia of pylon cross section
I	moment of inertia of pylon cross section
E_s	modulus of elasticity of cable steel
A_s	cross-sectional area of back-stay cable

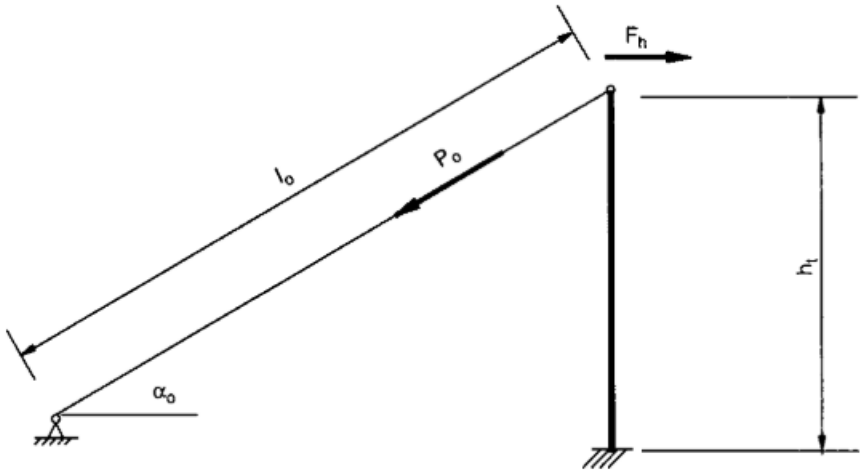

Figure 1.26. Backstay cable force PoBackstay force P_o (Brockenbrough & Merritt, 2011)

Influence lines for stay forces and girder moments are determined by treating the girder as a continuous, elastically supported beam. From Figure 1.27, the following relationships are obtained for a unit force at the connection of girder and stay:

$$P_i = \frac{1}{\sin \alpha_i} \tag{1.6}$$

$$\Delta l_{si} = \frac{P_i l_{si}}{A_{si} E_s} = \delta_i \sin \alpha_i \tag{1.7}$$

which lead to :

$$\delta_i = \frac{h_t \sigma_a}{A_{si} E_s sin^2 \alpha_i} \tag{1.8}$$

With equation (1.7) and $l_{si} = h_t \sin \alpha i$, the deflection at point i is given by

$$\delta_i = \frac{h_t \sigma_a}{R_i E_s sin^2 \alpha_i} \tag{1.9}$$

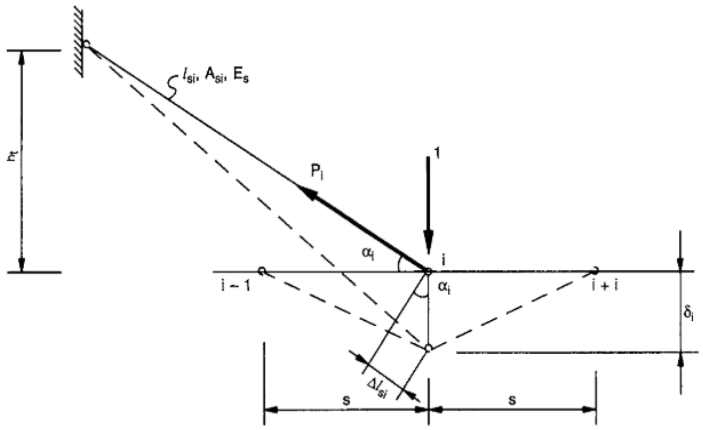

Figure 1.27. Unit force application at point of attachment of ith cable (Brockenbrough & Merritt, 2011)

With R_i taken as $s(w_{DL} + w_{LL})$, the product of the uniform dead and live loads and the stay spacing s, the spring stiffness of cable stay i is presented in equation (1.10):

$$k_i = \frac{1}{\delta_i s} = \frac{(w_{DL} + w_{LL}) E_s \sin^2 \alpha_i}{h_t \sigma_a} \tag{1.10}$$

For a vertical unit force applied on the girder at a distance x from the girder-stay connection, the equation for the cable force P_i is given by equation (1.11):

$$P_i = \frac{\xi W s}{2 \sin \alpha_i} \eta_p \tag{1.11}$$

Where :

$$\eta_p = e^{-\xi x}(\cos \xi x + \sin \xi x), \tag{1.12}$$

1.4.3 Stress verification methods

Stress in cable-stayed bridge elements have to satisfy the maximum allowed so that static analysis can be good. Different procedures can be applied to do verifications.

1.4.3.1 Eurocodes

Verifications pass through determination of stress in structural elements. We have to ensure that it is lower than allowable stress. Moreover, buckling due to shear or axial compression has to be checked. For steel elements, (*EN 1993-1-1*, 2011) is the reference for design. For the concrete part, details are given by (*EN 1991*, 2003).

a) Stress Constraints on Cables

As cables are considered as truss elements that are always in tension, only axial tensile constraints are imposed. To satisfy fatigue criteria, the material and cross-sectional dimensions of the cables must follow equation (1.13):

$$\sigma_{stay} < \sigma_{all} = 0{,}45.\, f_{uc} \qquad (1.13)$$

Where:

σ_{stay} is the computed axial tensile stress

σ_{all} is the allowable tensile stress

f_{uc} is the ultimate tensile strength of cable

b) Stress and Buckling Constraints on the Deck Girder and Towers

Deck girder and tower (beam) elements subject to both axial compression and bending must be proportioned to satisfy criterion presented in equation (1.14):

$$\frac{N_{Ed}}{A_{eff}} + \frac{M_y}{W_y} \leq \frac{f_y}{\gamma_{M0}} \qquad (1.14)$$

Where :

N_{ed} is the computed axial force

A_{eff} is the effective area

M_y is the computed bending moment

W_y is the resistance modulus

f_y is the yield stress

c) Shear verification

The design value of the shear force V_{Ed} at each cross section shall satisfy equation (1.15):

$$\frac{V_{Ed}}{V_{c,Rd}} \leq 1 \qquad (1.15)$$

Where $V_{c,Rd}$ is the design shear resistance.

1.4.3.2 Optimal design method

Bhatti et al. (1985) proposed an optimal design method for cable-stayed bridge. The procedure to verify stress in cables is the same as the one used in Eurocode. The difference is given by equation (1.16)

$$\sigma_{all} = \frac{1}{3}.f_u \qquad (1.16)$$

a) Axial and flexural stresses

Beam elements subject both to compression and bending must satisfy equations (1.17) and (1.18)

$$\frac{|f_a|}{F_a} + \frac{C_m|f_b|}{(1-|f_a|F'_e)F_b} - 1 \leq 0 \text{ where } \quad F'_e = \frac{12\pi^2 E}{23(kl/r)^2} \qquad (1.17)$$

$$\frac{|f_a|}{0.6F_y} + \frac{|f_b|}{F_b} - 1 \leq 0 \qquad (1.18)$$

With :

- f_a computed axial stress
- f_b computed bending stress
- F_a axial stress that would be permitted if only axial force existed
- F_b compressive bending stress that would be permitted if only bending existed.
- F_y yield stress
- k effective length factor in the plane of bending
- l actual unbraced length in the plane of bending
- C_m coefficient applied to the bending term of the interaction formula. This is conservatively taken as 0.85.

Allowable stresses in compression and bending for steel are given below. These expressions are applicable to any type of cross-section. Allowable axial compressive stresses are based on the following criteria:

- When $kl/r \leq C_c$, we have equations (1.19) and (1.20):

$$F_a = \frac{(-e^2/F_y)}{S} \text{ where } S = \frac{5}{3} + \left(\frac{3}{8}\right)e - \left(\frac{1}{8}\right)e^3 \quad (1.19)$$

$$C_c = \frac{2\pi^2 E}{F_y} (1.19) \text{ and } e = \frac{kl}{rC_c} 1.20 \quad (1.20)$$

- When $kl/r > C_c$ we have equation (1.21)

$$F_a = \frac{12\pi^2 E)}{23(kl/r)^2} \quad (1.21)$$

Allowable bending stresses are given by: $F_b = 0.66F_y$ (1.22)

b) Shear stresses

Members subjected to shear stresses must satisfy the condition expressed by equation (1.23).

$$|f_s|/F_s - 1 \leq 0 \quad (1.23)$$

Where :

f_s computed shear stress

F_s allowable shear stress

For steel structures $F_s = 0.4f_y$

However, if the web thickness is more than D/150 then the allowable shear stress is one-third of the yield stress. Here D is the unsupported depth of the web plate between flanges in m.

1.5 Advantages and disadvantages of cable-stayed bridge

The selection of the proper type of bridge for a particular site with a given set of conditions must take into account many parameters. The process of evaluating those parameters for various types of bridges under consideration is certainly more of an art than a science. For cable-stayed bridge, there are several advantages and disadvantages to consider.

1.5.1 Advantages of cable-stayed bridge

Cable-stayed bridges are a popular choice as they offer all the advantages of a suspension bridge but at a lesser cost for spans. They present many other advantages.

- Less Building time

The cable stayed design for a bridge is that it doesn't require the same degree of anchorages as other bridge designs. The deck for the bridge can be supported with fewer suspension cables as well. For smaller designs, a single tower may be enough to support the entire design.

- Strong and resilient structures

Compared to the traditional suspension bridge design, the cables involved with a cable stayed bridge are capable of handling more pressure. That provides the deck with a greater level of consistency for travel. It keeps its shape better, even under heavy live loads, because the overall design has more rigidity. At the same time, they have a natural level of environmental resistance that permits them to remain a viable option after events, such as an earthquake.

- An affordable design to build

Because there are fewer labour elements to consider with this design, the installation costs can be significantly less due to fewer manhours involved. That combination means this bridge design option can be up to 30% cheaper than other bridge designs. For that reason, the cable stayed bridge has come back into prominence, since the late 20th century, as it can replace aging bridges that no longer respond positively to ongoing maintenance and support.

- Large efficient span range

The natural design of a cable stayed bridge somewhat limits the distance that it can safely span for consumers. The only feature of this option is that each deck section can connected to one another through a series of pylons and anchors, creating bridges of almost indefinite length. The Jiaxing-Shaoxing Sea Bridge in China is currently the widest and longest cable stayed bridge in the world today. It carries 8 lanes of traffic and is over 10,000 m in length, extending across Hangzhou Bay. Even the main body of the bridge is over 2,600 m in length.

- Several design options

A cable stayed bridge can be built in a variety of ways, allowing each span to be created in a way that meets the needs of each community. A side-spar design has just one tower and is supported on just one side. A cantilever-spar design offers a single spar on one side of the span. There are multiple-span, extra-dosed bridge designs all included as options for this type of bridge as well.

- It allows each cable to support the needs of every other cable.

What makes this design unique is that the cables with the bridge are permanent and temporary supports simultaneously. If more weight needs to be supported in one specific section, the bridge is able to accommodate this need by displacing the weight throughout the cable structures. At the same time, the cables are also used to permanently maintain the deck, permitting the bridge to be safely used in the first place.

- Four different classes of rigging to create results**.**

Each offers unique benefits that can lead to a better user experience for the local community.

The mono design for a cable-stayed bridge uses a single cable from its towers to provide support. This option is rarely seen unless the span being crossed is relatively small.

The parallel design, referred to as a harp option, offers cables that are virtually parallel to each other so that the height of their attachment is proportion to their distance from the tower and their deck mounting.

The fan design requires that the cables all connect to or pass over the top of the towers. This option is preferred when access is necessary to the cables while maximum supports needed to create a stable deck. Engineers can modify this option for specific environmental requirements too.

The modified fan design spaces the cables on the tower, and was introduced when a greater number of stays was required.

- Several arrangements for their support columns.

Depending on the exact structure of the bridge, designers can have the columns be vertical, curved, or angled relative to the bridge deck. Bridge towers can be designed as H frame, A frame, and inverted Y frame pylons, diamond pylon, and twin-diamond pylon. For more details, refer to section 1.2.3.

1.5.2 Disadvantages of cable-stayed bridge

The cable-stayed bridge is related to the cantilever bridge. The cables are in tension, and the deck is in compression. The spans can be constructed as cantilevers until they are joined at the centre. In the longer sizes, the cantilevered halves are very susceptible to wind induced oscillation during construction. They have some disadvantages.

- Maximum span length

A cable stayed bridge is a good option for shorter spans that need to be crossed only. The maximum span recommended for this type of bridge design is just 1,000 m. In comparison, the maximum span length recommendation for a traditional suspension bridge can be nearly twice as long. The Akashi Kaikyo Bridge in Japan, for example, is nearly 2,000 m in length. The 10 longest suspension bridges in the world are all above 1,300 m.

- Unstablility design in certain environments

A cable stayed bridge should not be installed in a region that is known to experience high wind speeds on a consistent basis. The rigidity of the bridge gives it more overall durability, though it comes at the cost of flexibility. High wind speeds can cause the bridge to rock back and forth, which can loosen the cables which support the deck. In severe wind events, it is even possible for a cable stayed bridge to completely fail.

- Difficulty to inspect and repair

The design of a cable stayed bridge places the cable bundle areas in regions that are difficult to access for a physical inspection. Anchorage areas may be fewer with this bridge design, but they are equally difficult to access for routine maintenance and inspection. Although communities might be able to save upwards 30% on the installation costs, the increase in labour costs for ongoing maintenance will eventually eat into those savings.

- Susceptible to corrosion

The cables of this bridge design must be specifically built to handle the unique environmental elements of the region where it is installed. That is because the cables are already prone to higher levels of fatigue compared to other bridge designs. Exposure to salt air elements in a coastal region, for example, could reduce the natural lifespan of the bridge and even make using it dangerous during its later years of life.

1.6 Existing cable-stayed bridges

Cable-stayed bridges are a popular choice as they offer all the advantages of a suspension bridge but at a lesser cost for spans. Thus, a great number of cable-stayed bridges have been constructed in the world. We will present some examples in the following parts.

1.6.1 Cable-stayed bridges in the world

Since the 1950s, several cable-stayed bridges have been built all around the world.

1.6.1.1 Mariansky bridge

A notable cable stayed bridge was completed in 1998 across the Labe River in the Czech Republic. With a main span of 123 m, the bridge is of modest size but it shows an attractive shape of the steel pylon in a monolithic form that also incorporates the side span (Figure 1.28). In 2001, the Mariansky Bridge was ranked one of the ten most beautiful constructions of the twentieth century in an international survey by the well-known Structural Engineering International Magazine (Niels J. Gimsing, 2012).

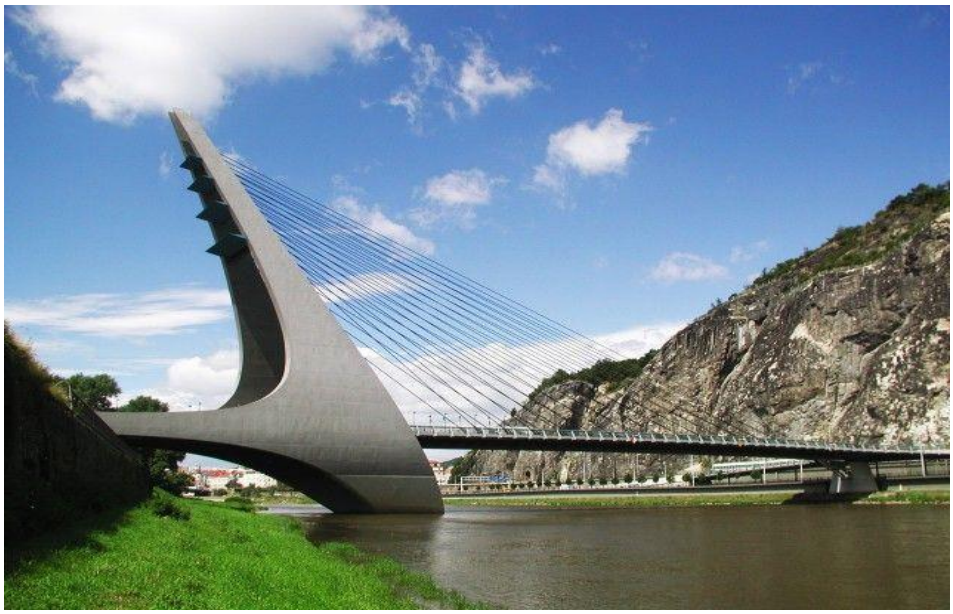

Figure 1.28. Mariansky bridge

1.6.1.2 Sutong Yangtze River Bridge

Located in Jiangsu province, in eastern china, the Sutong bridge crosses the Yangtze River and is 8,206 m long. With a span of 1,088 m, it was the cable-stayed bridge with the longest main span in the world in 2008-2012. Its two side spans are 300 m each, and there are also four small cable spans.

The bridge's two towers are inverted Y-shaped reinforced concrete structures. They are 306 m high and thus the fifth tallest in the world. Each tower has one connecting girder between its legs. The bridge deck is a steel box girder with internal transverse and longitudinal diaphragms, with fairing noses at both sides of the bridge deck. The total width of the deck is approximately 41 m, including the fairing noses.

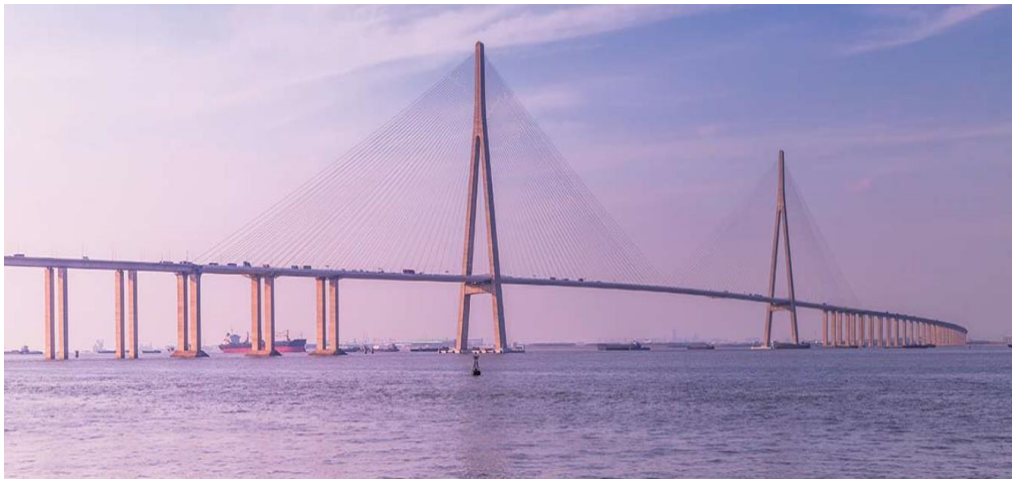

Figure 1.29. Sutong bridge (ICE, 2008)

1.6.1.3 Millau viaduct

No other high bridge in history caught the eye of the media more than the opening of the Millau Viaduct in 2005. Located in southern France, the bridge completes a hitherto missing link in the A75 autoroute from Clermont-Ferrand to Béziers across the Massif Central.

Comprised of 8 consecutive cable-stayed spans totalling 2,460 m, the metallic road deck is 32 m wide. The six central spans measure 342 m, and the outer 204 m. There are 173 central box beams, the spinal column of the construction, onto which the lateral floors and the lateral box are welded. Each of the seven pylons is supported by fours deep shafts, 15 m deep and 5 m in diameter. Its piers range in height from 75 m to 245 m, with the masts rising a further 87 m above the road deck. The abutment are concrete structures that provide anchorage for the road deck to the ground in the Causse du Larzac and the Causse rouge.

Figure 1.30. Millau Viaduct

1.6.2 Cable-stayed in Africa

In Africa, the concept of cable supported bridge is not really represented. Few examples of cable-stayed bridges will be presented below.

1.6.2.1 Mohammed VI Bridge

The Mohammed VI Bridge is a cable-stayed bridge that spans the valley of the Bouregreg River near Rabat in Morocco. The bridge is characterised by its architecture comprising two 200 m of high arched towers, which symbolize the new doors to the cities of Rabat and Salé. It is 954.3 m long and 30.4 m wide. The deck is supported by two sets of 20 pairs of parallel multi-strand stay cables.

Figure 1.31. Mohammed VI Bridge (Setec, 2016)

1.6.2.2 Lekki-Ikoyi bridge

Measuring 1.36 km in length, the bridge across Five Cowry Creek in Lagos is secured in the middle by a large pylon of 90 m height.

Figure 1.32. Lekki-Ikoyi bridge (Wikimedia, 2018)

Conclusion

In this chapter, cable-stayed bridges concept has been introduced, presenting an overview of its history, components and possible configurations. In order to know how those bridges can be design, some design procedures of cable-stayed bridges have been defined. After that a presentation of certain advantages and disadvantages have been made. Afterwards, we moved on some examples of cable-stayed bridges all around the world. To completely enter in our subject, accidental failures mechanisms that cable-stayed bridges faced, have to be highlighted. The next chapter will detail those failures, explain blast concept and show different analyses that have been investigated on cable-stayed bridges.

CHAPTER 2: ACCIDENTAL FAILURES MECHANISMS ON CABLE-STAYED BRIDGES

Introduction

Every structure is susceptible to failures during its design life. It can be due to design problem, fatigue phenomena or accidental events. This chapter outlines different triggering events and presents some accidental failures mechanisms on bridges. Progressive collapse concept and different classifications will be seen. Furthermore, a review of available literature on blast concept and its related parameters will be made. Finally, a selection of past investigations on cable breakage and blast studies will be presented.

2.1 Causes of accidental failures on bridges

Damages on bridge structures are several. They can take place gradually or suddenly, depending on the triggering event as discussed in following sections.

2.1.1 Fire

Fire is one of the most severe hazards to which built-infrastructure may be subjected during their lifetime. In recent years, due to rapid development of urban ground transportation systems, as well as increasing transport of hazardous materials (such as flammable materials, spontaneously combustible and poisonous materials), bridge fires have become a concern (Garlock et al., 2012).

As the fire grows, if there is sufficient fuel and good ventilation, then the fire will rapidly transit between being localised around the element first ignited to the other surrounding items. Therefore, bridge fires can lead to significant economic and public losses. In some cases, such intense fires can pose a severe threat to structural members and could lead to bridge collapse.

Garlock et al. summarize some of the major bridge fire incidents in the past 15 years.

- On the Mezcala cable-stayed bridge in Mexico, a traffic incident on March 17th, 2007, involving two school bus and a truck transporting coconut overturned (Figure 2.1) and produced a fire at deck level resulting in the failure of one stay cable and limited damage to an adjacent cable. The bridge was immediately closed to traffic and reopened to limited traffic prior to cable replacement.

- Xupu Bridge is a cable-stayed bridge span Huangpu River in Shanghai, China. Since its closing, Xupu Bridge has seen occasional fires in 2008 and 2011. On May 3, 2011, the bridge caught fire due to a chemical tank truck carrying xylene burst into flames (Figure 2.2). Similarly, the bridge was immediately closed to traffic (Liu et al., 2012).

Figure 2.1. Truck overturned on Mezcala Bridge (Garlock et al., 2012)

Figure 2.2. Close up of Xupu bridge fire, May 3, 2011 (Liu et al., 2012)

2.1.2 Blast

A blast is a process in which energy is dispersed in a very short period of time which is termed an explosion. On a commercial scale and for military purposes, Trinitrotolueme (TNT) is the most commonly used type of explosive. Other types of explosives are the C-4, Triacetone-Triperoxide (TATP), Hexamethlene Triperoxide Diamine (HMTD) (NCTC, 2014).

During an explosion, impact of the explosive and the high velocity impact of exploded fragments cause the primary damage to the structure. Furthermore, the blast waves are released at a very high pressure and in a very short period travelling through the surroundings in a uniform pattern until intercepted by a barrier. This wave propagation will be further explained in Section 2.3.1. (Winget et al., 2005)

- On the 12th of April, 2007 NBC News reported that a suicide truck bomb exploded on the Al-Sarafiya Bridge, a major steel bridge in Baghdad, Iraq (Figure 2.3), which led to 26 injuries and 10 deaths (NBC News, 2007).
- Another bridge in Iraq received serious damaged due to a small amount of explosive that was placed at the piers of the bridge, causing the collapse of the pier as shown in Figure 2.4.

Figure 2.3. Collapse of the Al-Sarafiya Bridge due to blast (NBC News, 2007)

Figure 2.4. The Iraqi bridge after blast (Agrawal and Yi, 2009)

2.1.3 Corrosion, fretting and fatigue of the cables

In cable stayed bridge the cables are inherently susceptible to corrosion damages. Corrosion of cables is usually highly concentrated at the anchorage of the cable.

Fretting fatigue is a corrosion-related phenomenon that can affect pre-stressing strand/wires used in post-tensioned applications. Fretting fatigue is an extension of fretting corrosion that occurs at the contact area between two materials under load with relative motion between the two surfaces. This motion must be sufficient to produce deformation which will lead to wear and corrosion in the presence of oxygen and resulting in progressive cracking under cyclic loading (fatigue) (Hamilton et al., 1995).

2.2 Consequences of failures on bridge

Depending on the location and type of failure, the bridge response varies. Some failures can be rapidly repaired after a good maintainance or they affect just a part of bridge. But others can conduct to bridge collapse.

2.2.1 Local effect of failures

Accidental events may lead to significant failures on bridge elements such as cable loss, damages on deck or on pylon.

2.2.1.1 Cable loss

The loss of cables must be considered as a possible local failure since the cross sections of cables have usually a low resistance against accidental lateral loads stemming from vehicle impact or malicious actions. This can lead to further overloading and rupture of the adjacent cables (M Wolff and Starossek, 2010). Furthermore, the dynamic effect on the entire bridge of the loss of a stay is not negligible.

The loss of a cable in the back stays of a cable-stayed bridge causes overstressing of the main span cables which will pull the pylon towards the main span thus bending the pylon (Zoli and Steinhouse, 2007; Mozos and Aparicio, 2010).

2.2.1.2 Deck damages

When a cable fails the deck can experience vertical displacement, vibration, and flexural/ buckling at the location of the lost cable (Zoli and Steinhouse, 2007). If breakage of the cable occurs at different locations, then the deck may experience vertical deformations causing varying uplifts along the deck. In decks with twin cable planes, cable loss along one

plane introduces eccentricity in the deck supports, leading to large deflections and with the live loads present is a potential cause of instability (Khan, 2010).

The response of the deck also depends on the stiffness of the deck. Where, the stiffer the deck is, the more the increase in stresses over its ultimate strength value is expected to be (Roura, 2011). Besides, the loss of a cable will lead to the loss of compression in the deck thus, reduction of bracing and therefore increase in the risk of buckling (Maren Wolff and Starossek, 2009).

2.2.1.3 Pylons damages

The pylons are not as susceptible to sudden loss as the stays since they have a larger cross-sectional area, but they are the only member that is part of both the substructure and superstructure and they are prone to ship collision and blast from terrorist attack. A number of research investigations have been carried out to consider the effect of blast ship collision on the pylons of cable-stayed bridges(Hao and Tang, 2010; Guo et al., 2020)

During the process of collision, nonlinear deformations occurs in impact regions, and the non-impact regions of the structure deform elastically (Wei & Chen, 2018).

2.2.2 Global effect of failures

The failure of one structural element can lead to the failure of further structural elements and thus to the collapse of large structural sections or the entire structure. This phenomenon refers to the term progressive collapse (M Wolff & Starossek, 2010). In many cases, the initial triggering event and the resulting damage are disproportionate. Although the disproportion between cause and effect is a defining and common feature, there are various differing mechanisms that produce such an outcome.

2.2.2.1 Zipper-type collapse

A zipper-type collapse is characterized by:

- Initial failure of one or a few structural elements;
- Redistribution of forces carried by these elements in the remaining structure;
- Impulsive loading due to the suddenness of the initial failure;
- Dynamic response of the remaining structure to that impulsive loading;

- Due to the combined static and dynamic effects, a force concentration in and failure of elements which are similar in type and function to and adjacent to or in the vicinity of the initially failing elements;
- Collapse progression in a direction transverse to the principal forces in the failing elements (Starossek, 2007).

2.2.2.2 Instability-type collapse

Instability of structures is characterized by small perturbations (imperfections, transverse loading) leading to large deformations or collapse. The failure of a bracing element due to some small triggering event, however, can make a system unstable and result in collapse (Starossek, 2007). An instability-type collapse exhibits the following features:

- Initial failure of elements which stabilize load-carrying elements in compression;
- Instability of the elements in compression that cease to be stabilized;
- Sudden failure of these destabilized elements due to small perturbations;
- Failure progression.

2.2.2.3 Domino-type collapse

The mechanism behind this type of collapse is as follows:

- Initial overturning of one element (i.e., of one domino block);
- Fall of that element in an angular rigid-body motion around a bottom edge;
- Transformation of potential energy into kinetic energy;
- Lateral impact of the upper edge of that element on the side face of an adjacent element; the horizontal pushing force transmitted by that impact is of both static and dynamic origin because it results from both the tilting and the motion of the impacting element;
- Overturning of the adjacent element due to the horizontal loading from the impacting element;
- Collapse progression in the overturning direction (Starossek, 2007).

2.2.2.4 Mixed-type collapse

The girders and towers of cable-stayed bridges are in compression. They are braced by the stay cables. Thus, the loss of one or a few cables can not only lead to unzipping, as mentioned above, but also to instability failure. In such a scenario, both the zipper-type and instability-type features will most likely interact and combine to produce collapse. Possible interactions are progressive destabilization through unzipping and an increase of force

concentration in the next element to fail (a zipper-type feature) by the transverse displacement increment caused by compression (an effect associated with instability). The propagating action would be both a force and a destabilization (Starossek, 2007).

2.2.3 Reduced serviceability

The loss of a major element may not lead to the collapse of the bridge but can lead to slacking of the cables and thus large deflections in the deck or large vibrations in the deck (M Wolff & Starossek, 2010). This invariably reduces the comfort of the bridge users. When extreme events lead to the loss of a cable, serviceability is no longer an issue.

2.3 Definition of blast load

An explosion can be defined as a very fast chemical reaction involving a solid, dust or gas, during which a rapid release of hot gases and energy takes place. The phenomenon lasts only some milliseconds and it results in the production of very high temperatures and pressures. Blast wave propagation depends on several parameters such as its impulse, the stand-off distance, weight of explosive…All these parameters will be presented below.

2.3.1 Ideal blast wave characteristics

During detonation the hot gases that are produced expand in order to occupy the available space, leading to wave type propagation through space that is transmitted spherically through an unbounded surrounding medium.

The blast wave contains a large part of the energy that was released during detonation and moves faster than the speed of sound. Figure 2.5 shows the idealised profile of the pressure in relation to time for the case of a free-air blast wave, which reaches a point at a certain distance from the detonation. The pressure surrounding the element is initially equal to the ambient pressure P_o, and it undergoes an instantaneous increase to a peak pressure P_{so} at the arrival time t_A, when the shock front reaches that point. The time needed for the pressure to reach its peak value is very small and for design purposes it is assumed to be equal to zero. The peak pressure P_{so} is also known as side-on overpressure or peak overpressure. The value of the peak overpressure decreases with increasing distance from the detonation centre. After its peak value, the pressure decreases with an exponential rate until it reaches the ambient pressure at t_A+t_o, t_o being called the positive phase duration. After the positive phase of the pressure-time diagram, the pressure becomes smaller (referred to as negative) than the ambient value, and finally returns to it. The negative phase is longer than the positive one, its minimum pressure value is

denoted as P_{so}^- and its duration as t_o^-. During this phase the structures are subjected to suction forces, which is the reason why sometimes during blast loading glass fragments from failures of facades are found outside a building instead in its interior.

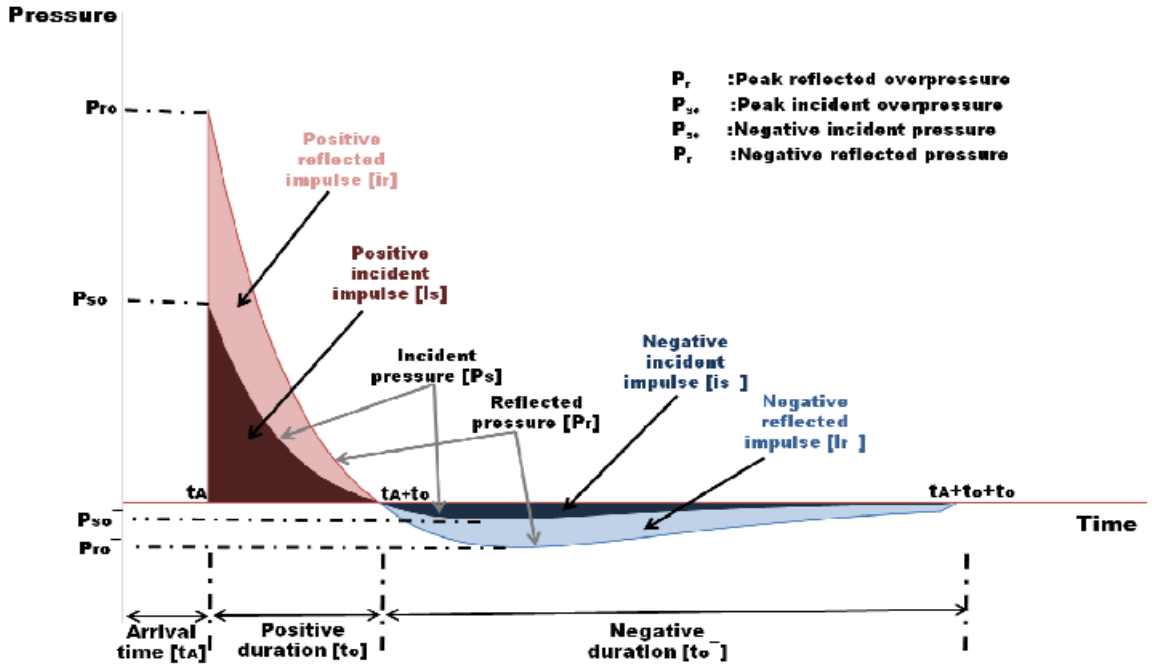

Figure 2.5. Incident and reflected pressure time histories (Karlos et al., 2016)

The negative phase of the explosive wave is usually not taken into account for design purposes as it has been verified that the main structural damage is connected to the positive phase. As can be seen from Figure 2.5, the positive incident pressure decreases exponentially. The following form of Friedlander's equation (2.1) has been proposed and is widely used to describe this rate of decrease in pressure values:

$$P_s(t) = P_{s0}\left(1 - \frac{t}{t_0}\right)e^{-b\frac{t}{t_0}} \qquad (2.1)$$

Where :

P_{so}	is the peak overpressure
t_o	is the positive phase duration
b	is a decay coefficient of the waveform
t	is the time elapsed, measured from the instant of blast arrival

The decay coefficient b can be calculated through a non-linear fitting of an experimental pressure time curve over its positive phase. Besides the peak pressure, for design purposes an even more important parameter of the blast wave pulse is its impulse because it relates to the

total force (per unit area) that is applied on a structure due to the blast. It is defined as the shaded area under the overpressure-time curve of Figure 2.5. The impulse is distinguished into positive i_s and negative i_s^-, according to the relevant phase of the blast wave time history. Equation (2.2) gives the expression in the case of the positive impulse, which is more significant than its negative counterpart in terms of building collapse prevention.

$$i_s = \int_{t_A}^{t_A+t_o} P_s(t)dt \tag{2.2}$$

For equation (2.1), the positive impulse can be analytically calculated as:

$$i_s = \frac{P_{so}t_o}{b^2}[b - 1 + e^{-b}] \tag{2.3}$$

This equation constitutes an alternative way for solving iteratively for the decay parameter b when the values of i_s, P_{so} and t_o are known from experimental data.

2.3.2 Blast parameters

The principal blast loads parameters are stand-off distance and explosive type and weight.

2.3.2.1 Stand-off distance

One of the most critical parameters for blast loading computations is the distance of the detonation point from the structure of interest. The peak pressure value and velocity of the blast wave, which were described earlier, decrease rapidly by increasing the distance between the blast source and the target surface (Figure 2.6). In the figure, only the positive phases of the blast waves are depicted, whose durations are longer whenever the distance from the detonation point increases.

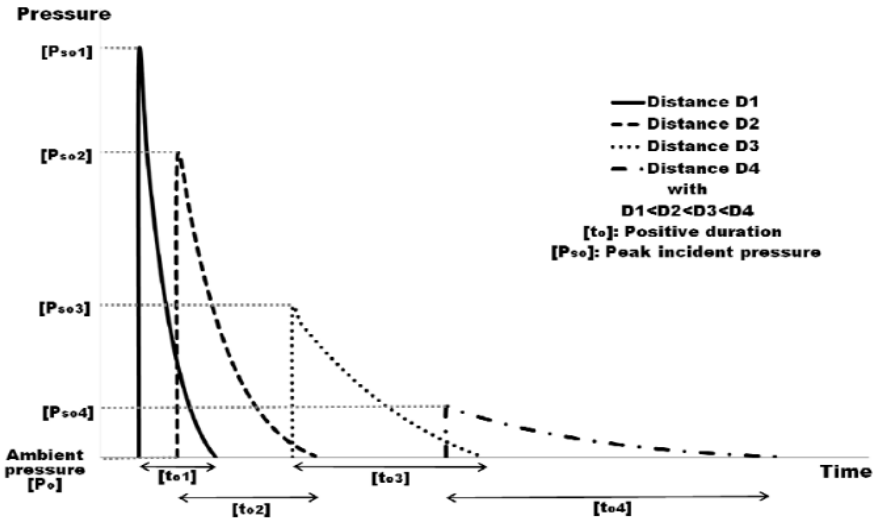

Figure 2.6. Influence of distance on the blast positive pressure phase (Karlos et al., 2016)

The effect of distance on the blast characteristics can be taken into account by the introduction of scaling laws. According to Hopkinson-Cranz law, a dimensional scaled distance is introduced as described by equation (2.4).

$$Z = \frac{R}{\sqrt[3]{W}} \tag{2.4}$$

Where:

R the distance from the detonation source to the point of interest

W the weight of the explosive

2.3.2.2 Explosive type and weight

The wide variety of explosives has led to the adoption of a universal quantity, which is used for all necessary computations of blast parameters. TNT (Trinitrotoluene) was chosen as its blast characteristics resemble those of most solid type explosives. An equivalent TNT weight is computed according to (2.5) that links the weight of the chosen design explosive to the equivalent weight of TNT by utilizing the ratio of the heat produced during detonation:

$$W_e = W_{exp} \frac{H^d_{exp}}{H^d_{TNT}} \tag{2.5}$$

Where :

W_e is the TNT equivalent weight

W_{exp} is the weight of the actual explosive

H^d_{exp} is the heat of detonation of the actual explosive

H^d_{TNT} is the heat of detonation of the TNT

2.3.3 Blast pressure determination

There are various relationships and approaches for determining the incident pressure value at a specific distance from an explosion. All the proposed relationships entail computation of the scaled distance, which depends on the explosive mass and the actual distance from the centre of the spherical explosion.

(Kinney and Graham, 1985) presents a formulation that is based on chemical type explosions. It is described by equation 2.6 and has been used extensively for computer calculation purposes.

$$P_{so} = P_o \frac{808\left[1+\left(\frac{Z}{4.5}\right)^2\right]}{\left\{\left[1+\left(\frac{Z}{0.048}\right)^2\right]\left[1+\left(\frac{Z}{0.32}\right)^2\right]\left[1+\left(\frac{Z}{1.35}\right)^2\right]\right\}^{0.5}} \quad (2.6)$$

Where:

Z is the scaled distance

P_o is the ambient pressure

Other relationships for the peak overpressure for spherical blast include those of (Brode, 1955) shown in Equations (2.7.a) and (2.7.b). The pressure P_{so} in bars:

$$P_{so} = \begin{cases} \frac{6.7}{Z^3}+1 & , for \quad P_{so} > 10\ bar \quad (2.7.a) \\ \frac{0.975}{Z}+\frac{1.455}{Z^2}+\frac{5.85}{Z^3}-0.019 & , for \quad 0.1 < P_{so} < 10 bar \quad (2.7.b) \end{cases}$$

Another formulation, that is widely used for computing peak overpressure values for ground surface blast has been proposed by Newmark and does not contain categorization according to severity of the detonation:

$$P_{so} = 6784\frac{W}{R^3} + 93\sqrt{\frac{W}{R^3}} \tag{2.8}$$

where, P_{so} is in bars,
W is the charge mass in metric tons (=1000kg) of TNT and
R is the distance of the surface from the center of a spherical explosion in m.

(Mills, 1987) have also introduced an expression of the peak overpressure in kPa, in which W is expressed in kg of TNT and the scaled distance Z is in m/kg$^{1/3}$, which reads:

$$P_{so} = \frac{1772}{Z^3} - \frac{114}{Z^2} + \frac{108}{Z} \tag{2.9}$$

Figure 2.7 shows a set of analytical relationships providing the above blast parameters in terms of polynomial functions of the logarithm of the scaled distance. Hence, we can determine arrival time.

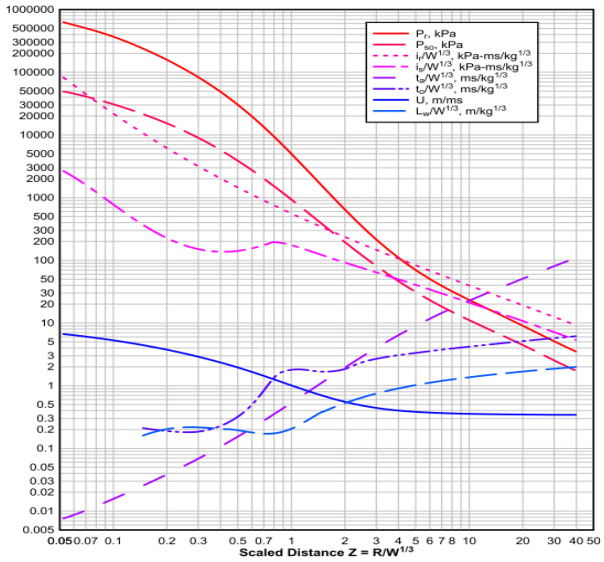

Figure 2.7. Parameters of positive phase of shock spherical wave of TNT charges from free-air bursts (Karlos et al., 2016)

2.3.4 Explosion and blast-loading types

As shown in Figure 2.8, they can be distinguished in three basic types, which depend on the relative position of the explosive source and the structure to be protected i.e., on the height H* above ground, where the detonation of a charge W occurs, and on the horizontal distance RG between the projection of the explosive to the ground and the structure. These three explosion types are:

(a) Free-air bursts: The explosive charge is detonated in the air; the blast waves propagate spherically outwards and impinge directly onto the structure without prior interaction with other obstacles or the ground.

(b) Air bursts: The explosive charge is detonated in the air, the blast waves propagate spherically outwards and impinge onto the structure after having interacted first with the ground: a Mach wave front is created.

(c) Surface bursts: The explosive charge is detonated almost at ground surface; the blast waves immediately interact locally with the ground and they next propagate hemi-spherically outwards and impinge onto the structure.

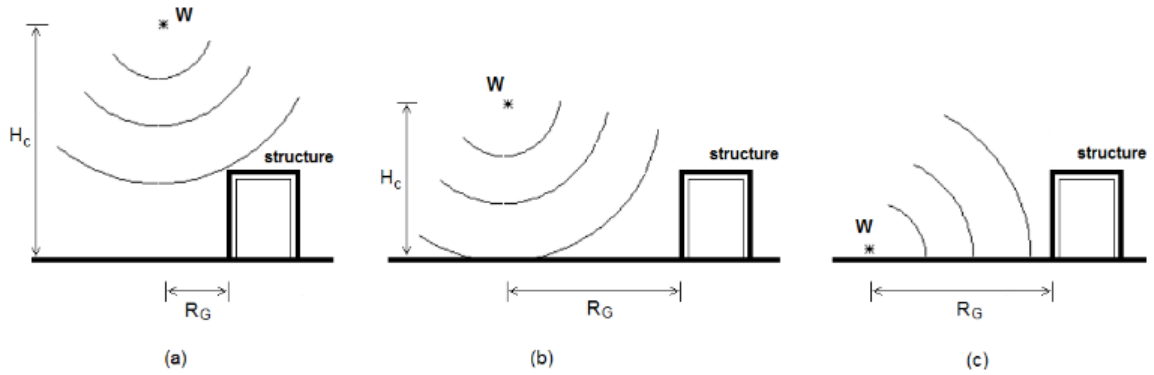

Figure 2.8. Types of external explosions and blast loadings (Karlos et al., 2016)

2.4 Dynamic analysis of cable-stayed bridge

A common situation in structural mechanics is that a structure is only affected by static forces. If the structure is affected by a dynamic force i.e., a force that varies with time, it may have a different response compared with the response of a static force. Dynamic equilibrium equations are solved using modal and direct-integration methods. Initial conditions may be set by continuing the structural state from the end of the previous analysis.

2.4.1 Modal-superposition method

The displacement of a structure is obtained from a linear superposition of modal displacements, which maintain orthogonal characteristics to one another. Using this, a more simplified time integral function can be used to calculate the dynamic response for a selected mode. The mode superposition method is used in many structural analysis programs and is an effective way to calculate the dynamic response for the linear dynamic analysis of large structures with little computational cost. However, the accuracy of the total response depends on the number of used natural modes and so, the number of modes used in the calculation need to be selected appropriately.

2.4.2 Direct-integration

For this option, two procedures can be used: Newmark or Hilber-Hughes-Taylor methods.

2.4.2.1 Newmark method

Iterative analysis by the Newton-Raphson method is carried out in each time step in the process of obtaining the displacement increment until the unbalanced force between the member force and external force is diminished. The unbalanced force is resulted from the change of stiffness in nonlinear elements of the Element Type (element that directly considers nonlinear properties by changing the element stiffness) and the change of member forces in nonlinear elements of the Force Type (element that indirectly considers nonlinear properties by replacing the nodal member forces with loads without changing the element stiffness). The equilibrium equation considered in each iteration step for obtaining response at the time (t+Δt) is as follows:

$$K_{eff}.\delta u = p_{eff} \tag{2.10}$$

$$K_{eff} = \frac{1}{\beta \Delta t^2} M + \frac{\gamma}{\beta \Delta t} C + K \tag{2.11}$$

$$p_{eff} = p(t + \Delta t) - f_E - f_F - K_S u - M\ddot{u} - C\dot{u} \tag{2.12}$$

Where :

Keff	is the effective stiffness matrix
Keff	is the global tangent stiffness matrix for elastic & inelastic elements
δu	is the incremental displacement vector at each iteration step
peff	is the effective load vector at each iteration step
β, γ	are parameters related to Newmark method
t, Δt	are time and time increment
f_E	nodal forces of element type nonlinear elements
f_F	nodal forces of force type nonlinear elements

For stability conditions, recommendations are to use β = 0.25 and γ = 2β = 0.5.

The above iterative process constantly updates the internal forces, f_E and f_F, of inelastic elements through state determination.

2.4.2.2 Hilber-Hughes-Taylor method

The HHT method (also known as the alpha-method) is a one-step implicit method for solving the transient problem which attempts to increase the amount of numerical dissipation present without degrading the order of accuracy. It is an extension to Newmark method.

2.5 Previous works on dynamic analysis of cable-stayed bridges

Since the September 11 attacks by terrorists, there has been increasing public concern about the threat of car bomb attacks on infrastructure such as bridges. Currently, information about blast-resistant design of bridges is limited, while more information about blast-resistant design of buildings is available in several codes and standards (e.g., ASCE codes, US Department of Defense criteria, and the European code).

Although some information about blast-resistant design of buildings is applicable to bridges, further development of such codes for the design of bridges is needed. Therefore, researchers have carried out experimental and numerical investigations to examine bridge structure's responses to explosive loads over the past decade.

2.5.1 Blast analysis studies

- Of the few previous studies of bridge structure response to blast loads, Winget et al. (2005) analysed bridge component responses to blast loads. In their study, a hypothetic bridge structure is considered. To reduce the computational effort, the bridge components (girder, deck and pier) are assumed to be uncoupled and simplified as single-degree-of-freedom (SDOF) systems. 1800 kg TNT explosive is placed at various positions to estimate the worst possible bridge responses. It was found that below deck explosion causes greater damage than above deck explosion because bridge span confinement on shock waves greatly enhances the blast pressures acting on the bridge. The pier fails by the combined flexural and shear failure mode. They suggested that round shaped piers should be used in constructing new bridge structures because the curved surface can increase the blast wave incident angles and hence reduce the blast loads acting on the pier.
- Son et al. (2005) performed nonlinear dynamic finite element analyses of steel orthotropic box and composite plate girder to simulate bridge deck responses to blast loads. By varying both steel and concrete material properties, a series of numerical simulations are carried out. Based on the results, they concluded that steel with high ductility exhibits better performance in both element and nodal responses in comparison with high strength steel.

Normal strength concrete girder with more reinforcements performed better than high strength concrete with relatively less reinforcement.

- Tetougueni et al. (2020) evaluated the structural performance of a cable-stayed bridge under blast loading using an extensive numerical analysis. Firstly, through non-linear dynamic analyses, they have studied the structural response of three configurations of cable-stayed bridges, then figured out the possible immediate and forthcoming damages considering different loading parameters and position. Finally, a displacement-controlled static non-linear pushover analysis of the structure has been performed to evaluate the limit state of the structure for a random position of blast loading and to predict the possible damage state during an accidental event such as blast loading. The results indicate significant effects of the structural configuration of the bridge and stay patterns. The Fan cable-stayed bridge is found to be the most effective among the considered configurations in reducing the dynamic effect induced by the blast loading on the structure. In addition, the deck is found to be less critical in terms of blast load mitigation close to the abutment and the pylon.

- Mishra (2021) studied the Charles River Cable-Stayed Bridge-Boston to assess its robustness and resistance against the progressive collapse resulting from localized failure due to blast loads. To interpret the bridge performance to blast loads, the blast was applicated at three different locations: near the tower location and at starting and end of main span. The results conclude that the bridge is too weak to sustain the blast loads near the tower location, and the progressive collapse is inevitable. Hence, to preserve this cable-stayed bridge from local and global failure, structural components should be more reinforced near the pylons.

2.5.2 Cable loss analyses

- In recent research papers, nonlinear static and dynamic Finite Element (FE) models were employed to estimate a more realistic dynamic amplification factor (DAF) for different cable loss scenarios and various deck geometry and configurations. (Maren Wolff & Starossek, 2009) stated that a DAF of 2.0 is necessary for safe design of cables but a much higher DAF should be applied for bending moments in towers. According to (Mozos & Aparicio, 2010), using the same D.A.F. for all of the cross sections and elements of the structure is not a rational approach to study the Accidental Limit State of failure of a stay. (Aoki et al., 2011) determined their own dynamic amplification factor. Each DAF was obtained as the ratio of the results from the transient dynamic analysis and the corresponding static analysis. The conclusion was that the approach adopted by PTI, may not be adequate for predicting the maximum possible dynamic bending moments.

- (Zhou & Chen, 2014) investigated the performance of a cable-stayed bridge subjected to abrupt cable breakage in the time domain and the influence of stochastic traffic load. They concluded that to consider traffic loads during cable-rupture events is necessary. Depending on the instant when the cable breakage occurs, the stochastic traffic load may cause larger bridge response than that from the static traffic load, which could control the design of the cable-breakage event. Also, material nonlinearity in the cables and frames is not significant, and progressive collapse will not occur after the single-cable breakage scenario for the bridge studied. However, geometric nonlinearity needs to be considered in the simulation to provide more accurate results.
- For Michaltsos et al. (2020), we must disassociate the case of a sudden fracture of one or more cables, caused by an accident, from the case of a programmed replacement of some cables. In general, a sudden rupture of cables induces high developed distresses and unforeseen oscillations of great amplitude.

Conclusion

In this chapter, accidental damages on cable-stayed bridges were the main point. To completely achieve that objective, possible triggering events of failures mechanisms have been first presented. After that, we moved to consequences of those failures on bridge at local and global levels. Some progressive collapse types have been presented. It has been followed by a summary of blast concept and its key parameters. We finished with several studies that have been done in blast load scenario against bridges and cable breakage. The next chapter will give in details the methodology used for investigation in this work.

CHAPTER 3: METHODOLOGY

Introduction

Following literature review presents in first chapters which enable us to have more knowledge on cable-stayed bridges and accidental failures on bridge, the main point of this part is to describe the methodology involved in the investigation of dynamic response of a cable-stayed bridge after a stay failure mechanism. The methodology is the part of the study that establishes the research procedure after the definition of the problem, so as to achieve the set objectives. The content of this chapter is divided in four main parts. First, a general recognition of site done by a documentary research. This is followed by data collection that will help us to model and analyse the bridge. Thereafter, this chapter will focus on a detailed presentation of analytical and numerical methods for static analysis -based on Eurocodes- and dynamic analysis procedure. Finally, because the analysis is made through finite element method, an overview of softwares used in this thesis and modelling will be made.

3.1 Site recognition

The general recognition of site of the building will be done from literature search whose essential goal is to know physical parameters specially the geographic location and climate, relief and ground in one side, and socio-economic parameters in the other side.

3.2 Data collection

The main type of data required for the purpose of this research is the geometrical and statistical data of the bridge.

3.2.1 Geometrical data

Geometrical data will be taken from plans in order to outcome different views of bridge. They show geometry of structural elements and surface area. Necessary steel reinforcement in slab will be presented after.

3.2.2 Statistical data

The collection of statistical data will present mainly the characteristics of materials. It concerns concrete and steel.

3.3 Methodology

A common situation in structural mechanics is that a structure is only affected by static forces. If the structure is affected by a dynamic force i.e., a force that varies with time, it may have a different response compared with the response of a static force. This section is dedicated to procedures used to outcome bridge reactions under static and dynamic loads.

3.3.1 Preliminary design

In order to have sections of structural elements, a preliminary design has been done according to some principles mentioned in section. Final sections of each element in this part will be presented.

3.3.2 Static and dynamic loading

Different types of actions act on the bridge. Regarding our study, we will focus on permanent, variable and blast loads. Permanent loads are represented by $G_{k,j}$; $Q_{k,i}$ express variable loads and A_d the accidental load.

3.3.2.1 Load combinations

A load combination defines a set of designed values used for the verification of the structural reliability for a limit state under the simultaneous influence of different actions. The designed value is the value obtained by multiplying the representative value by a partial factor.

a) Eurocodes

The main codes applied in this thesis are:

- EN 1990 Eurocode: Basis of structural design
- EN 1991 Eurocode 1: Actions on structures
- EN 1992 Eurocode 2: Design of concrete structures
- EN 1993 Eurocode 3: Design of steel structures
- EN 1994 Eurocode 4: Design of composite steel and concrete structures

b) Static load cases

As recommended in EN 1990, the following rules have been considered for the combination of loads with respect to static loads applied in a structure. In the case of a bridge, we have:

(i) Fundamental combination

This combination is used for Ultimate Limit State (ULS) associated to determining of structure resistance and is given by equation 3.1:

$$\sum_j \gamma_{G,j} * G_{k,j} + \gamma_{Q,1} * Q_{k,1} + \sum_{i>1} \gamma_{Q,i} * \psi_{0,i} * Q_{k,i} \quad (3.1)$$

Where the coefficients $\gamma_{G,j}$ *and* $\gamma_{Q,i}$ are partials factors which minimize the loads which tend to reduce the solicitations and maximise the ones that increase them. The recommended values preconized by the Eurocode 0 for the partial safety factors are given in table 3.1.

Table 3.1. Partial safety factors for ULS combination

Partial factor	Favourable	Unfavourable
$\gamma_{G,j}$	1.35	1.00
$\gamma_{Q,1}$	1.50	0.00
$\gamma_{Q,i}$	1.50	0.00

(ii) Characteristic combination (rare)

Usually used for non-reversible Serviceability Limit States (SLS), this combination (3.2) has to be used in the verifications with the allowable stress method:

$$\sum_j G_{k,j} + P + Q_{k,1} + \sum_{i>1} \psi_{0,i} * Q_{k,i} \quad (3.2)$$

(iii) Frequent combination

Frequent combination (3.3) is recommended for reversible SLS:

$$\sum_j G_{k,j} + P + \psi_{1,1} * Q_{k,1} + \sum_{i>1} \psi_{2,i} * Q_{k,i} \quad (3.3)$$

(iv) Quasi-permanent combination

Generally used for long-term effects, it is given by equation 3.4:

$$\sum_j G_{k,j} + P + \sum_{i\geq 1} \psi_{2,i} * Q_{k,i} \quad (3.4)$$

The values recommended for the reduction factors are given in table 3.2.

Table 3.2. Multipliers for the characteristic values of variable loads

	Temperature load	Wind load	Traffic load	
			TS	UDL
ψ0	0.6	0.6	0.75	0.4
ψ1	0.5	0.2	0.75	0.4
ψ2	0.5	0	0	0

c) Dynamic load cases

During the nominal life of a structure, actions such as explosions, fire can occur accidentally. In prevision of such an event, EN 1990 formulated a combination used for the ULS related to the design of accidental actions. Equation 3.5 presents the accidental load combination:

$$G + P + A_d + (\psi_1 \text{ or } \psi_2)Q_{k,1} + \sum \psi_2 Q_{k,i} \quad (3.5)$$

Where :

G: is the self-weight of the structure

A_d: is the design value of the accidental load (in this case the blast load)

$Q_{k,1}$: is the characteristic value of the leading variable load

$Q_{k,i}$: are the characteristic values of the accompanying variable loads

The values of $\psi_1$and ψ_2 depend on the relevant accidental design situation.

3.3.2.2 Load actions

This section focuses on the calculation of loads acting on the bridge. These loads include: permanent and variable loads. Blast load and its parameters will also be presented.

a) Permanent loads

Dead loads represent actions which remain relatively constant over the structure life cycle. They comprise the weight of bridge's structural elements (g_1) such as girders, slab, cables, and the others. Weight of non-structural elements (g_2) (barriers, road pavement, street lamps, …) are also included in dead loads.

b) Pretension loads

After preliminary calculations of cable area as explained in Section 1.4.2, we will proceed to an optimization of pretension forces. MIDAS software proposed an option of tuning

cable force so that the user can stay in interval of moment or displacement, that he had already fixed. It is an iterative process that goes until expectations are reached:

- The first step is to fix pretension forces in cables as 1 kN.
- Secondly, enter the different permanent loads and then run the analysis.
- When analysis is done, make a load combination with the different load factors that have been calculated by the software. Those load factors represent the first values of pretension forces before tuning.
- Enter the previous load combination in option ‘‘cable force tuning’’ so that the good values of pretension can be found.

c) Live loads

The live load on the bridge is moving load throughout bridge length. The moving loads are vehicles, pedestrians, etc.

(i) Number of lanes

The number and the width of notional lanes result from Table. 3.3(*EN 1991-2*, 2003).

Table 3.3. Multipliers for the characteristic values of variable loads (EN 1991-2, 2003)

Carriageway width w	Number of notional lanes	Width of a notional lane w_l	Width of the remaining area
$w < 5{,}4$ m	$n_1 = 1$	3 m	$w - 3$ m
$5{,}4$ m $\le w < 6$ m	$n_1 = 2$	$\frac{w}{2}$	0
6 m $\le w$	$n_1 = Int\left(\frac{w}{3}\right)$	3 m	$w - 3 \times n_1$
NOTE For example, for a carriageway width equal to 11m, $n_1 = Int\left(\frac{w}{3}\right) = 3$, and the width of the remaining area is 11 - 3×3 = 2m.			

(ii) Traffic loads

For the complete analysis of the vertical forces, the traffic Load Model 1 (LM1) has been considered. This Load Model is constituted of a tandem load (TS) and a uniformly distributed load (UDL) (see *EN 1991-2*, 2003). The class of the bridge is class 2. Table. 3.4 recaps the values to consider for loads due to traffic.

Table 3.4. Characteristic values of load model 1 (EN 1991-2, 2003)

Location	Tandem system *TS*	*UDL* system
	Axle loads Q_{ik} (kN)	q_{ik} (or q_{rk}) (kN/m^2)
Lane Number 1	300	9
Lane Number 2	200	2,5
Lane Number 3	100	2,5
Other lanes	0	2,5
Remaining area (q_{rk})	0	2,5

Correction factors α_{Qik}, α_{qik}, α_{qr} to be considered are shown in table 3.5:

Table 3.5. Values of adjustment factors (Marsassoum Project, 2020)

α_{Q1}	$\alpha_{Qi\ (i\geq 2)}$	α_{q1}	$\alpha_{qi\ (i\geq 2)}$	α_{qr}
0.9	0.8	0.7	1.0	1.0

In the following we adopt the load group gr1a from table. 3.6. It is displayed in equation (3.6)

$$gr1a = TS_k + UDL_k + q*_{fk} \tag{3.6}$$

Where $q*_{fk}$ represents the uniformly distributed load on footways and cycle tracks.

Table 3.6. Assessment of groups of traffic loads (EN 1991-2, 2003)

		CARRIAGEWAY						FOOTWAYS AND CYCLE TRACKS
Load type		Vertical forces				Horizontal forces		Vertical forces only
Reference		4.3.2	4.3.3	4.3.4	4.3.5	4.4.1	4.4.2	5.3.2-(1)
Load system		LM1 (TS and UDL systems)	LM2 (Single axle)	LM3 (Special vehicles)	LM4 (Crowd loading)	Braking and acceleration forces [a]	Centrifugal and transverse forces [a]	Uniformly Distributed load
Groups of Loads	gr1a	Characteristic values						Combination value [b]
	gr1b		Characteristic value					
	gr2	Frequent values				Characteristic value	Characteristic value	
	gr3 [d]							Characteristic value [c]
	gr4				Characteristic value			Characteristic value
	gr5	See annex A		Characteristic value				
	Dominant component action (designated as component associated with the group)							

[a] May be defined in the National Annex (for the cases mentioned).
[b] May be defined in the National Annex. The recommended value is 3 kN/m^2.
[c] See 5.3.2.1-(2). One footway only should be considered to be loaded if the effect is more unfavourable than the effect of two loaded footways.
[d] This group is irrelevant if gr4 is considered.

d) Wind load

The general expression of wind force F_w acting on a structure or a structural component can be determined directly by using equation 3.7

$$F_w = c_s . c_d . c_f . q_p(z_e) . d_{tot} \quad (3.7)$$

Where :

$q_p(z_e)$ is the peak velocity pressure at reference height Ze

dtot is the total depth of the structural element z_e

$c_s.c_d$ is the structural factor

c_f is the force coefficient

The peak velocity pressure at height z is expressed by equation 3.8:

$$q_p(z) = \frac{1}{2} . \left(1 + 7 . I_v(z)\right) . \rho . v_m^2(z) = c_e(z) . q_b \quad (3.8)$$

Where:

ρ is the air density

$v_m(z)$ is the mean wind velocity at height z and is given by equation 3.9

$$v_m(z) = c_r(z) . c_o(z) . v_b \quad (3.9)$$

$c_r(z)$ is the roughness coefficient

$c_o(z)$ is the orography coefficient

v_b is the basic wind velocity given by equation (3.11)

$I_v(z)$ is the turbulence intensity and can be obtained from equation (3.10)

$$(I_v(z) = \frac{k_l}{c_o(z) . ln(z/z_o)} \quad (3.10)$$

k_l is the turbulence factor

z_0 is the roughness length

$$v_b = c_{dir} * c_{season} * v_{b,0} \quad (3.11)$$

c_{dir} is the directionl factor

c_{season} is the season factor

Roughness length and coefficients depends on terrain category and parameters. The procedure to find values of different coefficients is detailed in (*EN 1991-1-4*)

The wind used for design will be wind acting on a loaded bridge.

e) Temperature load

Temperature load has two components.

(i) Uniform temperature component

It depends on the minimum and maximum temperature which a bridge will achieve. Having the minimum shade air temperature (Tmin) and maximum shade air temperature (Tmax) for the site, we can derive minimum and maximum uniform bridge temperature components Te.min and Te.max by using the graph on figure. 3.3

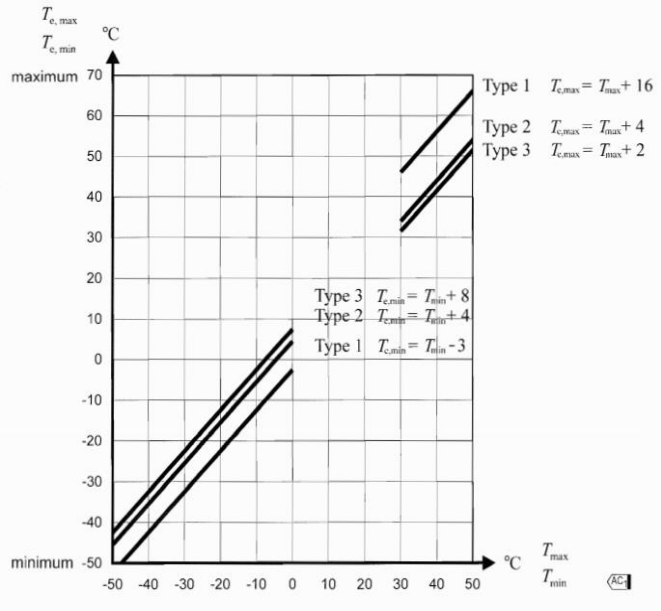

Figure 3.1. Correlation between minimum/maximum shade air temperature and minimum/maximum uniform bridge temperature component (EN 1991-1-5, 2011)

The initial bridge temperature To is important for calculating contraction down to the minimum uniform bridge temperature component and expansion up to the maximum uniform bridge temperature component.

Thus the characteristic value of the maximum contraction range of the uniform bridge temperature component, ΔTN,con should be taken as :

$$\Delta TN, con = T_0 - T_{e,min} \tag{3.12}$$

And the characteristic value of the maximum expansion range of the uniform bridge temperature component, ΔTN,exp should be taken as :

$$\Delta TN, exp = T_{e,max} - T_0 \tag{3.13}$$

The overall range of the uniform bridge temperature component is

$$\Delta TN = T_{e,max} - T_{e,min} \tag{3.14}$$

(ii) Vertical non-linear component

The vertical temperature gradient applied on bridge deck was defined according to table 3.7 in (*EN 1991-1-5*, 2011).

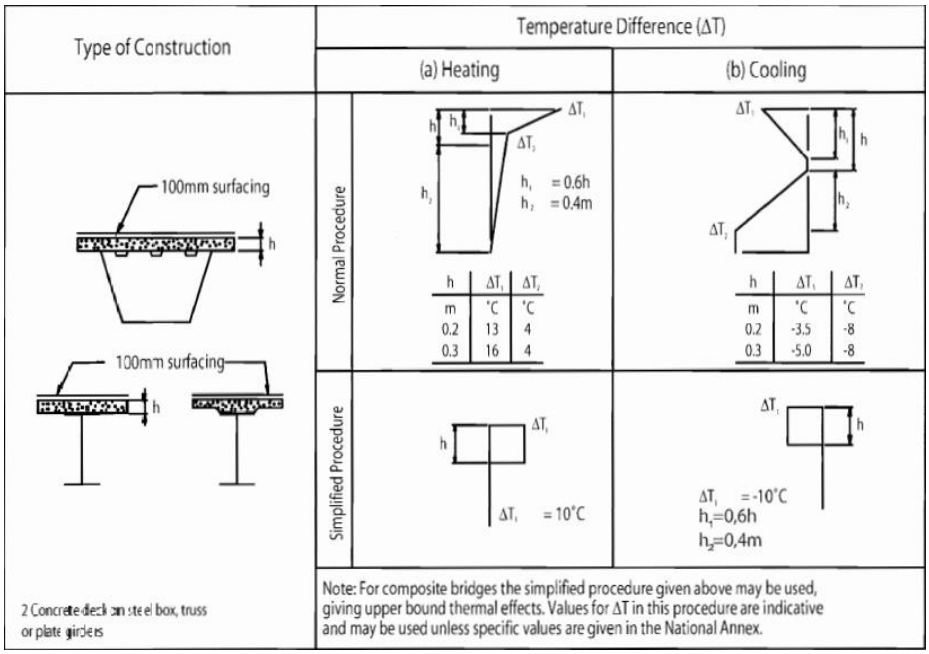

Table 3.7. Temperature differences for bridge decks type 2: composite decks (EN 1991-1-5, 2011)

The load (T_k) due to differential thermal variation (between slab and metal beams) is expressed by equation (3.15):

$$T_k = A_c . \varepsilon . E_{cm} \tag{3.15}$$

Where :

A_c is the slab area

ε is a thermal coefficient

E_{cm} is the concrete elastic modulus with $E_{cm} = 22000.(f_{cm}/10)^{0.3}$

Because we study an effective section of the bridge, we have to apply the corresponding temperature load. The force T_{beam} that will be considered is :

$$T_{beam} = T_k/n \quad \text{Where n is the number of girders.} \tag{3.16}$$

f) Shrinkage

In steel-concrete composite bridges, the slab is restrained by steel beam. The shear connectors resist the force arising out of shrinkage, by inducing a tensile force on the slab (global effect). This reduces the apparent shrinkage of composite structure with respect to the

free shrinkage of concrete. Shrinkage effect is combined to the creep effect; the latter is evaluated at infinite time.

(i) Creep

The effects of creep are taken into account by reducing concrete elastic modulus E_{cm} thus increasing the modular ratio.

Modular ratio at infinite time n_L is given by equation (3.17)

$$n_L = n_0(1 + \psi_L \rho_t) \tag{3.17}$$

Where:

n_0 is the modular ratio E_s/E_{cm} for the short-term loading

ρ_t is the creep coefficient depending on the age t of concrete and the age t_0 at loading

ψ_L is the creep multiplier depending on the type of loading ; to be taken as 1,1 for permanent loads ; 0,55 for primary and secondary effects of shrinkage ; 1,5 for pre-stressing by imposed deformations.

In order to determine the creep coefficient $\rho(t, t_0)$, we have to assume or calculate the following data :

Relative humidity	RH=70%
Reference zero time	t_0= 3 days
Fictitious dimension	h=2Ac/u

The value of $\rho(t, t_0)$ total shrinkage at $t=\infty$ will be found with software MIDAS/civil.

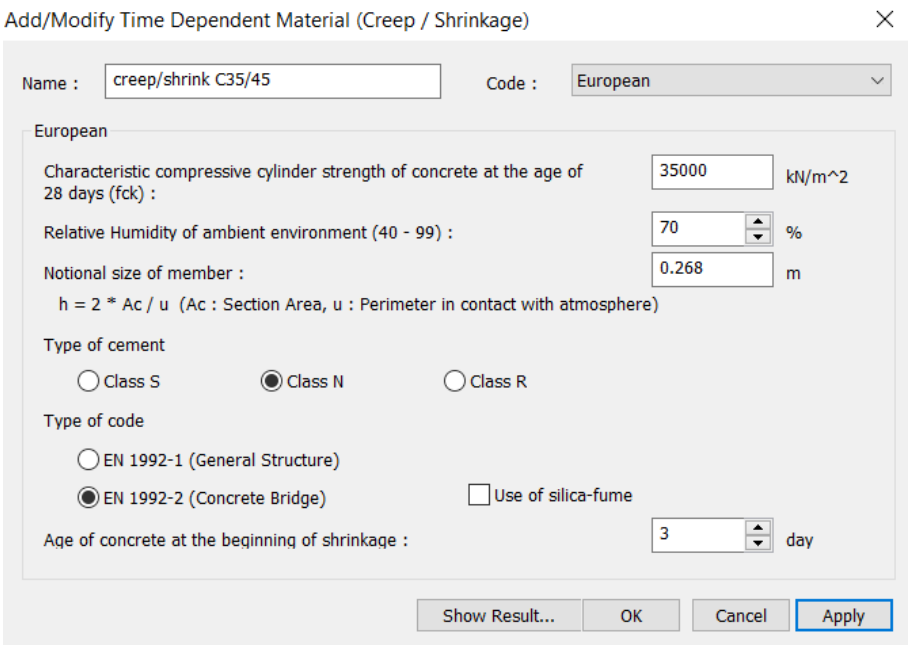

Figure 3.2. Time dependent concrete (MIDAS/civil software)

(ii) Shrinkage

Total shrinkage at infinite is calculated through equation 3.18

$$\varepsilon_{cs}(\infty) = \varepsilon_{ca}(\infty) + \varepsilon_{cd}(\infty) \tag{3.18}$$

Expressions of shrinkage strain components are reported in table 3.8.

Table 3.8. Shrinkage components

$\varepsilon_{ca} = 2.5.(f_{ck} - 10).10^{-6}$	(3.19)
$\varepsilon_{cd}(\infty) = k_h.\varepsilon_{c0}$	(3.20)
$\varepsilon_{c0} = 0.85.((220 + 110.\alpha_{ds1}).e^{(-\alpha ds2.f_{cm}/f_{cm0})}).10^{-6}.\beta_{RH}$	(3.21)
$\beta_{RH} = 1.55.(1 - \left(\frac{RH}{RH_0}\right)^3)$	(3.22)

Where: $\varepsilon_{cd}(\infty)$ is the dry shrinkage strain at infinite

$\varepsilon_{ca}(\infty)$ is the autogeneous shrinkage

Shrinkage of concrete is taken into account by applying an axial force at slab ends. It is given by equation (3.23)

$$N_{c,r\infty} = \varepsilon_{cs}(\infty).E_{c,eff}.A_c \tag{3.23}$$

Where $E_{c,eff}$ is the reduced modulus of elasticity for concrete and obtained from equation (3.24)

$$E_{c,eff} = \frac{E_{cm}}{1+\rho(\infty,t_0)} \tag{3.24}$$

Because we study an effective section of the bridge, we have to apply the corresponding temperature load. The force N_{beam} that will be considered is taken from equation (3.25)

$$N_{beam} = N_{c,r\infty}/n \tag{3.25}$$

Where n is the number of beams

g) Hydrostatic force (permanent load)

The value of hydrostatic force (F_{wa}) exerted on each pylon is given by equation 3.26 :

$$F_{wa} = \frac{1}{2}\, k\rho_{wa}hbv_{wa}^2 \tag{3.26}$$

Where:

v_{wa}	is the average water velocity
ρ_{wa}	is water density
h	is water depth
b	is the obstacle width
k	is a coefficient which depends on obstacle section k=1.44 for square section k=0.7 for circular section

h) Blast load

Blast loads are complex in nature. With the help of experimental results and scaling laws, charts are provided in the manual to calculate the blast load parameters for a given charge weight and standoff distance. The empirical formula to find the scaled distance, Z (m), is mentioned in the equation (3.27).

$$Z = \frac{R}{\sqrt[3]{W}} \tag{3.27}$$

Here, R = Standoff distance (m), W = Equivalent TNT weight of explosion (kg).

(i) Stand-off distance

Considering figure 3.5 below, the method used to determine the blast load parameters at point A is explained below.

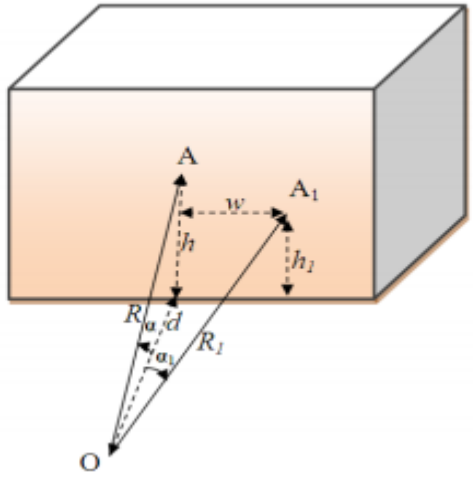

Figure 3.3. Scheme for blast parameters determination (Mbakop, 2020)

The blast origin is point O in figure 3.5, point A is the point where the blast parameters need to be calculated. It is located relative to point O at a horizontal distance d and at a height h. The angle of incidence is α which is the angle made between the shock wave and the line perpendicular to the target surface. We have expressions of R and α given by equations 3.28 and 3.29 respectively.

$$R = \sqrt{(d^2 + h^2)} \tag{3.28}$$

$$\alpha = \cos^{-1}\left(\frac{d}{R}\right) = \tan^{-1}\left(\frac{h}{d}\right) \tag{3.29}$$

(ii) Arrival time

Figure 3.6 describes all the required positive phase parameters in metric units with respect to the scaled distance Z. Hence, arrival time can be deduced.

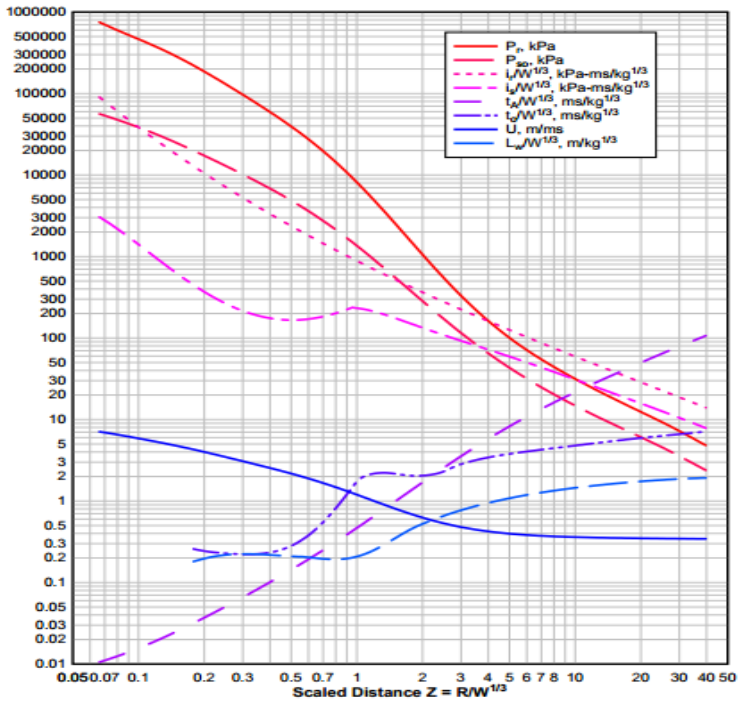

Figure 3.4. Positive phase parameters of shock hemispherical wave of TNT charges from surface bursts (TM5-1300 1990)

(iii) Pressure distribution

Using the scaled distance Z and the charts in TM 5-1300, Eric Jacques, an assistant professor at Virginia Tech developed a computer program names RCBlast to calculate the blast loads for known values of charge weight and stand-off distance. RCBlast software is widely used to determine the equivalent blast pressure distribution due to an explosion. The peak pressure is determined with Mills expression (3.30).

$$P_{s0} = \frac{1}{Z}(108 + \frac{1772}{Z^2} - \frac{114}{Z^2}) \tag{3.30}$$

3.3.3 Static analysis

The static analysis will pass through stress verification at bottom and top of girder and at slab level. Investigation in tower subjected to compression will also be done.

3.3.3.1 Effective width of mixed section

The effective width of a mixed section depends on the position on bridge (edge, middle, supports…). Equation (3.31) gives expression of b_{eff}.

$$b_{eff} = b_0 + b_{e1} + b_{e2} \tag{3.31}$$

Where: $b_{ei} = min(L_e/8\ ;\ b_i)$ (3.32)

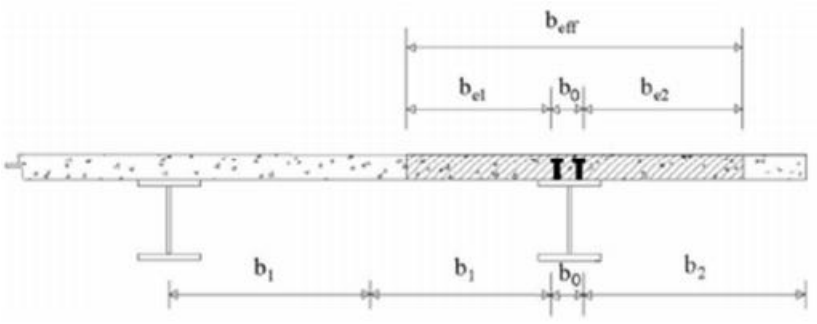

Figure 3.5. Effective width of composite deck

At the end support sections; we have equation 3.33 as formula of b_{eff} and equation (3.34) for value of β_i.

$$b_{eff} = b_0 + \beta_1 b_{e1} + \beta_2 b_{e2} \quad (3.33)$$

$$where:\ \beta_i = (0.55 + 0.025.\frac{L_e}{beff,_i}) \leq 1.0 \quad (3.34)$$

The value of influence length (Le) can be obtained from Figure3.8.

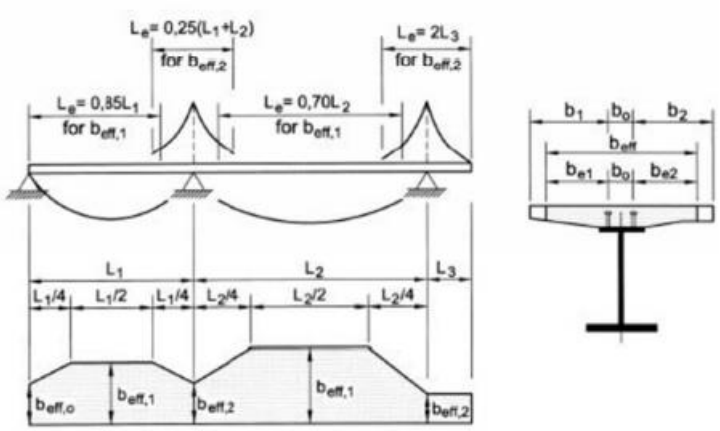

Figure 3.6. Influence length diagram

3.3.3.2 Geometric mixed section characteristics

The characteristics of mixed-section were calculated with respect to Figure 3.9, using the displayed local axis.

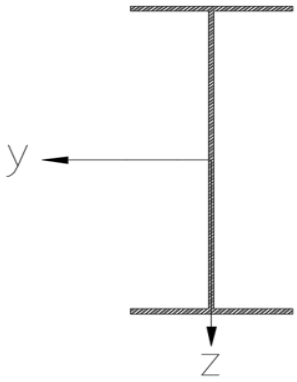

Figure 3.7. Mixed section with local axis (Self-made)

Geometric characteristics are summarized in table 3.9.

Table 3.9. Geometric characteristics of mixed-section

Steel-concrete homogenization coefficient at short-term	$n_0 = \frac{Es}{Ecm}$	(3.35)
Area of ideal mixed section	$A_{id} = A_{steel} + \frac{A_{slab}}{n_0}$ where $A_{slab} = b_{eff}.h_{slab}$	(3.36)
Coordinate y of gravity centre	$y_{id} = \frac{\sum A_i.y_i + (A_{slab}.y_{slab}/n_0)}{A_{id}}$	(3.37)
Moment of inertia of ideal mixed section	$J_{id} = J_{steel} + \frac{b_{eff}.h_{slab}^3}{n_0} + \frac{A_{slab}}{n_0}(y_{id} - y_{slab})^2 + A_{steel}(y_{id} - y_s)^2$	(3.38)
Resistance modulus relative to slab upper section	$W_{up,slab} = \frac{J_{id}.n_0}{y_{id} - h_{tot}}$ where $h_{tot} = \sum h_i + h_{slab}$	(3.39)
Resistance modulus relative to slab lower section	$W_{low,slab} = \frac{J_{id}.n_0}{y_{id} - y_{slab}}$	(3.40)
Resistance modulus relative to steel upper section	$W_{up,steel} = \frac{J_{id}}{(y_{id} - h_{steel})}$ where $h_{steel} = \sum h_i$	(3.41)
Resistance modulus relative to steel lower section	$W_{low,steel} = \frac{J_{id}}{y_{id}}$	(3.42)

At time t=∞, n_0 is replaced by n_L for long-term effects (phase 2).

3.3.3.3 Ultimate limit state

a) Stresses computation

To check the sections of the main beams, the stresses deriving from the application of the loads in the various phases must be found. These stresses are calculated considering the geometric and inertia characteristics relating to the analysed phase and their expressions are reported in Table 3.10.

Table 3.10. Stress calculation

Stress at slab upper section	$\sigma_{up,slab} = \frac{N}{A_{id}.n_0} + \frac{M}{W_{up,slab}}$	(3.43)
Stress at slab lower section	$\sigma_{low,slab} = \frac{N}{A_{id}.n_0} + \frac{M}{W_{low,slab}}$	(3.44)
Stress at steel upper section	$\sigma_{up,steel} = \frac{N}{A_{id}} + \frac{M}{W_{up,steel}}$	(3.45)
Stress at steel lower section	$\sigma_{low,steel} = \frac{N}{A_{id}} + \frac{M}{W_{low,steel}}$	(3.46)

At time t=∞, n_0 is replaced by n_L for long-term effects (phase 2).

For each section, allowable stresses for steel and concrete are given equations (3.47) and (3.48) respectively:

- $\sigma_{steel} < \sigma_{all} = f_{yk}/1.05$ (3.47)
- $\sigma_{slab} < f_{cd} = \frac{0.85 f_{ck}}{1.5}$ or $f_{ctd} = \frac{0.15 f_{ck}}{1.5}$ for parts in compression and tension respectively. (3.48)

b) Classification of section

Table 3.11 permits us to classify sections depending on maximum solicitations obtained from static analysis.

Table 3.11. Maximum width-to-thickness ratios for compression parts (EN 1993-2, 2011)

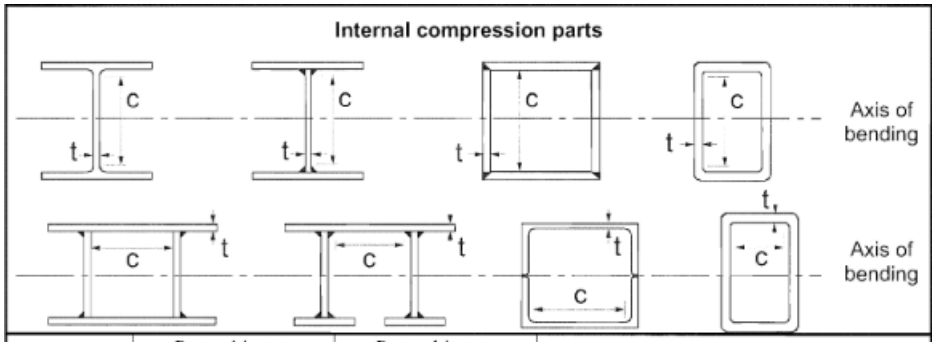

Class	Part subject to bending	Part subject to compression	Part subject to bending and compression
Stress distribution in parts (compression positive)	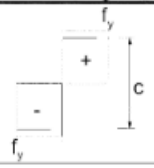	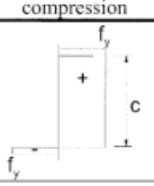	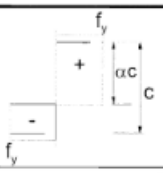
1	$c/t \le 72\varepsilon$	$c/t \le 33\varepsilon$	when $\alpha > 0{,}5$: $c/t \le \frac{396\varepsilon}{13\alpha - 1}$ when $\alpha \le 0{,}5$: $c/t \le \frac{36\varepsilon}{\alpha}$
2	$c/t \le 83\varepsilon$	$c/t \le 38\varepsilon$	when $\alpha > 0{,}5$: $c/t \le \frac{456\varepsilon}{13\alpha - 1}$ when $\alpha \le 0{,}5$: $c/t \le \frac{41{,}5\varepsilon}{\alpha}$
Stress distribution in parts (compression positive)	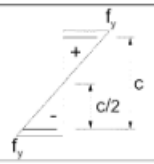	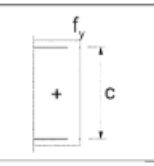	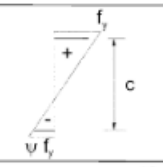
3	$c/t \le 124\varepsilon$	$c/t \le 42\varepsilon$	when $\psi > -1$: $c/t \le \frac{42\varepsilon}{0{,}67 + 0{,}33\psi}$ when $\psi \le -1^{*)}$: $c/t \le 62\varepsilon(1-\psi)\sqrt{(-\psi)}$

$\varepsilon = \sqrt{235/f_y}$	f_y	235	275	355	420	460
	ε	1,00	0,92	0,81	0,75	0,71

*) $\psi \le -1$ applies where either the compression stress $\sigma \le f_y$ or the tensile strain $\varepsilon_y > f_y/E$

c) Shear verification

The maximum shear under previous load combinations will be considered. A look at plastic resistance of sections to vertical shear, shear buckling resistance will be done. It will be checked if there is no interaction between moment and shear.

(i) Plastic resistance

For verifying the design plastic shear resistance $V_{c.Rd}$ the criterion expressed by equation (3.49) for a critical point of the cross section may be used :

$$V_{Ed} \le V_{pl,Rd} = A_v \frac{f_y}{\gamma_a \sqrt{3}} \tag{3.49}$$

Where :

V_{Ed} is the design value of the shear force

A_v is the resisting shear area

(ii) Shear buckling resistance

The shear buckling resistance $V_{b,Rd}$ of steel web is taken from equation (3.50)

$$V_{b,Rd} = V_{bw,Rd} + V_{bf,Rd} \leq \frac{\eta f_{yw} h_w t}{\sqrt{3}\gamma_{M1}} \tag{3.50}$$

In which the contribution from the web is given by equation (3.51)

$$V_{bw,Rd} = \frac{\chi f_{yw} h_w t}{\sqrt{3}\gamma_{M1}} \tag{3.51}$$

And $V_{bf,Rd}$ the contribution from the flanges. η is taken as 1,00.

(iii) Interaction between shear and moment

To attest that there is no interaction between shear (V_{Ed}) and bending moment M_{Ed}, the criterion in equation (3.52) has to be verified:

$$V_{Ed} \leq 0.5\min\{V_{pl,Rd}; V_{b,Rd}\} \tag{3.52}$$

d) Studs design

Shear connectors shall be capable of preventing separation of the concrete element from the steel element. To prevent it, they will be designed under previous designed shear T_{Ed}.

The design shear resistance of a stud is given by equation (3.53):

$$P_{Rd} = min \begin{cases} P_{Rd1} = \dfrac{0.8 f_u \pi d^2/4}{\gamma_v} \\ P_{Rd2} = \dfrac{0.29 \alpha d^2 \sqrt{f_{ck} E_{cm}}}{\gamma_v} \end{cases} \tag{3.53}$$

Where:

$$\alpha = 0.2\left(\frac{hs}{d} + 1\right) \text{ for } 3 \leq hs/d \leq 4 \quad \text{or } \alpha = 1 \text{ for } h/d > 4$$

P_{Rd1} is the stud resistance;

P_{Rd2} is the concrete resistance;

d is the diameter of the shank of the stud, 16 mm ≤ d ≤ 25 mm;

f_u is the specified ultimate tensile strength of the material of the stud

hs is the overall nominal height of the stud;

γ_v is the partial factor and the recommended value is 1,25.

Considering ULS and dynamic load the stud will be designed with value from equation (3.54).

$$\overline{P_{Rd}} = \frac{P_{Rd}}{\gamma_s \gamma_d} \tag{3.54}$$

Where $\gamma_s = \gamma_d = 1.5$ are ULS and dynamic factors respectively.

To obtain the number of studs per meter, we have to get first the shear stress per meter. It is taken from equation (3.55)

$$\tau_b = \frac{V_{Ed} \cdot S}{J_{id}} \quad \text{with } S = \frac{A_{slab}}{n_0}(y_{slab} - y_{id}) \tag{3.55}$$

Where:

τ_b is the shear stress per meter;

V_{Ed} is the design shear force;

S is the static moment of the mixed section;

J_{id} is the moment of inertia of the mixed section.

The number of studs per meter is then:

$$n_s = \frac{\tau_b}{\overline{P_{Rd}}} \tag{3.56}$$

e) Buckling resistance

Members which are subjected to axial compression should satisfy equation (3.57)

$$\frac{N_{Ed}}{N_{b,Rd}} \leq 1{,}0 \tag{3.57}$$

Where $N_{b,Rd}$ is the design buckling resistance of the compression member. It is expressed by equation 3.58

$$N_{b,Rd} = \frac{\chi . A_{eff} . f_y}{\gamma_{M1}} \tag{3.58}$$

$$\bar{\lambda} = \frac{L_{cr}}{i}\frac{1}{\lambda_1} \tag{3.59}$$

Where:

$\bar{\lambda}$ is the slenderness;

χ is the reduction factor;

L_{cr} is the buckling length in the buckling plane considered;

i is the radius of gyration about the relevant axis.

f) Pylon design

Verifications will be done according to *EN 1993-1.1*. Classification of pylon will be done according to table 3.11. Following that, resistance to compression has to be checked. The design value of the compression force N_{Ed} at each cross-section shall satisfy equation (3.60)

$$\frac{N_{Ed}}{A_{eff}} + \frac{M_y}{W_y} \leq \frac{f_y}{\gamma_{M0}} \tag{3.60}$$

The buckling resistance will be evaluated on the same way as explained in previous section e.

3.3.3.4 Serviceability Limit State

Combinations are detailed in section. We are going to check stress, cracking and deflection of slab. It will be followed by stress determination in cables.

a) Slab verification

For this purpose stress limit, control cracking and deflection will be presented.

(i) Stress

Frequent combination (3.3) will be used to verify stress in slab. In this condition, stress criterion from equation (3.61) have to be satisfied

$$\begin{cases} \sigma_c \leq 0.6 f_{ck} \\ \sigma_s \leq 0.8 f_{yk} \end{cases} \tag{3.61}$$

$$\text{With } \sigma_c = \frac{My}{J} \text{ and } \sigma_s = \frac{n_0 M(d-y)}{J} \tag{3.62}$$

Where:

σ_c is the stress in concrete;

σ_s is the stress in steel;

y is the neutral axis position;

J is the moment of inertia of the section.

(ii) Cracking

Cracking shall be limited to an extent that will not impair the proper functioning or durability of the structure or cause its appearance to be unacceptable. We will employ quasi-permanent combination. Because it is at long term, we will consider n_L of section 3.2.2.1.

The calculated crack width w_k from table 3.12 has to be less than the corresponding w_{max} taking from table 3.13.

Table 3.12. Maximum bar diameters Φs for crack control (EN 1991-2, 2003)

Steel stress[2] [MPa]	Maximum bar size [mm] w_k= 0,4 mm	w_k= 0,3 mm	w_k= 0,2 mm
160	40	32	25
200	32	25	16
240	20	16	12
280	16	12	8
320	12	10	6
360	10	8	5
400	8	6	4
450	6	5	-

Table 3.13. Recommended values of wmax (mmm (EN 1991-2, 2003)

Exposure Class	Reinforced members and prestressed members with unbonded tendons	Prestressed members with bonded tendons
	Quasi-permanent load combination	Frequent load combination
X0, XC1	0,4[1]	0,2
XC2, XC3, XC4	0,3	0,2[2]
XD1, XD2, XD3, XS1, XS2, XS3		Decompression

Note 1: For X0, XC1 exposure classes, crack width has no influence on durability and this limit is set to give generally acceptable appearance. In the absence of appearance conditions this limit may be relaxed.

Note 2: For these exposure classes, in addition, decompression should be checked under the quasi-permanent combination of loads.

(iii) Deflection control

Next, quasi-permanent combination will be used. The deflection has to be less than span/250 and is given by equation (3.63.a) and (3.63.b)

$$\frac{l}{d} = K\left[11 + 1{,}5\sqrt{f_{ck}}\frac{\rho_0}{\rho} + 3{,}2\sqrt{f_{ck}}\left(\frac{\rho_0}{\rho} - 1\right)^{3/2}\right] \quad \text{if } \rho \le \rho_0 \qquad (3.63.a)$$

$$\frac{l}{d} = K\left[11 + 1{,}5\sqrt{f_{ck}}\frac{\rho_0}{\rho - \rho'} + \frac{1}{12}\sqrt{f_{ck}}\sqrt{\frac{\rho'}{\rho_0}}\right] \quad \text{if } \rho > \rho_0 \qquad (3.63.b)$$

Where:

l/d	is the limit span/depth;
K	is the factor to take into account the different structural systems;
ρ_0	is the reference reinforcement ratio $\rho_0 = 10^{-3}\sqrt{f_{ck}}$;
ρ	is the required tension reinforcement ratio at mid-span to resist the moment due to the design loads $\rho = \frac{As}{bd}$;
ρ'	is the required tension compression ratio at mid-span to resist the moment due to the design loads $\rho' = \frac{As'}{bd}$;

b) Cable verification

With quasi-permanent combination, stresses in cables will be calculated to satisfy fatigue criterion. We have to verify:

$$\sigma_{stay} < \sigma_{all} = 0{,}45.f_u \tag{3.64}$$

3.3.4 Dynamic analysis

Entering in the principal part of this thesis, a presentation of the procedure that will used to perform time-history analysis will be shown.

3.3.4.1 Explosive weights and positions of explosion

- Blast will occur at three different positions. The considered cases are: blast at start of side span; blast at tower location and blast at middle of bridge.
- Assuming that the bomb is transported in a vehicle (car, truck…), we have considered a size that one of these vehicles carry. We will study two masses of bomb: 250 and 500 kg.

3.3.4.2 Blast load analysis

The minimum height above which the blast can happen will be 1m. The effect of explosion diminishes as the scaled distance increases. Thus, the maximum stand-off distance of 3m is considered. The charges are blasted on the bridge centre. Blast wave considered dispersing in all directions and affect all girders surrounded by the blast.

3.3.4.3 Nonlinear time-history analysis

When big loadings (blast in case) are applied to a structure thereby resulting in high stresses in the range of nonlinear stress-strain relationship, material nonlinear behaviours are encountered. The presence of elements such as cable that are geometrically non-linear and can undergo large displacements, we enter in the domain of nonlinear analysis. That is why we choose to do a nonlinear time-history analysis for our dynamic study.

The dynamic equilibrium equations to be solved are given by equation 3.65.

$$[M]\ddot{u}(t) + [C]\dot{u}(t) + [K]u(t) = p(t) \quad (3.65)$$

Where:

[K], [C], [M] are the stiffness matrix, the damping matrix and the diagonal mass matrix respectiely

u, $\dot{u}$, and $\ddot{u}$: are the displacement, velocity and acceleration of the structure respectively

$p(t)$ represents the applied load.

Modal-superposition is a good procedure to the non-linear problems. Therefore, we will use this option to solve the dynamic equilibrium equation in order to obtain the time-history response of the bridge against blast load.

3.3.4.4 Robustness study of cable-stayed bridge

After performing time-history analysis, we will suppose breakage of cables that crossed the fixed strain limit of 2.7% due to shock front wave. Those cables will be removed and a static analysis will be run in order to outcome the corresponding collapse behaviour of cable-stayed bridge for each case study.

3.4 Numerical modelling

In this section, softwares used for modelling and different analyses will be presented. The software used in this thesis for different analyses starting by optimization of cable pretension forces and static analysis is MIDAS/civil. For dynamic analysis, software SAP2000 was chosen.

3.4.1 Cable-stayed bridge modelling

A three-dimensional computational model of the bridge was created in MIDAS/Civil for pretension forces calculation throughout an optimization process in order to compensate permanent loads with the maximum displacement limited to 15 cm.

The structural elements (girder, pylons, cross and transverse beams) for numerical simulation are modelled using 1D fibre beam element since the variation in the section due to the torsional stress is prevented. In the analysis, those elements are connected to each other by a fixed joint with zero degrees of freedom as is done in the practice of such bridges.

The slab is modelled as a 2D plate element. The connection between slab and girders is done node to node with rigid bars each 1m.

Cable stays are directly connected to pylons while rigid links are used to create the appropriate connection between the deck and cables. Cables were considered as truss elements with a linear elastic behaviour.

The base of the pylons is considered fully restrained in rotation and translation since they are supposed to be embedded in a massive concrete foundation at their bases. The end spans of the bridge are connected to the end spans substructure (abutments) with bearings. Abutments were replaced by fixed constraints and elastic links with high vertical stiffness were used as bearing at both bridge end. They were also placed above transversal beam as bearings.

High strength steel material was considered for deck, pylons, and piers whereas the stress distribution was considered elastic in the cables and was limited to $0.45 \times fu$ to satisfy the fatigue criteria. On the other hand, to consider the cable's sag effect due to the change in the shape under varying stresses, Ernst's equation (3.66) has been used to derive the equivalent elastic modulus of the cable (Freire et al., 2006).

$$E_r = \frac{E_c}{1 + \frac{g^2 L_h^2}{12T^3} E_c A} \tag{3.66}$$

Where :

- E_r is the reduced modulus of elasticity
- E_c is the elastic modulus of cable material
- A is the cable cross section
- T is the cable tension
- L_h is the horizontal component of the cable chord
- g is the weigth per unit length of the cable

For modelling in SAP2000, the same procedure has been employed. The only difference is the replacement of rigid bars by rigid links.

3.4.2 MIDAS/civil description

To do static analysis of the bridge under permanent and variable loads, MIDAS/civil was used.

The different modules that will be used are presented as follows:

- Properties: this section is meant for definition of material and section properties of different elements (cables, girders, slab, cross beams, pylons and transversal beams)
- Structure: this module permits us to define the geometry of our cable-stayed bridge and affect the different sections and the corresponding material properties.
- Boundary: here we can define boundary restrains, rigid and elastic links of our bridge.
- Loads: loads cases are defined here (self-weight, moving loads, element loads, nodal loads).
- Cable control (results): in order to get pretension forces in cables, we have to tuned them so that we can have a displacement less than 15 cm under permanent loads of the bridge. It is possible after analysis has been performed.
- Results: different results (displacements, stresses, moments, axial, shear forces…) can be displayed.

3.4.3 SAP2000 description

SAP2000 version 22 was used to perform nonlinear time-history analysis on bridge subjected to blast load.

For dynamic analysis, we used the following options:

- Time-history functions: after having blast pressure distribution, we will convert it in a function of distributed force changing with time. We have to create time-history functions which represented blast loads that will act on our bridge.
- Load cases: depending on the number of time-history functions, we have to create the same number of load cases.

For damping method, we opted for modal damping and assume a damping ratio of 3% because cable-stayed bridges have really low damping ratios.

We choose Eigen vectors to find natural frequencies and mode shapes.

- Display: once analysis performance is ended, we can outcome time-history graph/results depending on the parameters we want to study.

Conclusion

This chapter discussed in a chronological manner, the methodology used in this thesis in order to have response of a cave-stayed bridge under blast load. We started off by establishing the procedure of collecting data from field to material properties. In order to perform righteous analyses, a clear methodology to obtain loads acting on the structure and various loads combination was done. The design limit state follows and different verifications were explained. We moved on to blast analysis approach presentation and we explained how we will do collapse prediction and evaluate robustness of the bridge. Finally, softwares used and bridge modelling were presented. and the theories related to blast loads prediction, modelling and FEM analysis involved. The final chapter will present the results of previous detailed methods and the response to the main objective of this thesis.

CHAPTER 4: RESULTS AND INTERPRETATION

Introduction

This section presents the results obtained from previous detailed methodology outlined in chapter 3. First, our case study which is a hypothetical cable-stayed bridge in Marsassoum with the different structural elements will be shown; details on materials will be given. Second, we have to do a dynamic analysis on this bridge, static analysis under Ultimate Limit state and verifications under Serviceability Limit State have to be made in order to assess bridge stability. Next, nonlinear time-history analysis will be performed to outcome effects of blast load on our bridge. At the end, some scenarios of cable breakage will be made to check possible collapse types and look at robustness of the bridge.

4.1 General presentation of the site

This section is a brief presentation of Marsassoum. The city will be presented geographically, the climate, the relief and economic conditions in order to know the different conditions which generally have a major influence on the design of structures.

4.1.1 Geographical location of the site

Marsassoum is a small town of Marsassoum arrondissement in Ziguinchor province in Senegal. It is located at: 12° 49′ 39″ N and 15° 58′ 50″ W. The site is in East region of Marsassoum; there we can find the Soungrourou river which separate Marsassoum from Diéba on the other river bank.

Figure 4.1. Marsassoum location (Google Map)

4.1.2 Climatic conditions

With an average temperature of 27.1°C, Marsassoum has tropical climatic conditions. During the year, the temperature generally ranges from 17 °C to 38°C and is rarely below 15°C or above 41°C. It has an annual rainfall of 1300.5 mm. The rainiest month is August with 426.7 mm of precipitation and the driest one is January. Figure details some meteorologic characteristics of Marsassoum town.

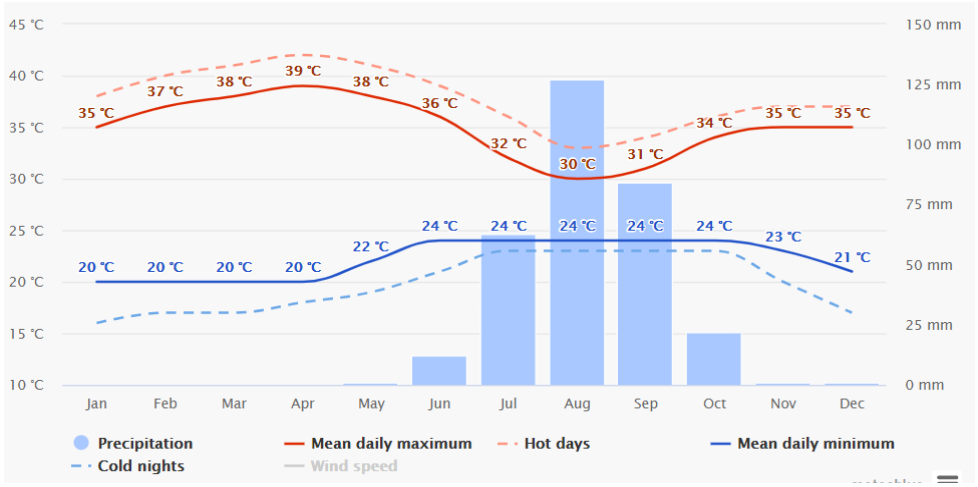

Figure 4.2. Average temperature and precipitation per month in Marsassoum (Meteoblue, 2021)

4.1.3 Relief and ground

The relief is essentially made up of plateaus, valleys and lowlands. The types of soil encountered around the site are as follows:

- Ferralitic soils: They cover most of the region. They are suitable for growing cereals and peanuts.
- The loamy clay soils located on the slopes of the valleys. This is the domain where palm groves and an area suitable for arboriculture and market gardening.
- Hydro-morphic soils are found at the bottom of the slopes. These soils are suitable for rice cultivation. The hydro-morphic soils are the result of alluvial fluviomarin contact and border the Soungrougrou river. These soils are suitable for rice cultivation winter but are often exposed to intrusion of the salty tongue.
- Halomorphic soils acidified by the high salt content which makes them unusable.

4.1.4 Socio-economic aspect

The regional economy is essentially an agricultural economy. The agriculture sector employs more than half of the work population. The dominant agricultural productions remain peanuts and millet. Logging and arboriculture, in particular fruit production, constitute a sector with growth and job creation for the populations. We also find cattle breeding and fishing.

Marsassoum has a population of around 7,000. It is an area with a fairly low schools enrolment; however, a lot of efforts have been made in strengthening the system in recent years. This is also the case in the field of health. Very few households have access to drinking water.

4.1.5 Physical description of the site

Some pictures of the site are going to be presented. It is an area with roads that need rehabilitation. The access road to Diéba side is almost submersible, especially during the rainy period with a total length of approximately 4Km.

Figure 4.3. Access road from Soungrourou river to Diéba (Geotechnical notes of Marsassoum, 2012)

Figure 4.4. Access road from Soungrourou river to Marsassoum (Geotechnical notes of Marsassoum, 2012)

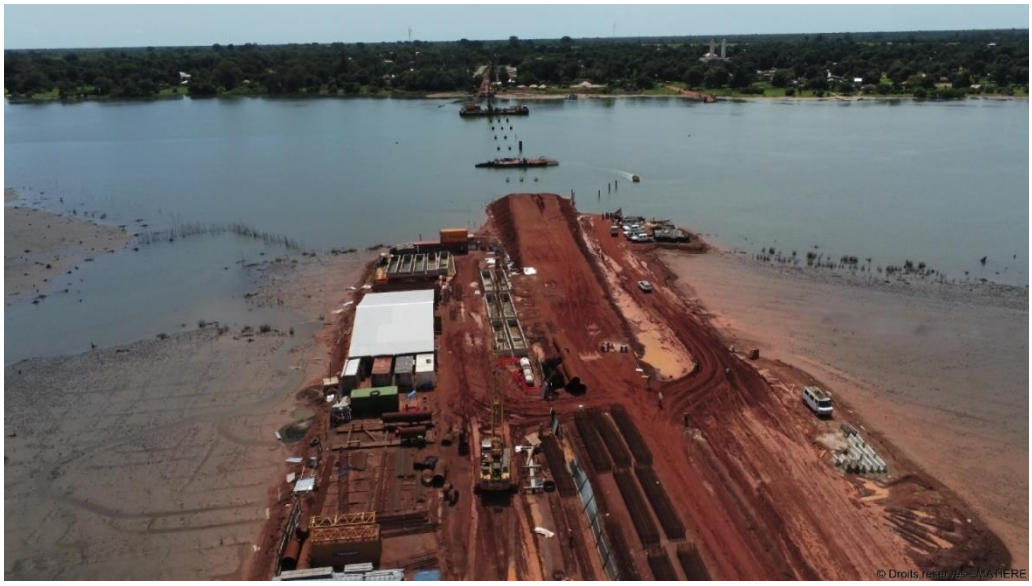

Figure 4.5. Marsassoum bridge construction (Notes of Marsassoum project, 2020)

4.2 Presentation of case study

Elements which allow us to present the case study building are geometric data and statistic data.

4.2.1 Geometrical data

Geometric data are essentially bridge geometry with its different cross section or views.

4.2.1.1 Bridge geometry

The generic bridge under this study is a cable-stayed bridge with a modified fan configuration and double plane cable arrangement. Cables are anchored and spaced of 12 m each other.

The analysed bridge indeed consists of two lateral spans of 120 m long and a main span of 245.5 m long. The bridge deck has a composite multi-girder section, with three steel beams of 2.5 m depth and a concrete slab of 24 cm thickness. The centre-to-centre spacing between main girders is 5.26 m. Bridge transversal section is 11.52 m wide, including a carriageway of 8.70m width and two footways.

Rectangular closed box sections have been considered for the pylon, the transverse beam, and the base pylon. The pylon is considered as the vertical element above the steel deck whereas the base pylon is taken as a vertical element below the steel deck. Two transverse beams are used to connect the vertical elements and form with the vertical element the "H" shaped pylon.

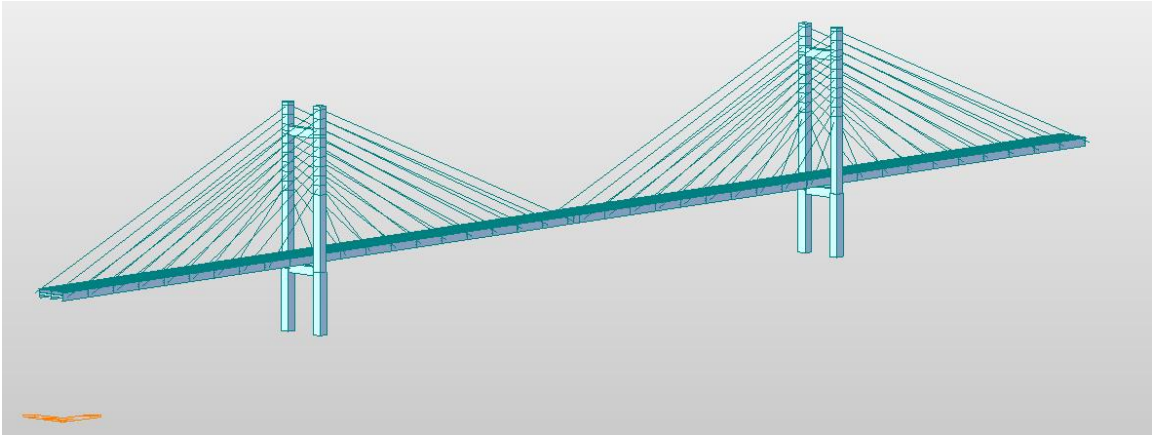

Figure 4.6. Longitudinal view of bridge model

On this view, the bridge length is along the x direction. Y direction is for transversal width of bridge and z axis is for height.

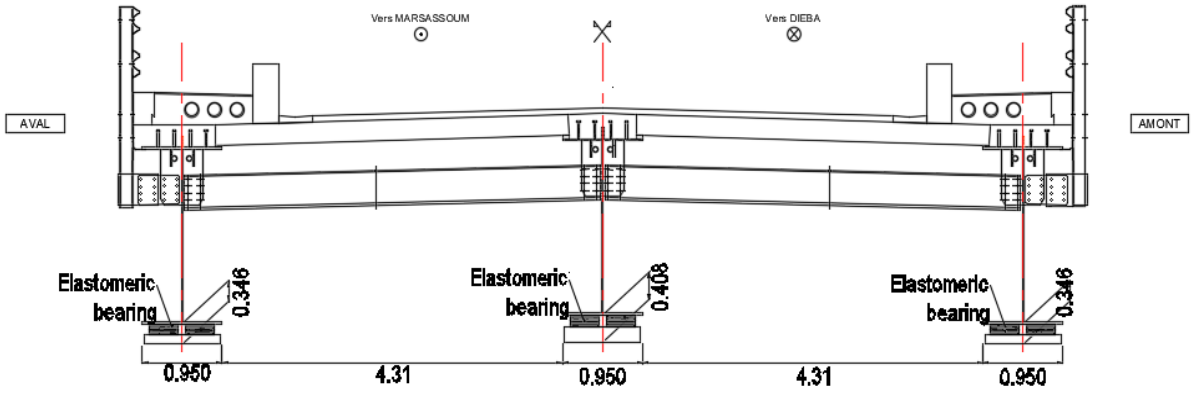

Figure 4.7. Transversal section of the Deck

The preliminary design that permits us to obtain the cross-sections used to model the structural elements will be presented later.

4.2.2 Statistical data

Statistic data will deal with presentation of data link to characteristics of concrete and steel used.

a) Characteristics of slab

The slab concrete belongs to C35/45 resistance class with normal setting (N). For steel reinforcement, Fe500 was considered. The principal characteristics of concrete and steel reinforcement used in this analysis are reported in tables 4.1 and 4.2 respectively.

Table 4.1. Characteristics of concrete

Designation	Values	Units
Characteristic cubic Compressive strength of concrete fck	35.00	N/mm^2
Characteristic cylinder Compressive strength of concrete fck	45.00	N/mm^2
Mean tensile strength of concrete $fctm$	3.21	N/mm^2
Designed compressive strength of concrete fcd	19.83	N/mm^2

Concrete Elastic Modulus Ecm	34077.15	N/mm^2

Table 4.2. Characteristics of steel reinforcement

Designation	Values	Units
Characteristic yield strength of steel fyk	500	N/mm^2
Design yield strength of steel fyd	434.78	N/mm^2
Steel Elastic modulus Es	210000.00	N/mm^2

b) Steel reinforcement

The distribution of reinforcing bars in slab is presented in figure 4.8. We have Φ20 spaced of 12.5 cm at top of girders and spacing bars increase to 20 cm at the interspace between them.

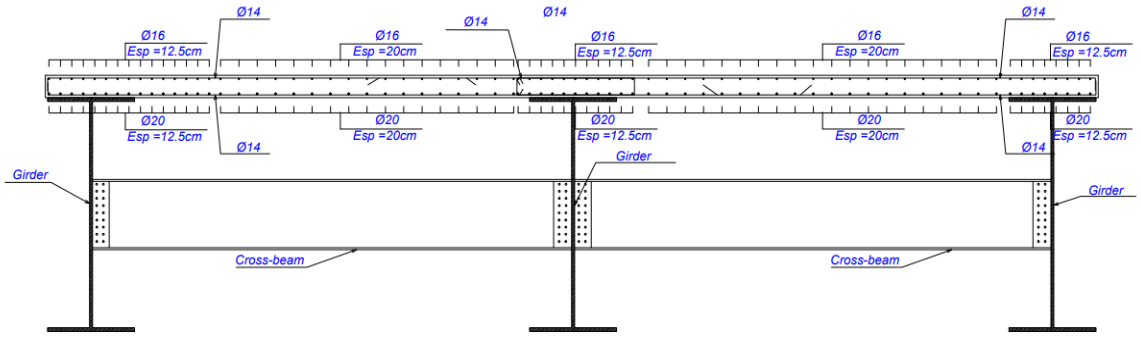

Figure 4.8. Steel reinforcement in slab

c) Exposure classes and concrete cover

The design working life is of bridge is 100 years. Requirements on concrete cover are establishing based on the link between the environmental conditions and the protection of reinforcement. Exposure classes of concrete are the following:

- For top of slab: XC3 due to moderate humidity
- For slab bottom: XC4 (concrete surfaces subject to water contact) and XS3 (parts of marine structures)

- For concrete cast-in place: XC4 and XS1 (exposed to airborne salt but not in direct contact with sea water).

The basic data for the concrete cover is detailed in Table 4.3.

Table 4.3. Concrete cover calculation

Exposure class	Bond type	Cmin,b (mm)	Cmin,dur (mm)	
XC3	Reinforcing bars	20	30	10
XC4	Reinforcing bars	25	40	10
XS1	Reinforcing bars	25	45	10

Cmin=max (cmin,b ;cmin,dur ;10mm)

Concrete cover will be considered as 50mm.

d) Shear connectors

Stud shear connectors in S235J2G3 steel grade are adopted. Their ultimate strength is fu = 450MPa.

e) Structural steel

We have materials features of structural elements reported in table 4.4.

Table 4.4. Materials of structural steel elements

Structural elements	Steel grade	Yield strength [Mpa]	Failure strain	Elastic modulus [Mpa]	Weight density [kN/m3]	Thermal coefficient [1/C]
Cables	Y1770S7	1570		195000	76,98	$1.2.10^{-5}$
Deck (girder)	S420	420	5%	210000	76,98	$1.2.10^{-5}$
Pylons, transversal beam, cross beam	S355	355	3%	210000	76,98	$2.06.10^{-7}$

Plastic properties for S355 and S420 are defined following Tresca yield criterion which is suitable for ductile materials such as metals. Plastic materials are defined because of dynamic nonlinear analysis that will be done further.

4.3 Structural analysis of cable-stayed bridge

According to some principles enumerated in the first chapter, a preliminary design has been done and modified to find good cross sections. Eurocodes and some physical properties of materials help us to calculate different loads values and do static analysis verifications.

4.3.1 Preliminary design of structural elements

This part presents preliminary design and shows good sections of structural bridge elements.

4.3.1.1 Span proportions

Span ratios for the conventional three-span cable-stayed structure vary according to use. For highway bridges, back-span to main-span ratios of 0.45 to 0.48 have been used for contemporary composite bridges.

We choose to round up the ratio to 0.5 and took a bridge that consists of two lateral spans of 120 m long and a main span of 245.5 m long.

4.3.1.2 Cables

Seven wire high tensile strength strands of 15.2 mm diameter are used to make the cables (Figure 4.9). These seven-wire strands are assembled to form a parallel-strand cable composed of 75 strands. They are hot-dipped galvanized and are sheathed with a tight high-density polyethylene coating to prevent corrosion. The bundled mono strands are supplemented with an outer sheathing to reduce the cable anchorage connection's wind and rain effects.

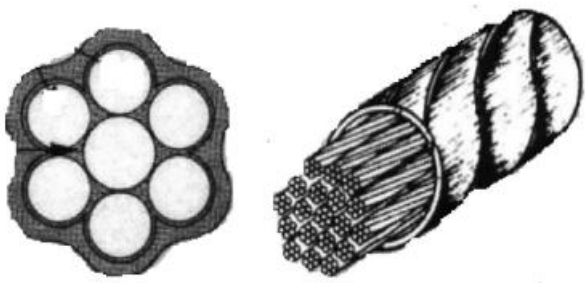

Figure 4.9. Cable cross-section

Right pretensions in cables and corresponding areas obtained after the optimization process are reported in table 4.5.

Table 4.5. Cables pretension forces and areas

Cable No (towards bridge middle)	Area [m2]	Pretension [kN]
1	4029,11	3209,1826
2	4365,40	3477,0442
3	4506,50	3589,4284
4	4917,33	3916,6558
5	5076,25	4043,2299
6	4723,78	3762,4942
7	4689,15	3734,9099
8	6391,86	5091,1132
9	9296,97	7405,0374
10	10215,65	8136,762
11	9040,74	7200,9469
12	6686,64	5325,9074
13	6295,35	5014,2459
14	6039,40	4810,3808
15	5564,21	4431,8972
16	5800,74	4620,2914
17	5449,80	4340,7648
18	4793,37	3817,9214
19	5386,32	4290,2011
20	4924,45	3922,3236

4.3.1.3 Deck cross-section

Depth of stayed girders range from 1/150 to 1/200 of the main span for composite-girder designs. We first took a depth of 1.8 m but the static analysis was not verified. Thus, we opted for a depth girder of 2.5 m. Characteristics of deck elements are reported in table 4.6.

Table 4.6. Girder geometry

Geometry	Properties	Values	Units
	Total height *htot*	2500	mm
	Flange thickness *tf*	40	mm

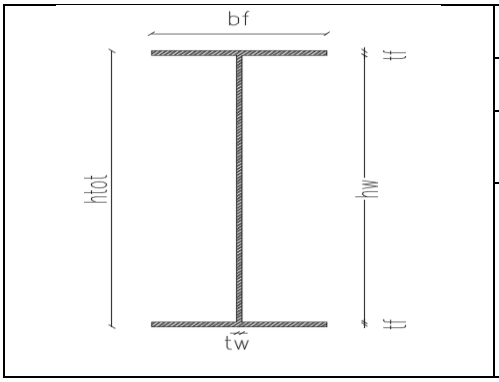	Flange width *bf*	950 mm	mm
	Web thickness *tw*	40	mm
	Area	148600	mm^2
	Moment of inertia *Iyy*	1,50422E+11	mm^4

For cross-beams, geometrical characteristics figured in table 4.7.

Table 4.7. Cross-beam geometry

Geometry	Properties	Values	Units
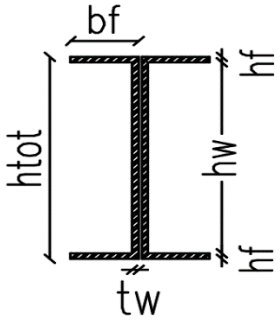	Total height *htot*	**750**	**mm**
	Flange thickness *tf*	**20**	**mm**
	Flange width *bf*	**210**	**mm**
	Web thickness *tw*	**16**	**mm**
	Area	**39520**	**mm2**
	Moment of inertia *Iyy*	**3.193E+9**	**mm4**

4.3.1.4 Tower sections

For the pylon height and dimensions, we choose the same sections that Tetougueni et al., (2020) took for his work. The upper portion of tower is high of 48.5 m while for the base pylon, we have 12 m. Tables 4.8 and 4.9 detailed their geometry.

Table 4.8. Pylon geometry

Geometry	Properties	Values	Units
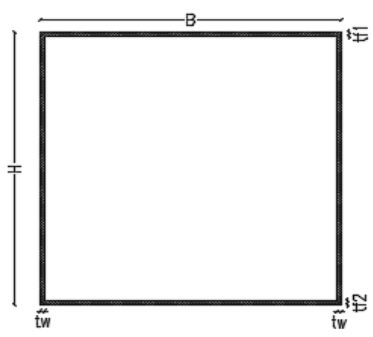	Total height *htot*	2800	mm
	Flange thickness *tf*	40	mm
	Flange width *bf*	2800	mm
	Web thickness *tw*	40	mm
	Area	441600	mm^2
	Moment of inertia *Iyy*	5.61E+11	mm^4

Table 4.9. Base pylon geometry

Geometry	Properties	Values	Units
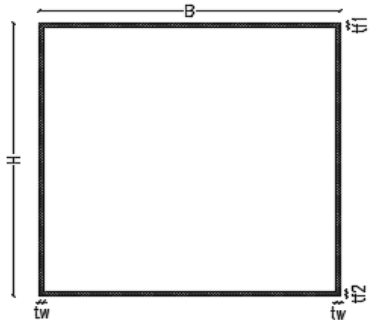	Total height *htot*	3200	mm
	Flange thickness *tf*	40	mm
	Flange width *bf*	3200	mm
	Web thickness *tw*	40	mm
	Area	505600	mm^2
	Moment of inertia *Iyy*	8.42E+11	mm^4

Pylons sections are followed by geometry of transversal beam that link them under the deck.

Table 4.10. Transversal beam geometry

Geometry	Properties	Values	Units
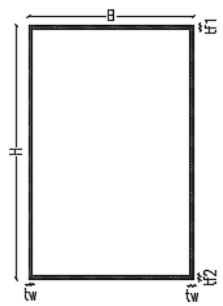	Total height *htot*	2800	mm
	Flange thickness *tf*	40	mm
	Flange width *bf*	1800	mm
	Web thickness *tw*	40	mm
	Area	361600	mm^2
	Moment of inertia *Iyy*	4.08E+11	mm^4

4.3.1.5 Shear connectors

A section with h=200mm and d=22mm has been assumed. Figure 4.10 represents studs section.

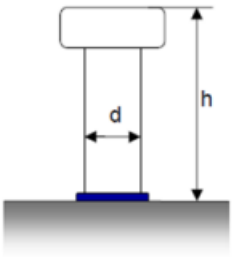

Figure 4.10. Studs section (Notes of Marsassoum project, 2020)

4.3.2 Loads computation

We have to find permanent and variable loads values acting on the bridge.

4.3.2.1 Self-weight of structural elements (g1)

Table 4.11 shows a self-weight estimation concerning structural steel ($g_{1,s}$) and concrete slab ($g_{1,c}$), both expressed as distributive loads. In order to take into account the weight of the joints, stiffening plates, etc. the weight of the steel box is increased by a 20% factor.

Table 4.11. Self-weight of structural elements

Loads	Weight density [kN/m3]	g_1 [kN/m]
$g_{1,s}$	76.98	14.87
$g_{1,c}$	25	69.12
Total	/	**83.99**

4.3.2.2 Self-weight of non-structural elements (g2)

Self-weights of non-structural elements are summarised in following table:

Table 4.12. Self-weight of structural elements

Elements	Number	Weight density [kN/m3]	Width/diameter [m]	Thickness/height [m]	Characteristic value [kN/m]
Left footway					
Safety barrier	1	/	/	/	0,6
Footway concrete	1	25	1,455	0,37	10,77457324
Concrete cornice	1	23	0,4	0,075	0,69
Cable sheaths	3	89	0,16		2,68
Low wall	1	25	0,3	0,68	5,1
Right footway					
Safety barrier	1	/	/	/	0,6
Footway concrete	1	25	1,455	0,37	10,77457324
Concrete cornice	1	23	0,4	0,075	0,69
Cable sheaths	3	89	0,16		2,68
Low wall	1	25	0,3	0,68	5,1
Street lamps (each 12 m)					0,077
Roadway					
Waterproofing layer	1	24	10,9	0,005	1,308
Asphalt layer	1	24	6,9	0,07	11,592

4.3.2.3 Shrinkage

On Figure 4.11 we can see that at t=∞, $\rho = 2.009$.

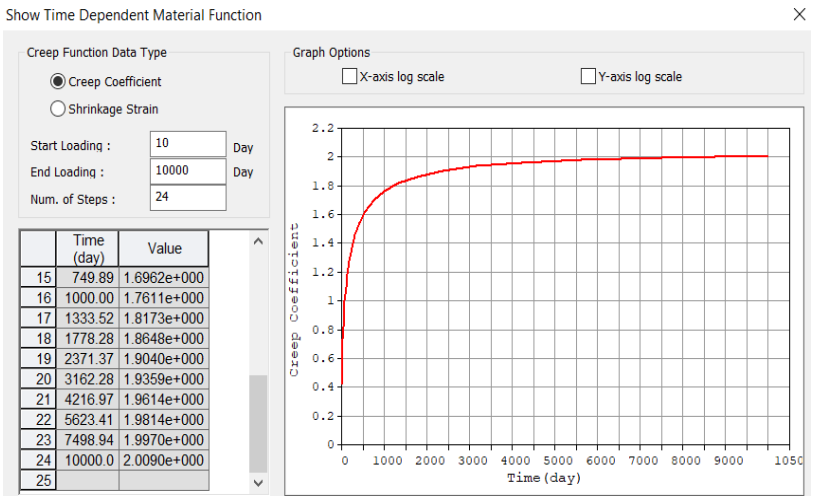

Figure 4.11. Creep coefficient graph

Looking at graph on figure 4.12, we have $\varepsilon_{cs}(\infty) = -3.2457E-04$

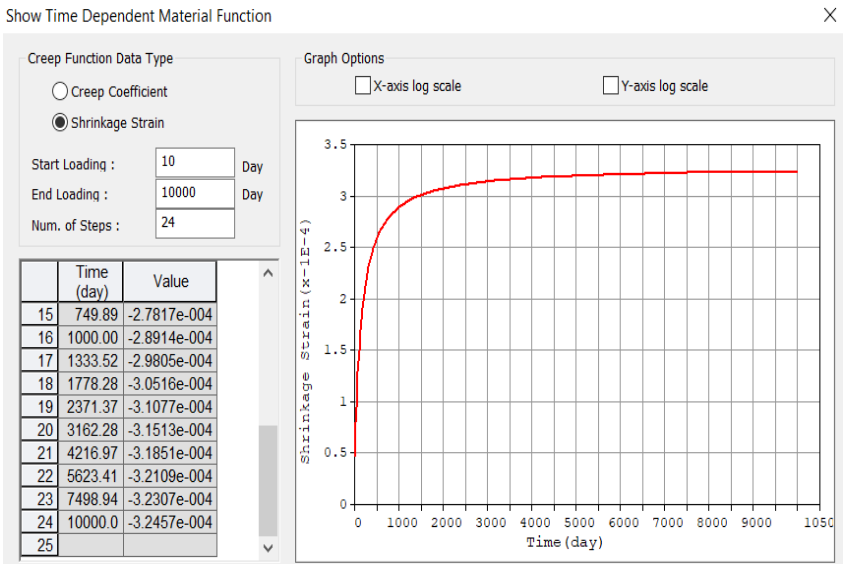

Figure 4.12. Shrinkage strain graph

Values of different coefficients and axial force value obtained for shrinkage figured in table 4.13.

Table 4.13. Shrinkage computation

Designation	Values	Units
Concrete-steel homogeneity coefficient for short-term loading n_0	6.16	/
Concrete-steel homogeneity coefficient for long-term loading $_{n}$L	13.65	/
Effective elastic modulus of concrete $E_{c,eff}$	11325.1	N/mm^2

Total shrinkage force $N_{c,r\infty}$	10118.68	kN
Shrinkage force per effective section N_{beam}	3372.9	kN

4.3.2.4 Live loads

For traffic distribution, load values of traffic are reported in table 4.14.

Table 4.14. Load values for group 1a

	Lane 1	**Lane 2**	**Residual area**	**Footway**
Width of the notional lane [m]	3	3	0,875	1,885
Uniformly distributed load UDL [kN/m2]	9	2,5	2,5	3
Concentrated load TS [kN] (value of single axle)	300	200	0	0

4.3.2.5 Wind load

This project faces a terrain of category II (z_0=0.05 m and z_{min}=2 m). We assume a reference velocity of $V_{b,0}$=32m/s (obtained from project notes). The values of coefficients at height z=3 m used in this process are reported in table 4.15.

Table 4.15. Coefficients of wind

Coefficients	**Values**
Roughness coefficient $c_r(z)$	0.778
Orography coefficient $c_o(z)$	1
Turbulence factor k_l	1
Directional factor c_{dir}	1
Season factor c_{season}	1

For wind force applied in y direction, the computed value figure in table 4.16.

Table 4.16. Wind force computation

Designation	Values	Units
Basic wind velocity v_b	32	m/s
Mean velocity v_m	24.89	m/s
Turbulence intensity $I_v(z)$	0.244	/
Peak velocity pressure $q_p(z)$	1028.49	N/m^2
Total depth d_{tot}	5.74	m
Force coefficient c_f	2.471	/
Wind force $F_{w,y}$	3.64	kN/m

4.3.2.6 Temperature load

Table 4.17 presents temperature load calculation.

Table 4.17. Temperature force computation

Designation	Values	Units
Slab area A_c	2.75	m^2
Thermal coefficient ε	1.2E-05	/
Total temperature load T_k	11256.91	kN
Temperature force per effective section	3752.3	kN

4.3.2.7 Hydrostatic force

This section concerns force of water applied on pylon. Table 4.18 presents hydrostatic force parameters and their values.

Table 4.18. Hydrostatic force computation

Designation	Values	Units
Average water velocity v_{wa}	0.7	m/s
Water density ρ_{wa}	1000	kg/m^3
Water depth h	4.15	m
Obstacle width b	3.2	m
Force of water F_{wa}	4.69	kN

4.3.3 Verification at Ultimate Limit State

Stresses depend on mixed-section geometrical characteristics. Those characteristics change, they are different at short and long term. Verification will be done at three sections.

4.3.3.1 Geometrical characteristics

To check the sections of the main beams, the stresses deriving from the application of the loads in the various phases must be found. These stresses are calculated considering the geometric and inertia characteristics relating to the analysed phase. The stress state of the subsequent phases consists in the sum of all the stress states acting up to that point.

We assume to check bridge at edge beam. Its effective width value is equal to 3.09m. We obtained the following characteristics for short-term:

Table 4.19. Mixed-section characteristics at t=0

Mixed section t=0		
A_{id}	0.269	m^2
Y_{id}	1.863	m
J_{id}	0.276	m^4
$W_{low,\ steel}$	0.148	m^3
$W_{up,\ steel}$	-0.433	m^3
$W_{low,\ slab}$	-2.668	m^3
$W_{up,\ slab}$	-1.938	m^3

At long-term loading we have data recorded in table 4.20.

Table 4.20. Mixed-section characteristics at t=∞

Mixed section t=∞		
A_{id}	0.203	m^2
Y_{id}	1.617	m
J_{id}	0.225	m^4
$W_{low,\ steel}$	0.139	m^3
$W_{up,\ steel}$	-0.255	m^3

$W_{low,\ slab}$	-0.3479	m^3
$W_{up,\ slab}$	-0.2736	m^3

4.3.3.2 Stresses

Stresses calculated will be compared to $\sigma_{all} = \frac{420}{1.05} = 400\ MPa$ for steel and to $f_{cd} = \frac{0.85*35}{1.5} = 19.83\ MPa$ for compressed parts; $f_{ctd} = \frac{0.15*35}{1.5} = 3.5\ MPa$ for parts in tension. We have considered the following phases.

a) Phase 1

This phase characterises short-term loading.

(i) Section 1

Table 4.21 resumes computed stress values at bridge start.

All stresses in concrete and steel are below the limit fixed previously. Section 1 is subjected to bending; the top is compressed and bottom is in tension.

Table 4.21. Stress verification at section 1

	Actions from model FEM			ULS		Design actions			Stresses			
Loads	N [kN]	M[kN/m]	T [kN]	Combination	Factor	N [kN]	M [kN/m]	T [kN]	σup,slab [Mpa]	σlow,slab [Mpa]	σup,steel [Mpa]	σlow,steel [Mpa]
g1	1069,22	789,14	2,85	**I**	1,35	1443,45	1065,34	3,85	0,32	0,47	2,91	12,56
Temperature (+)	2237,23	-2205,68	-57,47		0,90	2013,51	-1985,11	-51,72	2,24	1,96	12,07	-5,92
Wind Y	1207,02	2259,15	-188,29		0,90	1086,32	2033,24	-169,46	-0,39	-0,11	-0,66	17,77
Traffic (distributed)	1457,02	6340,73	492,55		1,35	1966,98	8559,99	664,94	-3,23	-2,02	-12,46	65,14
Traffic (tandem)	343,24	2396,45	92,39		1,35	463,37	3235,21	124,73	-1,39	-0,93	-5,75	23,58
g2	532,05	300,51	100,17		1,35	718,27	405,69	135,23	0,22	0,28	1,73	5,41
					Total	**7691,89**	**13314,34**	**707,56**	**-2,23**	**-0,35**	**-2,15**	**118,54**
	Actions from model FEM			**ULS**		**Design actions**			**Stresses**			
Loads	N [kN]	M[kN/m]	T [kN]	Combination	Factor	N [kN]	M [kN/m]	T [kN]	σup,slab [Mpa]	σlow,slab [Mpa]	σup,steel [Mpa]	σlow,steel [Mpa]
g1	1069,22	789,14	2,85	**II**	1,35	1443,45	1065,34	3,85	0,32	0,47	2,91	12,56
Temperature (+)	2237,23	-2205,68	-57,47		1,50	3355,85	-3308,52	-86,21	3,73	3,26	20,12	-9,87
Wind Y	1207,02	2259,15	-188,29		0,90	1086,32	2033,24	-169,46	-0,39	-0,11	-0,66	17,77
Traffic (distributed)	1457,02	6340,73	492,55		0,54	786,79	3423,99	265,98	-1,29	-0,81	-4,98	26,05
Traffic (tandem)	343,24	2396,45	92,39		1,01	347,53	2426,41	93,54	-1,04	-0,70	-4,31	17,68
g2	532,05	300,51	100,17		1,35	718,27	405,69	135,23	0,22	0,28	1,73	5,41
					Total	**7738,20**	**6046,14**	**242,93**	**1,55**	**2,40**	**14,81**	**69,61**
	Actions from model FEM			**ULS**		**Design actions**			**Stresses**			
Loads	N [kN]	M[kN/m]	T [kN]	Combination	Factor	N [kN]	M [kN/m]	T [kN]	σup,slab [Mpa]	σlow,slab [Mpa]	σup,steel [Mpa]	σlow,steel [Mpa]

g1	1069,22	789,14	2,85	**III**	1,35	1443,45	1065,34	3,85	0,32	0,47	2,91	12,56
Temperature (+)	2237,23	-2205,68	-57,47		0,90	2013,51	-1985,11	-51,72	2,24	1,96	12,07	-5,92
Wind Y	1207,02	2259,15	-188,29		1,50	1810,53	3388,73	-282,44	-0,66	-0,18	-1,09	29,62
Traffic (distributed)	1457,02	6340,73	492,55		0,54	786,79	3423,99	265,98	-1,29	-0,81	-4,98	26,05
Traffic (tandem)	343,24	2396,45	92,39		1,01	347,53	2426,41	93,54	-1,04	-0,70	-4,31	17,68
g2	532,05	300,51	100,17		1,35	718,27	405,69	135,23	0,22	0,28	1,73	5,41
					Total	**7120,07**	**8725,04**	**164,44**	**-0,21**	**1,03**	**6,32**	**85,41**
	Actions from model FEM			**ULS**		**Design actions**			**Stresses**			
Loads	N [kN]	M[kN/m]	T [kN]	Combination	Factor	N [kN]	M [kN/m]	T [kN]	σup,slab [Mpa]	σlow,slab [Mpa]	σup,steel [Mpa]	σlow,steel [Mpa]
g1	1069,22	789,14	2,85	**IV**	1,35	1443,45	1065,34	3,85	0,32	0,47	2,91	12,56
Temperature (-)	-2237,23	2205,68	57,47		0,90	-2013,5	1985,11	51,72	-2,24	-1,96	-12,07	5,92
Wind Y	1207,02	2259,15	-188,29		0,90	1086,32	2033,24	-169,5	-0,39	-0,11	-0,66	17,77
Traffic (distributed)	1457,02	6340,73	492,55		1,35	1966,98	8559,99	664,94	-3,23	-2,02	-12,46	65,14
Traffic (tandem)	343,24	2396,45	92,39		1,35	463,37	3235,21	124,73	-1,39	-0,93	-5,75	23,58
g2	532,05	300,51	100,17		1,35	718,27	405,69	135,23	0,22	0,28	1,73	5,41
					Total	**3664,88**	**17284,57**	**811,01**	**-6,71**	**-4,27**	**-26,29**	**130,38**
	Actions from model FEM			**ULS**		**Design actions**			**Stresses**			
Loads	N [kN]	M[kN/m]	T [kN]	Combination	Factor	N [kN]	M [kN/m]	T [kN]	σup,slab [Mpa]	σlow,slab [Mpa]	σup,steel [Mpa]	σlow,steel [Mpa]
g1	1069,22	789,14	2,85	**V**	1,35	1443,45	1065,34	3,85	0,32	0,47	2,91	12,56
Temperature (-)	-2237,23	2205,68	57,47		1,50	-3355,8	3308,52	86,21	-3,73	-3,26	-20,12	9,87
Wind Y	1207,02	2259,15	-188,29		0,90	1086,32	2033,24	-169,46	-0,39	-0,11	-0,66	17,77

Traffic (distributed)	1457,02	6340,73	492,55		0,54	786,79	3423,99	265,98	-1,29	-0,81	-4,98	26,05
Traffic (tandem)	343,24	2396,45	92,39		1,01	347,53	2426,41	93,54	-1,04	-0,70	-4,31	17,68
g2	532,05	300,51	100,17		1,35	718,27	405,69	135,23	0,22	0,28	1,73	5,41
					Total	**1026,51**	**12663,18**	**415,34**	**-5,91**	**-4,13**	**-25,43**	**89,36**
	Actions from model FEM			**ULS**		**Design actions**			**Stresses**			
Loads	N [kN]	M[kN/m]	T [kN]	Combination	Factor	N [kN]	M [kN/m]	T [kN]	σup,slab [Mpa]	σlow,slab [Mpa]	σup,steel [Mpa]	σlow,steel [Mpa]
g1	1069,22	789,14	2,85		1,35	1443,45	1065,34	3,85	0,32	0,47	2,91	12,56
Temperature (-)	-2237,23	2205,68	57,47		0,90	-2013,5	1985,11	51,72	-2,24	-1,96	-12,07	5,92
Wind Y	1207,02	2259,15	-188,29	**VI**	1,50	1810,53	3388,73	-282,44	-0,66	-0,18	-1,09	29,62
Traffic (distributed)	1457,02	6340,73	492,55		0,54	786,79	3423,99	265,98	-1,29	-0,81	-4,98	26,05
Traffic (tandem)	343,24	2396,45	92,39		1,01	347,53	2426,41	93,54	-1,04	-0,70	-4,31	17,68
g2	532,05	300,51	100,17		1,35	718,27	405,69	135,23	0,22	0,28	1,73	5,41
					Total	**3093,06**	**12695,26**	**267,89**	**-4,68**	**-2,89**	**-17,82**	**97,26**

(ii) Section 2

Table 4.22 resumes computed stress values at pylons. All the stresses are lower than design strength for concrete and steel. They are also negative from top of slab to bottom of girder, it means that the section is totally compressed. We will verify buckling resistance in the following section.

Table 4.22. Stress verification at section 2

	Actions from model FEM			ULS	Design actions				Stresses			
Loads	N [kN]	M[kN/m]	T [kN]	combination	factor	N [kN]	M [kN/m]	T [kN]	σup,slab [Mpa]	σlow,slab [Mpa]	σup,steel [Mpa]	σlow,steel [Mpa]
g1	-8714,0	1864,45	-383,6	**I**	1,35	-11763,91	2517,01	-517,89	-8,40	-8,04	-49,55	-26,74
Temperature (+)	2551,10	209,25	-16,78		0,90	2295,99	188,33	-15,10	1,29	1,31	8,10	9,81
Wind Y	-2926,7	-701,91	38,65		0,90	-2634,04	-631,72	34,79	-1,26	-1,35	-8,34	-14,06
Traffic (distributed)	224,62	1995,48	116,07		1,35	303,24	2693,90	156,69	-1,21	-0,83	-5,09	19,32
Traffic (tandem)	74,88	1501,69	34,40		1,35	101,09	2027,28	46,44	-0,99	-0,70	-4,31	14,07
g2	-4171,6	847,30	-106,4		1,35	-5631,70	1143,86	-143,60	-3,99	-3,83	-23,58	-13,21
					Total	**-17329,34**	**7938,65**	**-438,67**	**-14,55**	**-13,43**	**-82,77**	**-10,81**
	Actions from model FEM			**ULS**	**Design actions**				**Stresses**			
Loads	N [kN]	M[kN/m]	T [kN]	combination	factor	N [kN]	M[kN/m]	T [kN]	σup,slab [Mpa]	σlow,slab [Mpa]	σup,steel [Mpa]	σlow,steel [Mpa]
g1	-8714,0	1864,45	-383,6	**II**	1,35	-11763,91	2517,01	-517,89	-8,40	-8,04	-49,55	-26,74
Temperature (+)	2551,10	209,25	-16,78		1,50	3826,65	313,88	-25,17	2,15	2,19	13,50	16,35
Wind Y	-2926,7	-701,91	38,65		0,90	-2634,04	-631,72	34,79	-1,26	-1,35	-8,34	-14,06
Traffic (distributed)	224,62	1995,48	116,07		0,54	121,29	1077,56	62,68	-0,48	-0,33	-2,04	7,73
Traffic (tandem)	74,88	1501,69	34,40		1,01	75,82	1520,46	34,83	-0,74	-0,52	-3,23	10,55
g2	-4171,6	847,30	-106,4		1,35	-5631,70	1143,86	-143,60	-3,99	-3,83	-23,58	-13,21
					Total	**-16005,89**	**5941,04**	**-554,36**	**-12,72**	**-11,88**	**-73,24**	**-19,38**
	Actions from model FEM			**ULS**	**Design actions**				**Stresses**			
Loads	N [kN]	M[kN/m]	T [kN]	combination	factor	N [kN]	M[kN/m]	T [kN]	σup,slab [Mpa]	σlow,slab [Mpa]	σup,steel [Mpa]	σlow,steel [Mpa]

g1	-8714,0	1864,45	-383,6	**III**	1,35	-11763,91	2517,01	-517,89	-8,40	-8,04	-49,55	-26,74
Temperature (+)	2551,10	209,25	-16,78		0,90	2295,99	188,33	-15,10	1,29	1,31	8,10	9,81
Wind Y	-2926,7	-701,91	38,65		1,50	-4390,07	-1052,87	57,98	-2,11	-2,25	-13,89	-23,44
Traffic (distributed)	224,62	1995,48	116,07		0,54	121,29	1077,56	62,68	-0,48	-0,33	-2,04	7,73
Traffic (tandem)	74,88	1501,69	34,40		1,01	75,82	1520,46	34,83	-0,74	-0,52	-3,23	10,55
g2	-4171,6	847,30	-106,4		1,35	-5631,70	1143,86	-143,60	-3,99	-3,83	-23,58	-13,21
					Total	**-19292,58**	**5394,34**	**-521,11**	**-14,42**	**-13,66**	**-84,19**	**-35,30**
	Actions from model FEM			**ULS**	**Design actions**				**Stresses**			
Loads	N [kN]	M[kN/m]	T [kN]	combination	factor	N [kN]	M[kN/m]	T [kN]	σup,slab [Mpa]	σlow,slab [Mpa]	σup,steel [Mpa]	σlow,steel [Mpa]
g1	-8714,0	1864,45	-383,6	**IV**	1,35	-11763,91	2517,01	-517,89	-8,40	-8,04	-49,55	-26,74
Temperature (-)	-2551,1	-209,25	16,78		0,90	-2295,99	-188,33	15,10	-1,29	-1,31	-8,10	-9,81
Wind Y	-2926,7	-701,91	38,65		0,90	-2634,04	-631,72	34,79	-1,26	-1,35	-8,34	-14,06
Traffic (distributed)	224,62	1995,48	116,07		1,35	303,24	2693,90	156,69	-1,21	-0,83	-5,09	19,32
Traffic (tandem)	74,88	1501,69	34,40		1,35	101,09	2027,28	46,44	-0,99	-0,70	-4,31	14,07
g2	-4171,6	847,30	-106,4		1,35	-5631,70	1143,86	-143,60	-3,99	-3,83	-23,58	-13,21
					Total	**-21921,32**	**7562,00**	**-408,47**	**-17,13**	**-16,06**	**-98,97**	**-30,43**
	Actions from model FEM			**ULS**	**Design actions**				**Stresses**			
Loads	N [kN]	M[kN/m]	T [kN]	combination	factor	N [kN]	M[kN/m]	T [kN]	σup,slab [Mpa]	σlow,slab [Mpa]	σup,steel [Mpa]	σlow,steel [Mpa]
g1	-8714,0	1864,45	-383,6	**V**	1,35	-11763,91	2517,01	-517,89	-8,40	-8,04	-49,55	-26,74
Temperature (-)	-2551,1	-209,25	16,78		1,50	-3826,65	-313,88	25,17	-2,15	-2,19	-13,50	-16,35
Wind Y	-2926,7	-701,91	38,65		0,90	-2634,04	-631,72	34,79	-1,26	-1,35	-8,34	-14,06
Traffic (distributed)	224,62	1995,48	116,07		0,54	121,29	1077,56	62,68	-0,48	-0,33	-2,04	7,73

Traffic (tandem)	74,88	1501,69	34,40		1,01	75,82	1520,46	34,83	-0,74	-0,52	-3,23	10,55
g2	-4171,6	847,30	-106,4		1,35	-5631,70	1143,86	-143,60	-3,99	-3,83	-23,58	-13,21
					Total	**-23659,19**	**5313,29**	**-504,02**	**-17,02**	**-16,27**	**-100,24**	**-52,08**
	Actions from model FEM			**ULS**	**Design actions**				**Stresses**			
Loads	N [kN]	M[kN/m]	T [kN]	combination	factor	N [kN]	M[kN/m]	T [kN]	σup,slab [Mpa]	σlow,slab [Mpa]	σup,steel [Mpa]	σlow,steel [Mpa]
g1	-8714,0	1864,45	-383,6	**VI**	1,35	-11763,91	2517,01	-517,89	-8,40	-8,04	-49,55	-26,74
Temperature (-)	-2551,1	-209,25	16,78		0,90	-2295,99	-188,33	15,10	-1,29	-1,31	-8,10	-9,81
Wind Y	-2926,7	-701,91	38,65		1,50	-4390,07	-1052,87	57,98	-2,11	-2,25	-13,89	-23,44
Traffic (distributed)	224,62	1995,48	116,07		0,54	121,29	1077,56	62,68	-0,48	-0,33	-2,04	7,73
Traffic (tandem)	74,88	1501,69	34,40		1,01	75,82	1520,46	34,83	-0,74	-0,52	-3,23	10,55
g2	-4171,6	847,30	-106,4		1,35	-5631,70	1143,86	-143,60	-3,99	-3,83	-23,58	-13,21
					Total	**-23884,56**	**5017,69**	**-490,90**	**-17,00**	**-16,29**	**-100,40**	**-54,92**

(iii) Section 3

Stress do not reach the limit; we have a section partially subjected to compression and tight at bottom.

Table 4.23. Stress verification at section 3

	Actions from model FEM			**ULS**		**Design actions**			**Stresses**			
Loads	N [kN]	M[kN/m]	T [kN]	Combination	Factor	N [kN]	M [kN/m]	T [kN]	σup,slab [Mpa]	σlow,slab [Mpa]	σup,steel [Mpa]	σlow,steel [Mpa]
g1	3460,45	5120,09	181,87	**I**	1,35	4671,61	6912,12	245,52	-0,75	0,23	1,41	64,06
Temperature (+)	2623,40	-454,76	3,95		0,90	2361,06	-409,28	3,56	1,64	1,58	9,72	6,01
Wind Y	-4215,87	1746,92	0,83		0,90	-3794,28	1572,23	0,75	-3,10	-2,88	-17,74	-3,49

Traffic (distributed)	1950,41	3738,76	583,44		1,35	2633,05	5047,33	787,64	-1,02	-0,30	-1,87	43,89
Traffic (tandem)	255,05	1995,73	143,09		1,35	344,32	2694,24	193,17	-1,18	-0,80	-4,94	19,48
g2	1621,52	2005,84	118,42		1,35	2189,05	2707,88	159,87	-0,08	0,31	1,89	26,43
					Total	**8404,81**	**18524,51**	**1390,51**	**-4,49**	**-1,87**	**-11,53**	**156,38**
	Actions from model FEM			**ULS**		**Design actions**			**Stresses**			
Loads	N [kN]	M[kN/m]	T [kN]	Combination	Factor	N [kN]	M [kN/m]	T [kN]	σup,slab [Mpa]	σlow,slab [Mpa]	σup,steel [Mpa]	σlow,steel [Mpa]
g1	3460,45	5120,09	181,87	**II**	1,35	4671,61	6912,12	245,52	-0,75	0,23	1,41	64,06
Temperature (+)	2623,40	-454,76	3,95		1,50	3935,10	-682,14	5,93	2,73	2,63	16,21	10,02
Wind Y	-4215,87	1746,92	0,83		0,90	-3794,28	1572,23	0,75	-3,10	-2,88	-17,74	-3,49
Traffic (distributed)	1950,41	3738,76	583,44		0,54	1053,22	2018,93	315,06	-0,41	-0,12	-0,75	17,55
Traffic (tandem)	255,05	1995,73	143,09		1,01	258,24	2020,68	144,88	-0,89	-0,60	-3,71	14,61
g2	1621,52	2005,84	118,42		1,35	2189,05	2707,88	159,87	-0,08	0,31	1,89	26,43
					Total	**8312,94**	**14549,70**	**872,00**	**-2,49**	**-0,44**	**-2,69**	**129,19**
	Actions from model FEM			**ULS**		**Design actions**			**Stresses**			
Loads	N [kN]	M[kN/m]	T [kN]	Combination	Factor	N [kN]	M [kN/m]	T [kN]	σup,slab [Mpa]	σlow,slab [Mpa]	σup,steel [Mpa]	σlow,steel [Mpa]
g1	3460,45	5120,09	181,87	**III**	1,35	4671,61	6912,12	245,52	-0,75	0,23	1,41	64,06
Temperature (+)	2623,40	-454,76	3,95		0,90	2361,06	-409,28	3,56	1,64	1,58	9,72	6,01
Wind Y	-4215,87	1746,92	0,83		1,50	-6323,81	2620,38	1,25	-5,17	-4,80	-29,57	-5,81
Traffic (distributed)	1950,41	3738,76	583,44		0,54	1053,22	2018,93	315,06	-0,41	-0,12	-0,75	17,55
Traffic (tandem)	255,05	1995,73	143,09		1,01	258,24	2020,68	144,88	-0,89	-0,60	-3,71	14,61
g2	1621,52	2005,84	118,42		1,35	2189,05	2707,88	159,87	-0,08	0,31	1,89	26,43
					Total	**4209,37**	**15870,71**	**870,13**	**-5,65**	**-3,41**	**-21,00**	**122,86**

	Actions from model FEM			**ULS**		**Design actions**			**Stresses**			
Loads	N [kN]	M[kN/m]	T [kN]	Combination	Factor	N [kN]	M [kN/m]	T [kN]	σup,slab [Mpa]	σlow,slab [Mpa]	σup,steel [Mpa]	σlow,steel [Mpa]
g1	3460,45	5120,09	181,87	**IV**	1,35	4671,61	6912,12	245,52	-0,75	0,23	1,41	64,06
Temperature (-)	-2623,40	454,76	-3,95		0,90	-2361,06	409,28	-3,56	-1,64	-1,58	-9,72	-6,01
Wind Y	-4215,87	1746,92	0,83		0,90	-3794,28	1572,23	0,75	-3,10	-2,88	-17,74	-3,49
Traffic (distributed)	1950,41	3738,76	583,44		1,35	2633,05	5047,33	787,64	-1,02	-0,30	-1,87	43,89
Traffic (tandem)	255,05	1995,73	143,09		1,35	344,32	2694,24	193,17	-1,18	-0,80	-4,94	19,48
g2	1621,52	2005,84	118,42		1,35	2189,05	2707,88	159,87	-0,08	0,31	1,89	26,43
					Total	**3682,69**	**19343,08**	**1383,40**	**-7,76**	**-5,03**	**-30,98**	**144,36**
	Actions from model FEM			**ULS**		**Design actions**			**Stresses**			
Loads	N [kN]	M[kN/m]	T [kN]	Combination	Factor	N [kN]	M [kN/m]	T [kN]	σup,slab [Mpa]	σlow,slab [Mpa]	σup,steel [Mpa]	σlow,steel [Mpa]
g1	3460,45	5120,09	181,87	**V**	1,35	4671,61	6912,12	245,52	-0,75	0,23	1,41	64,06
Temperature (-)	-2623,40	454,76	-3,95		1,50	-3935,10	682,14	-5,93	-2,73	-2,63	-16,21	-10,02
Wind Y	-4215,87	1746,92	0,83		0,90	-3794,28	1572,23	0,75	-3,10	-2,88	-17,74	-3,49
Traffic (distributed)	1950,41	3738,76	583,44		0,54	1053,22	2018,93	315,06	-0,41	-0,12	-0,75	17,55
Traffic (tandem)	255,05	1995,73	143,09		1,01	258,24	2020,68	144,88	-0,89	-0,60	-3,71	14,61
g2	1621,52	2005,84	118,42		1,35	2189,05	2707,88	159,87	-0,08	0,31	1,89	26,43
					Total	**442,74**	**15913,98**	**860,15**	**-7,94**	**-5,70**	**-35,11**	**109,14**
	Actions from model FEM			**ULS**		**Design actions**			**Stresses**			
Loads	N [kN]	M[kN/m]	T [kN]	Combination	Factor	N [kN]	M [kN/m]	T [kN]	σup,slab [Mpa]	σlow,slab [Mpa]	σup,steel [Mpa]	σlow,steel [Mpa]
g1	3460,45	5120,09	181,87	**VI**	1,35	4671,61	6912,12	245,52	-0,75	0,23	1,41	64,06

Temperature (-)	-2623,40	454,76	-3,95		0,90	-2361,06	409,28	-3,56	-1,64	-1,58	-9,72	-6,01
Wind Y	-4215,87	1746,92	0,83		1,50	-6323,81	2620,38	1,25	-5,17	-4,80	-29,57	-5,81
Traffic (distributed)	1950,41	3738,76	583,44		0,54	1053,22	2018,93	315,06	-0,41	-0,12	-0,75	17,55
Traffic (tandem)	255,05	1995,73	143,09		1,01	258,24	2020,68	144,88	-0,89	-0,60	-3,71	14,61
g2	1621,52	2005,84	118,42		1,35	2189,05	2707,88	159,87	-0,08	0,31	1,89	26,43
					Total	**-512,75**	**16689,28**	**863,02**	**-8,92**	**-6,56**	**-40,45**	**110,83**

b) Phase 2

Including shrinkage in stress calculation is considering long term effects on elements. We have the following stresses:

(i) Section 1

Beam and slab stresses under different load combination in table 4.24 are lower than maximum allowable stress for steel and concrete

Table 4.24. Stress at section 1 (phase 2)

	Actions from model FEM		**SLU**		**Design actions**		**Stresses**			
Loads	N [kN]	M[kN/m]	Combination	Factor	N [kN]	M [kN/m]	σup,slab [Mpa]	σlow,slab [Mpa]	σup,steel [Mpa]	σlow,steel [Mpa]
g1	1069,22	789,14	**I**	1,35	1443,45	1065,34	0,13	0,22	2,94	14,75
Temperature (+)	2219,23	-2150,66		0,90	1997,31	-1935,59	1,43	1,28	17,41	-4,05
Wind Y	1207,02	2259,15		0,90	1086,32	2033,24	-0,35	-0,19	-2,61	19,93
Traffic (distributed)	1457,02	6340,73		1,35	1966,98	8559,99	-2,42	-1,75	-23,82	71,09

Traffic (tandem)	343,24	2396,45		1,35	463,37	3235,21	-1,02	-0,76	-10,38	25,49
Shrinkage	-3372,90	2266,59		1,20	-4047,48	2719,91	-2,46	-2,25	-30,58	-0,42
g2	532,05	300,51		1,35	718,27	405,69	0,11	0,14	1,95	6,45
				Total	**3628,21**	**16083,77**	**-4,57**	**-3,31**	**-45,09**	**133,24**
	Actions from model FEM		**SLU**		**Design actions**		**Stresses**			
Loads	N [kN]	M[kN/m]	Combination	Factor	N [kN]	M [kN/m]	σup,slab [Mpa]	σlow,slab [Mpa]	σup,steel [Mpa]	σlow,steel [Mpa]
g1	1069,22	789,14	**IV**	1,35	1443,45	1065,34	0,13	0,22	2,94	14,75
Temperature (-)	-2219,23	2150,66		0,90	-1997,31	1935,59	-1,43	-1,28	-17,41	4,05
Wind Y	1207,02	2259,15		0,90	1086,32	2033,24	-0,35	-0,19	-2,61	19,93
Traffic (distributed)	1457,02	6340,73		1,35	1966,98	8559,99	-2,42	-1,75	-23,82	71,09
Traffic (tandem)	343,24	2396,45		1,35	463,37	3235,21	-1,02	-0,76	-10,38	25,49
Shrinkage	-3372,90	2266,59		1,20	-4047,48	2719,91	-2,46	-2,25	-30,58	-0,42
g2	532,05	300,51		1,35	718,27	405,69	0,11	0,14	1,95	6,45
				Total	**-366,40**	**19954,96**	**-7,43**	**-5,87**	**-79,92**	**141,34**

(ii) Section 2

Beam and slab stresses under different load combination in table 4.25 are lower than maximum allowable stress for steel and concrete

Table 4.25. Stress at section 2 (phase 2)

	Actions from model FEM		**SLU**		**Design actions**		**Stresses**			
Loads	N [kN]	M[kN/m]	Combination	Factor	N [kN]	M [kN/m]	σup,slab [Mpa]	σlow,slab [Mpa]	σup,steel [Mpa]	σlow,steel [Mpa]
g1	3460,45	5120,09	**II**	1,35	4671,61	6912,12	-0,84	-0,30	-4,05	72,59
Temperature (+)	2623,61	-540,57		1,50	3935,42	-810,86	1,72	1,66	22,56	13,57
Wind Y	-4215,87	1746,92		0,90	-3794,28	1572,23	-1,95	-1,82	-24,84	-7,41
Traffic (distributed)	1950,41	3738,76		0,54	1053,22	2018,93	-0,36	-0,20	-2,72	19,67
Traffic (tandem)	255,05	1995,73		1,01	258,24	2020,68	-0,65	-0,49	-6,64	15,77
Shrinkage	-3372,90	-312,99		1,20	-4047,48	-375,59	-1,33	-1,36	-18,46	-22,63
g2	1621,52	2005,84		1,35	2189,05	2707,88	-0,20	0,01	0,18	30,21
				Total	**4265,77**	**14045,40**	**-3,59**	**-2,49**	**-33,97**	**121,76**
	Actions from model FEM		**SLU**		**Design actions**		**Stresses**			
Loads	N [kN]	M[kN/m]	Combination	Factor	N [kN]	M [kN/m]	σup,slab [Mpa]	σlow,slab [Mpa]	σup,steel [Mpa]	σlow,steel [Mpa]
g1	3460,45	5120,09	**IV**	1,35	4671,61	6912,12	-0,84	-0,30	-4,05	72,59
Temperature (-)	-2623,61	540,57		0,90	-2361,25	486,51	-1,03	-0,99	-13,53	-8,14
Wind Y	-4215,87	1746,92		0,90	-3794,28	1572,23	-1,95	-1,82	-24,84	-7,41

Traffic (distributed)	1950,41	3738,76		1,35	2633,05	5047,33	-0,89	-0,50	-6,79	49,17
Traffic (tandem)	255,05	1995,73		1,35	344,32	2694,24	-0,86	-0,65	-8,85	21,02
Shrinkage	-3372,90	-312,99		1,20	-4047,48	-375,59	-1,33	-1,36	-18,46	-22,63
g2	1621,52	2005,84		1,35	2189,05	2707,88	-0,20	0,01	0,18	30,21
				Total	**-364,98**	**19044,72**	**-7,09**	**-5,61**	**-76,35**	**134,81**

(iii) Section 3

Beam and slab stresses under different load combination in table 4.26 are lower than maximum allowable stress for steel and concrete.

Table 4.26. Stress at section 3 (phase 2)

	Actions from model FEM		**SLU**		**Design actions**		**Stresses**			
Loads	N [kN]	M[kN/m]	Combination	Factor	N [kN]	M [kN/m]	σup,slab [Mpa]	σlow,slab [Mpa]	σup,steel [Mpa]	σlow,steel [Mpa]
g1	3460,45	5120,09	**II**	1,35	4671,61	6912,12	-0,84	-0,30	-4,05	72,59
Temperature (+)	2623,61	-540,57		1,50	3935,42	-810,86	1,72	1,66	22,56	13,57
Wind Y	-4215,87	1746,92		0,90	-3794,28	1572,23	-1,95	-1,82	-24,84	-7,41
Traffic (distributed)	1950,41	3738,76		0,54	1053,22	2018,93	-0,36	-0,20	-2,72	19,67
Traffic (tandem)	255,05	1995,73		1,01	258,24	2020,68	-0,65	-0,49	-6,64	15,77

Shrinkage	-3372,90	-312,99		1,20	-4047,48	-375,59	-1,33	-1,36	-18,46	-22,63
g2	1621,52	2005,84		1,35	2189,05	2707,88	-0,20	0,01	0,18	30,21
				Total	**4265,77**	**14045,40**	**-3,59**	**-2,49**	**-33,97**	**121,76**
	Actions from model FEM		**SLU**		**Design actions**		**Stresses**			
Loads	N [kN]	M[kN/m]	Combination	Factor	N [kN]	M [kN/m]	σup,slab [Mpa]	σlow,slab [Mpa]	σup,steel [Mpa]	σlow,steel [Mpa]
g1	3460,45	5120,09	**IV**	1,35	4671,61	6912,12	-0,84	-0,30	-4,05	72,59
Temperature (-)	-2623,61	540,57		0,90	-2361,25	486,51	-1,03	-0,99	-13,53	-8,14
Wind Y	-4215,87	1746,92		0,90	-3794,28	1572,23	-1,95	-1,82	-24,84	-7,41
Traffic (distributed)	1950,41	3738,76		1,35	2633,05	5047,33	-0,89	-0,50	-6,79	49,17
Traffic (tandem)	255,05	1995,73		1,35	344,32	2694,24	-0,86	-0,65	-8,85	21,02
Shrinkage	-3372,90	-312,99		1,20	-4047,48	-375,59	-1,33	-1,36	-18,46	-22,63
g2	1621,52	2005,84		1,35	2189,05	2707,88	-0,20	0,01	0,18	30,21
				Total	**-364,98**	**19044,72**	**-7,09**	**-5,61**	**-76,35**	**134,81**

4.3.3.3 Verifications of girder

a) Classification of section

Classes of different parts of main beam are presented in tables 4.27 and 4.28. It concerns web classification and next table is for flanges.

Table 4.27. Web classification

Web classification	Sections 1 and 3
c [mm]	2420
t [mm]	40
c/t	60.5
ε	0.75
82ε	61.5
⟶Class 2	
Web classification	**Section 2**
c [mm]	2420
t [mm]	40
c/t	60.5
ε	0,75
42ε	31,5
⟶Class 4	

Table 4.28. Flanges classification

Flange classification	Sections 1,2,3
c [mm]	950
t [mm]	40
c/t	23,75
ε	0,75
33ε	24,75
⟶Class 1	

b) Shear verifications

The maximum shear found in previous load combinations is at section 3 with a value of 1390.5 kN.

The verification of shear has been done in three steps. Table 4.9 presents it.

Table 4.29. Verification of shear resistance

Shear force	$V_{Ed} = 1390.5\ kN$
Plastic resistance	$V_{Ed} < V_{pl,Rd} = 30492\ kN$
Buckling resistance	$V_{Ed} < V_{b,Rd} = 30492\ kN$
Interaction between shear and moment	$V_{Ed} < \frac{V_{b,Rd}}{2} = 15246\ kN$

According to table 4.29, we can conclude resistance of girders to shear. We neglected area of holes in computing effective area because the shear resistance is too great.

c) Shear connectors design

This section summarises the design of studs in order to assume a good transmission of stresses between slab and main beam. Design is shown in table 4.30.

$$P_{Rd} = min\begin{cases} P_{Rd1} = 109.48\ kN \\ P_{Rd2} = 122.63\ kN \end{cases} = 109.48\ kN$$

Table 4.30. Studs design

Stud design resistance	$\overline{P_{Rd}} = 48.66\ kN$
Static moment	$S = 0.0911\ m^3$
Inertia moment	$J_{id} = 0.276\ m^4$
Shear stress per meter	$\tau\_b = 458.97\ kN/m$
Number of studs per meter	$n_s = 10\ studs/m$

For more security, 15 studs/m will be used.

d) Buckling verification at section 2

Looking at the results of stresses at ULS, we can testify that section 2 at bridge tower is compressed. We have to check its buckling resistance.

Table 4.31. Buckling resistance of section 2

Axial force	$N_{Ed} = 23884.56\ kN$
Slenderness	$\bar{\lambda} = 0.28$
Reduction factor	$\chi = 0.98$

Buckling resistance	$N_{b,Rd} = 121265.2\ kN$

$N_{Ed} < N_{b,Rd}$ thus, buckling resistance of section 2 is verified.

e) Pylon verification

This section concerns different verifications done on pylon sections which are classifications and buckling resistance.

(i) Classification and stress calculation

Classification of pylon cross sections is shown in table 4.32.

Table 4.32. Pylon sections classification

	Pylon	Base pylon
c [mm]	2720	3120
t [mm]	40	40
c/t	68	78
42ε	34.02	34.02

The conclusion is that pylon sections are from class 4.

The stresses calculation is presented below in table 4.33.

Table 4.33. Stresses in pylon sections

	A [m2]	W_{low} [m3]	W_{up} [m3]	N [kN]	M [kN/m]	σ_{low} [Mpa]	σ_{up} [Mpa]
Pylon	0.442	0.401	- 0.401	-44783.59	-47442.68	-219.855	17.031
Base pylon	0.506	0.526	-0.526	-47085.4	-64457.72	-215.673	29.417

All the stresses are lower than f_{yd}=338.1 MPa

(ii) Buckling resistance

For buckling of pylon, we have:

- Pylon buckling resistance is presented in table 4.34.

Table 4.34. Buckling resistance of pylon

Axial force	$N_{Ed} = 44783.59kN$
Slenderness	$\bar{\lambda} = 1.41$

Reduction factor	$\chi = 0.4$
Buckling resistance	$N_{b,Rd} = 59721.84\ kN$

- Base pylon buckling resistance is presented in table 4.35.

Table 4.35. Buckling resistance base pylon

Axial force	$N_{Ed} = 47085.4\ kN$
Slenderness	$\bar{\lambda} = 0.63$
Reduction factor	$\chi = 0.84$
Buckling resistance	$N_{b,Rd} = 143592.42\ kN$

For both sections of pylons $N_{Ed} < N_{b,Rd}$, thus buckling resistance is verified.

4.3.4 Serviceability Limit State

Focus will be on slab and cables verifications.

4.3.4.1 Slab

We have to check stress, cracking and deflection of slab.

a) Stress verification

The Eurocode 2 recommends to limit the stress in the concrete and the reinforcement steel to a certain value to mitigate the apparition of cracks. These values are:

$$\sigma_{c,lim} = 0.6 f_{ck} = 21\ MPa$$
$$\sigma_{s,lim} = 0.8 f_{yk} = 400\ \ MPa$$

When using frequent combination, we obtain:

Table 4.36. Stress verification for slab

Neutral axis	$y = 61.43\ mm$
Inertia moment	$J = 9.88 * 10^8 mm^4$
Moment at SLS	$M = 206.58\ kN.m$
Stress in concrete	$\sigma_c = 12.84\ MPa$
Stress in steel	$\sigma_s = 165.6\ Mpa$

According to table 4.36, stresses are lower than the limit values presented above for both steel reinforcement and concrete.

b) Cracking control

For cracking, we considered quasi-permanent load combination. Cracking control figures in table 4.37.

Table 4.37. Cracking control in slab

Neutral axis	$y = 83.23\ mm$
Inertia moment	$J = 1.74 * 10^9 mm^4$
Moment at SLS	$M = 179.67\ kN.m$
Stress in steel	$\sigma_s = 150.16\ Mpa$

The maximum crack width allowed for exposure classes used in this project is $w_{max} = 0.3\ mm$.

The maximum bar size is $\phi = 20\ mm$. When we check table, we compute that the limit of stress in reinforcement bar is 192 MPa. It is greater than σ_s previously calculated. Cracking is controlled.

c) Deflection

The limit of a span deflection is span/250. Table 4.38 shows us deflection computation.

Table 4.38. Deflection verification

Factor K	1.2
Reference reinforcement ratio	$\rho_0 = 0.59\%$
Bottom reinforcement ratio	$\rho = 0.65\% > \rho_0$
Top reinforcement ratio	$\rho' = 0.60\%$
Deflection	$l/d = 1270\ mm \rightarrow d = 193.31\ mm$

The limit for main span long of 245.5 m is 982 mm. The deflection is checked.

According to results presented above, we can conclude that our slab fulfills the serviceability limit state requirements.

4.3.4.2 Cables

Looking at figure 4.13, we can see that the maximum stress under quasi-permanent condition is 231.13 MPa. $\sigma_{all} = 796.5\ MPa$

The requirement for cables is satisfied.

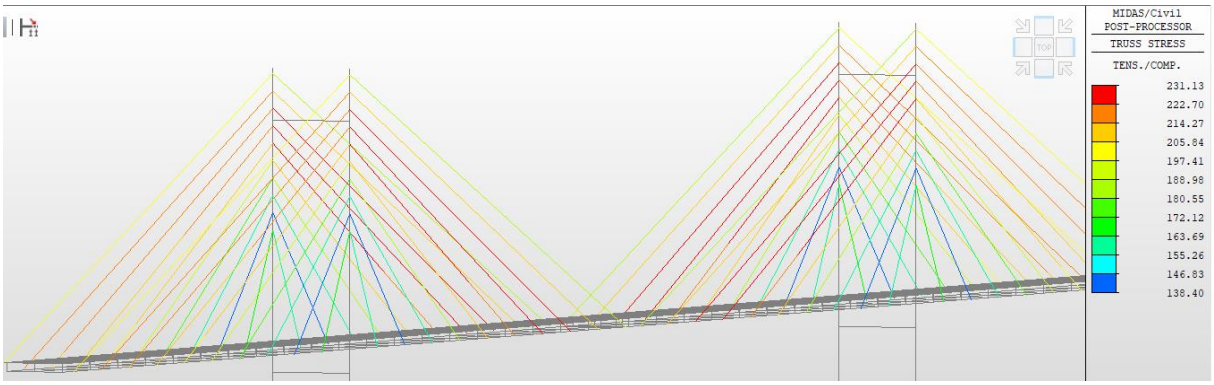

Figure 4.13. Stresses in cables

4.4 Dynamic analysis

This analysis was performed with the software SAP2000. We proceed to a nonlinear modal time-history analysis.

4.4.1 Blast functions

Blast load will be applied as distributed load at the considered position. We have blast loads for 3 stand-off distances: $R = \{1,2,3\}\ m$.

Blast wave parameters for each mass with varied stand-off distances are summarised in table 4.39.

Table 4.39. Blast parameters

Charge weight [kg]	Standoff distance [m]	Scaled distance [m/kg1/3]	Time of arrival [ms]	Peak over-pressure [kPa]	Impulse [kPa-ms]
250	1	0.16	0.158	261450.4	100200.8
	2	0.32	0.44	88182.5	30314,0
	3	0.48	1.01	43286.7	16053.3
500	1	0.15	0.152	354273	194439
	2	0.25	0.390	129088	56001
	3	0.38	0.794	65507.1	28896.6

4.4.2 Parametric study

A parametric study will be carried out on our model considering different blast load scenarios with varying charge weights, positions of blast occurrance and standoff distances.

4.4.2.1 Study cases

Tables 4.40 and 4.41 present the different study cases that will be run for nonlinear time-history analysis.

Table 4.40. Study cases varying positions and masses

Blast location	Case study	Charge weight [kg]	Standoff [m]
Start of the bridge at x=6 m	Case 1	250	1
	Case 2	500	1
Tower at x=120 m	Case 3	250	1
	Case 4	500	1
Middle of the bridge at x= 242.75 m	Case 5	250	1
	Case 6	500	1

Table 4.41. Study cases varying stand-off distances

Blast location	Case study	Charge weight [kg]	Standoff [m]
Start of the bridge at x=6 m	Case 7	250	2
	Case 8	250	3

4.4.2.2 Results of the parametric study

The results obtained for all the blast scenarios of our parametric study are discussed in this section.

a) Variation of weight and blast location

For these purposes, the standoff distance has been fixed to 1 m. The following results are obtained.

(i) Blast at start of the bridge

The results of displacement of girders in x and y directions for both masses will be compared. After we will display stress in cables at peak time of each mass. Contour of stresses will be presented at same time.

- Displacement in x direction

The maximum joint displacement is observed at x=184.7 m. Figure 4.14 shows that, as the charge weight of the blast is increased considering the same standoff distance, the displacements increase.

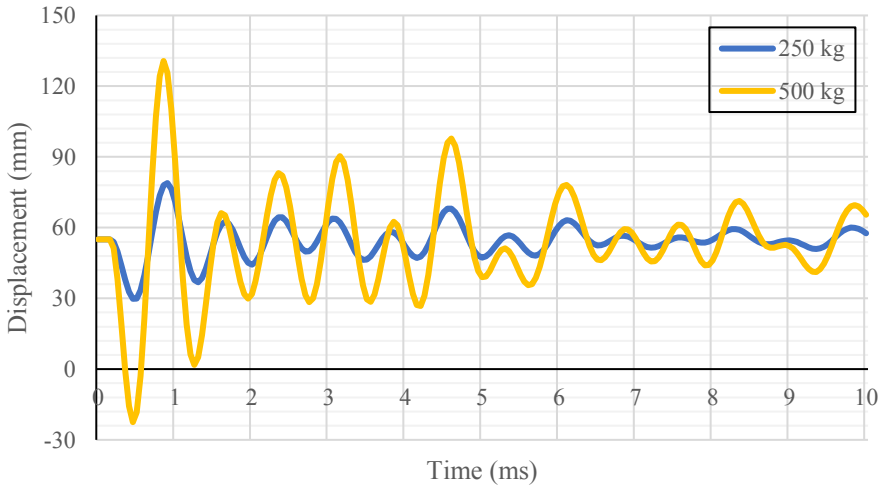

Figure 4.14. Displacement in x direction for blast at x=6m

Global displacement of bridge in x direction for each mass of TNT is presented in figures 4.15 and 4.16 Cable joints with pylon are the most potential to high displacement. It goes up to 840 mm for cables around blast location.

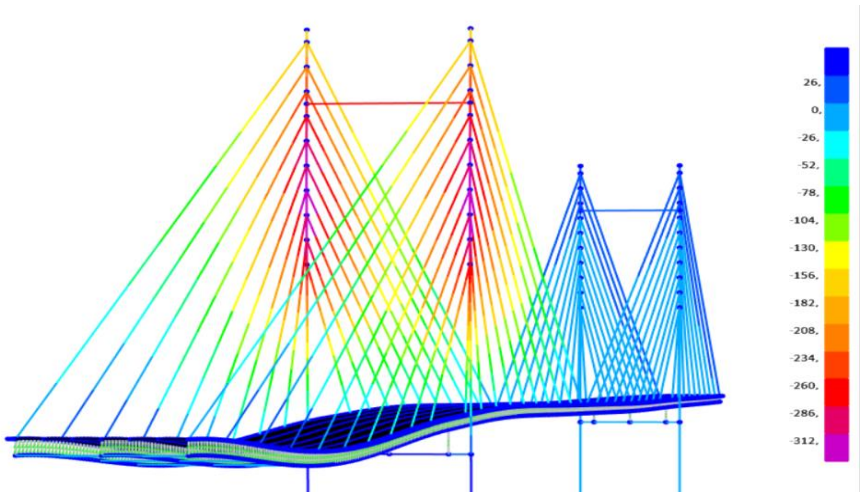

Figure 4.15. Bridge displacement in x direction at t=0.55 ms for 250 kg

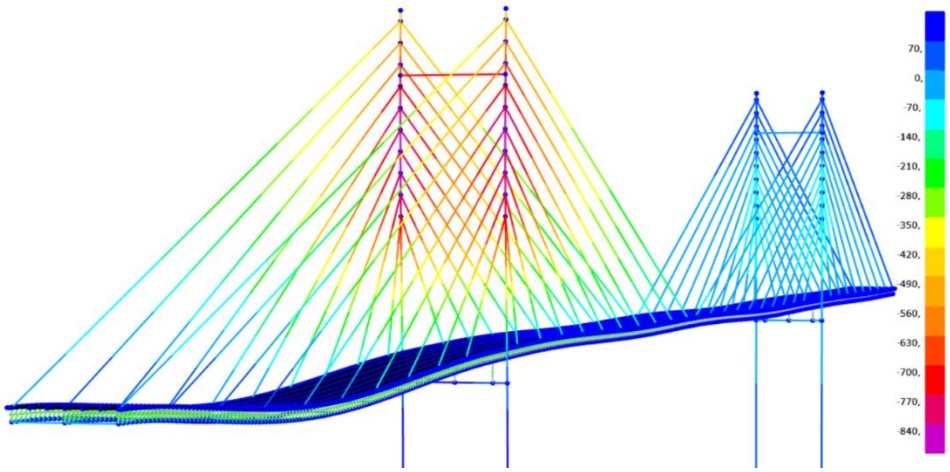

Figure 4.16. Bridge displacement in x direction at t=0.45 ms for 500 kg

- Displacement in z direction

The higher displacement occurs at x=55m. Figure 4.17 shows that the amount of displacement in the direction of blast loading (z direction) grows at an increasing rate.

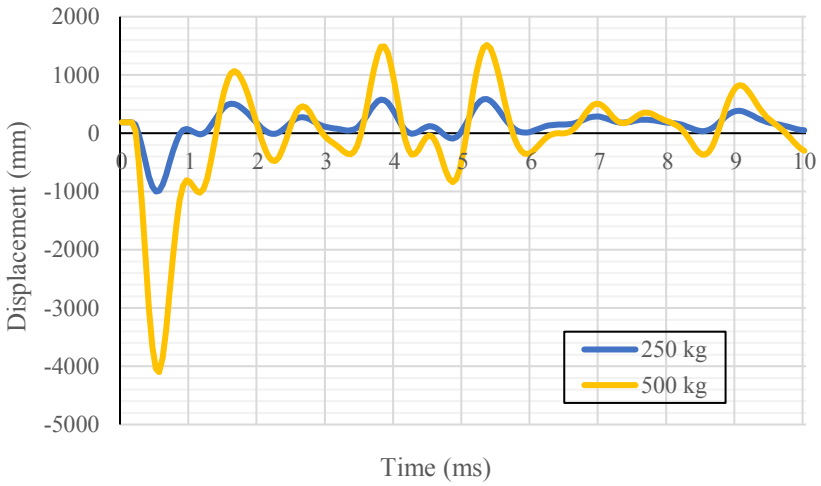

Figure 4.17. Displacement in z direction for blast at x=6m

Figures 4.18 and 4.19 below illustrate how the bridge moves in z direction under blast load for both masses.

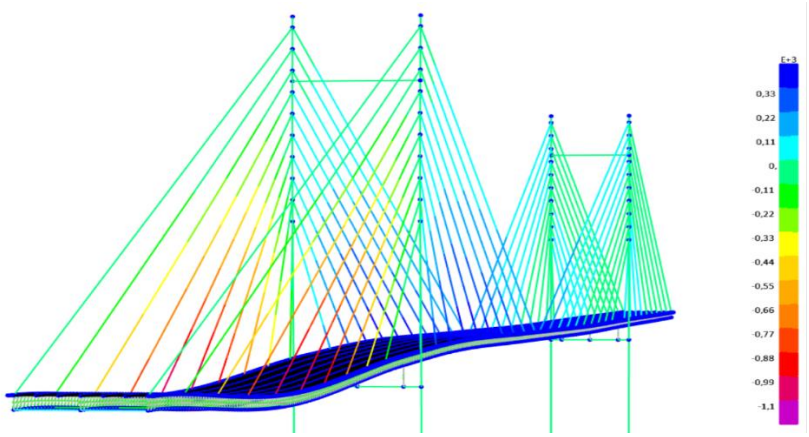

Figure 4.18. Bridge displacement in z direction at t=0.55 ms for 250 kg

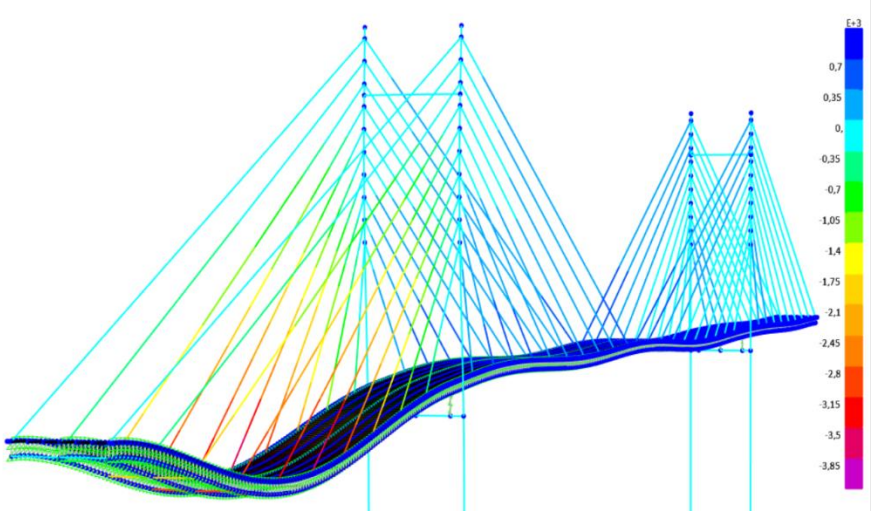

Figure 4.19. Bridge displacement in z direction at t=0.45 ms for 500 kg

The maximum displacements occur near middle of side span at x=55m.

- Strain in x direction

Strain in girder (main span) varies with time as describes in figure 4.20. The maximum strain is 0.6% for 500 kg of TNT at t = 0.85 ms; compared to failure strain $\varepsilon_{ud} = 4.5\%$, it is below the limit.

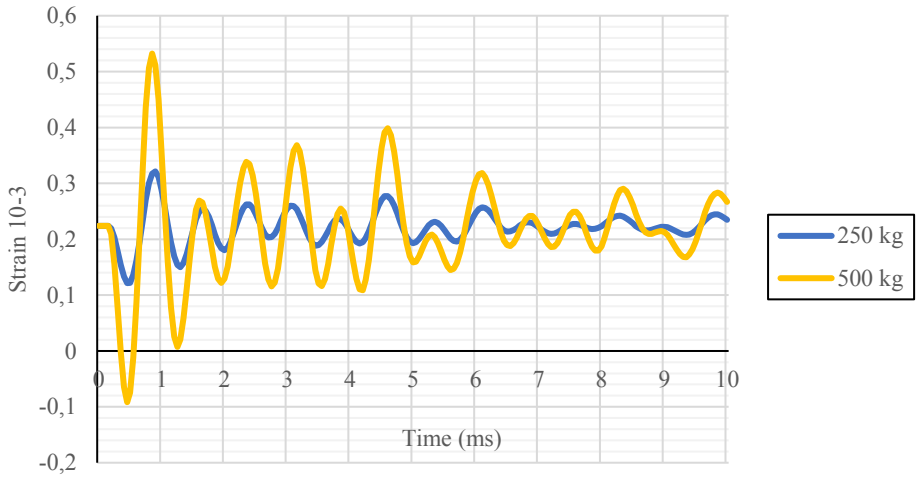

Figure 4.20. Strain variation in time

- Stress in girders

The structural component subjected to the blast loading reaches quickly the allowable stresses just after detonation. For cases 1 and 2, all the equivalent weights of TNT considered succeed in creating stress reaching the stress limit at a very short time step (Figure 4.21)

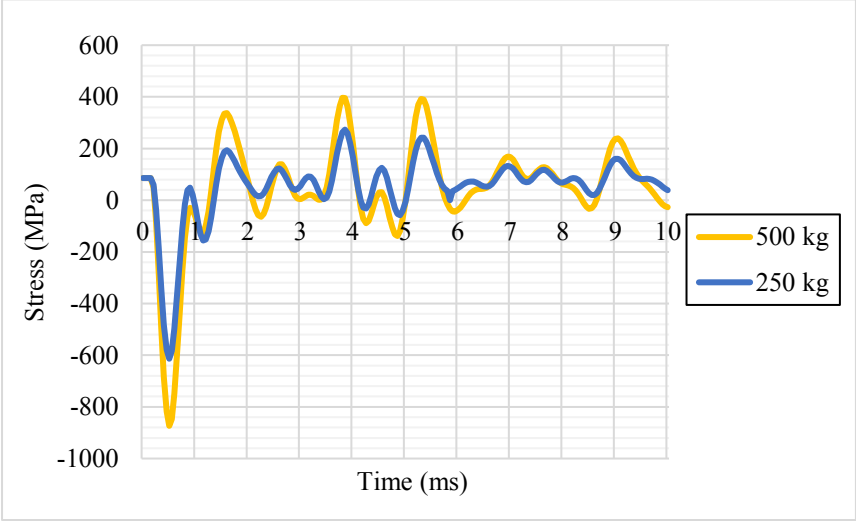

Figure 4.21. Girder stress variation

- Stress in cables

Cables considered are the first twentieth cables from at bridge start to bridge middle. Figure 4.22 displays stress in cables for both masses. For explosive weight of 250 kg, four cables have crossed the allowable stress of 796.5 MPa. Concerning 500 kg of TNT, six cable stresses remain under stress limit.

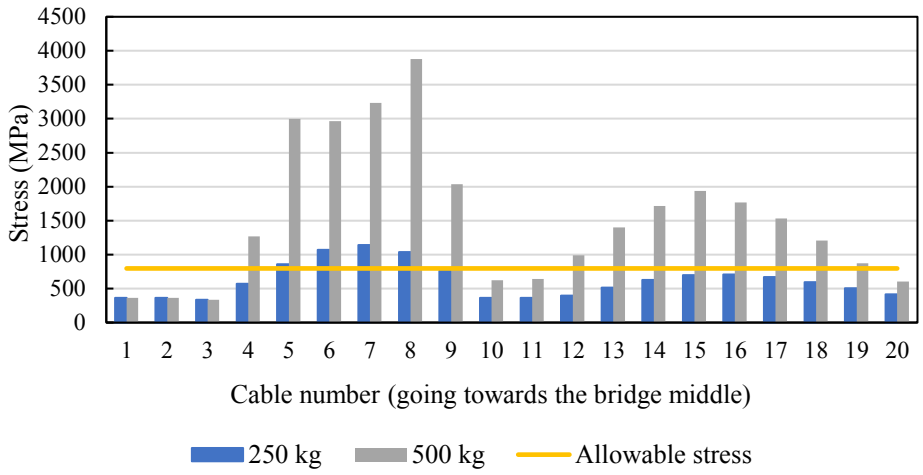

Figure 4.22. Cable stress for blast at x = 6 m

- Strain in cables

Because displacements of symmetric cables are similar, we display only first part of cables strains. Figure 4.23 shows that short cables have reached the strain limit of 2.7%. They will be considered failed for progressive collapse prediction and will be removed.

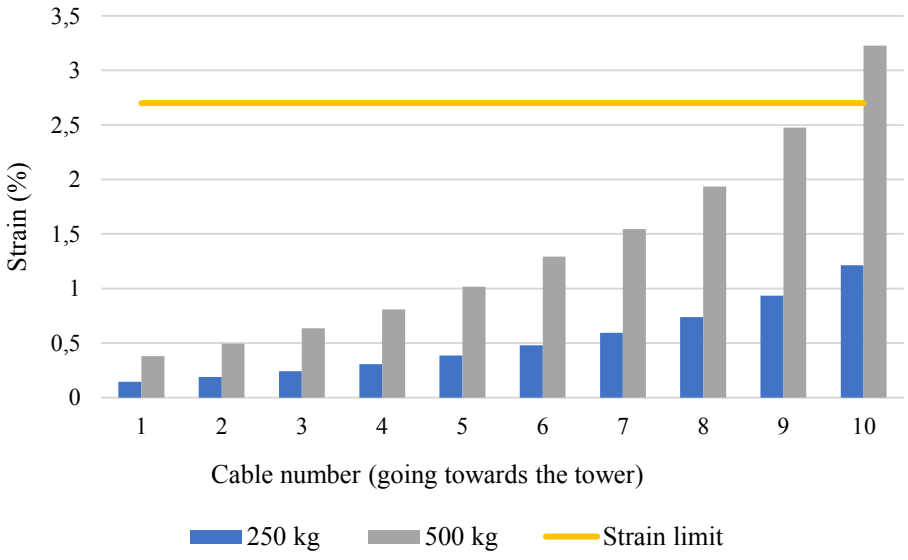

Figure 4.23. Cable strain for blast at x = 6 m

- Blast analysis case 1

Figure 4.24 presents the contour of stresses in slab. We observe that parts of the slab near the explosion location (until x= 13 m) have exceeded the concrete yield strength.

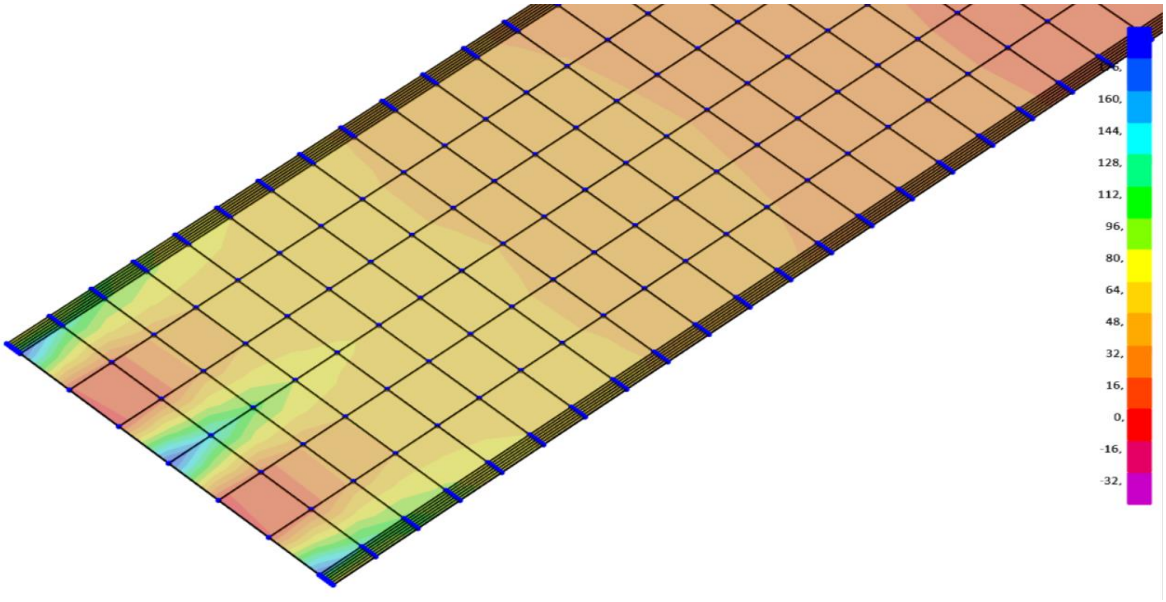

Figure 4.24. Stress contour in slab

Figure 4.25 presents the contour of stresses in girders. Main beams and cross beams have gone beyond stress limit at bridge start until x=14m.

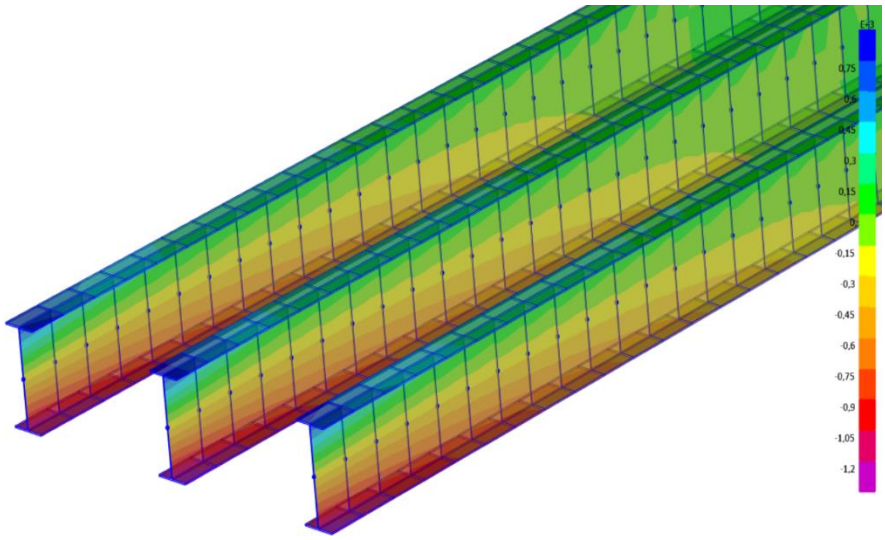

Figure 4.25. Stress contour in girders

- Blast analysis case 2

Stresses in slab (Figure 4.26) exceeded the allowable stress everywhere from the bridge start to x=93m.

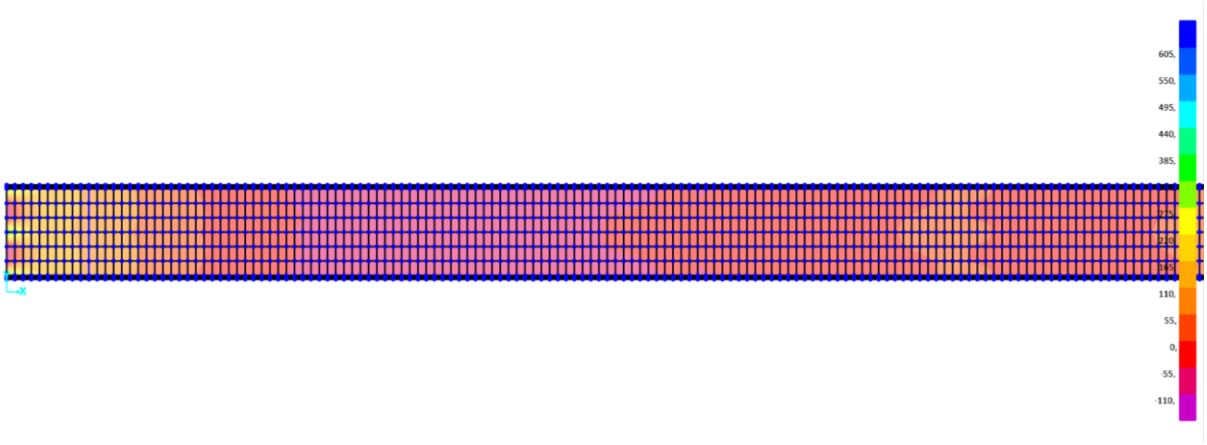

Figure 4.26. Stress contour in slab

For girders (Figure 4.27), we have half of the bridge that exceeded the design yield limit f_{yd}.

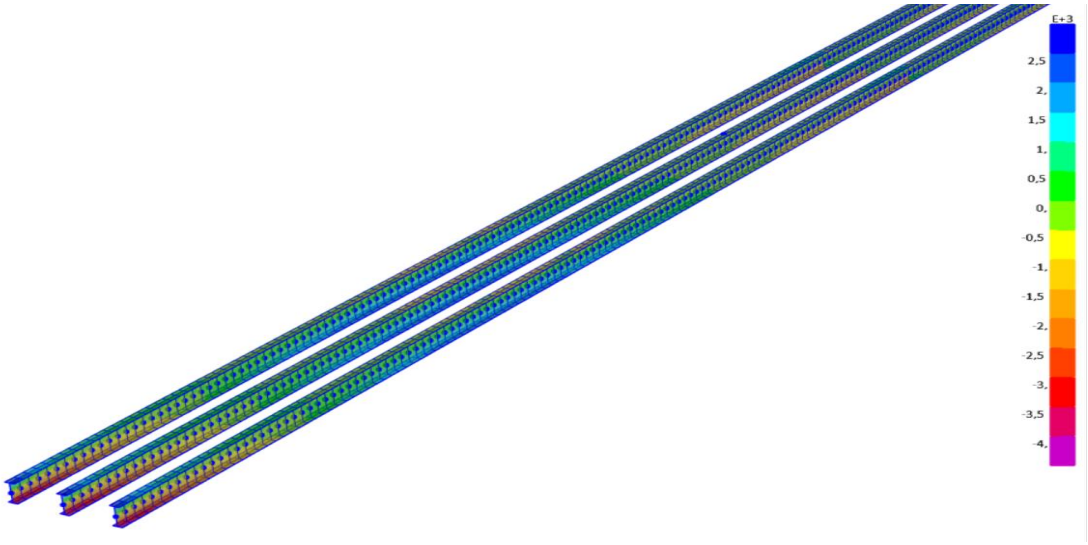

Figure 4.27. Girder stress contour

(ii) Blast at bridge tower

The results of displacement in x, y directions for both masses will be presented. After we will display stress in cables at peak time of the corresponding mass.

- Displacement in x direction

For cases 3 and 4, it is observed that the maximum displacement is 110mm at mid-span (Figure 4.28). Displacement due to blast can be neglected because, the total move is principally due to permanent and live loads; at t = 0 ms displacement is 100 mm.

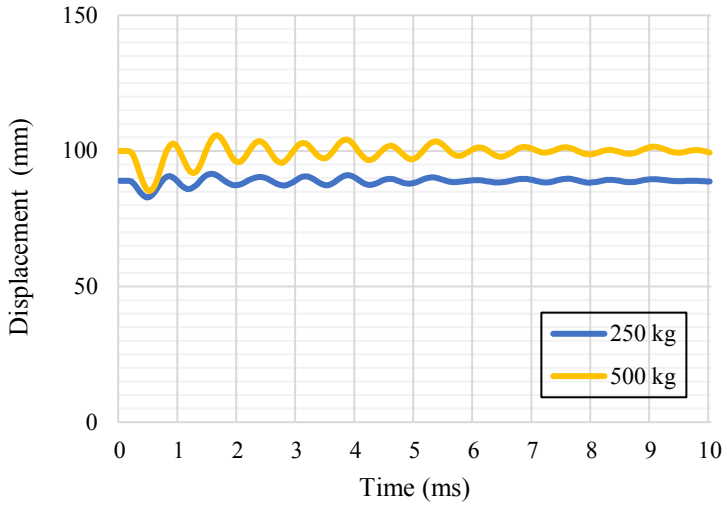

Figure 4.28. Displacement in x direction for blast at x=120m

- Displacement in z direction

Blast effect on displacements in z direction (Figure 4.29) is negligeable as previously seen in x direction. The maximum is 513,5 mm which comes from permanent and live loads; at t = 0 ms, displacement is 320 mm.

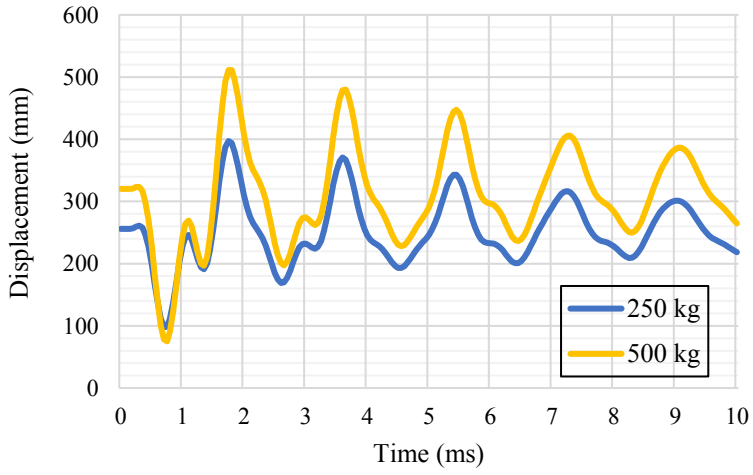

Figure 4.29. Displacement in z direction for blast at x=120m

- Strain in x direction

Having a small displacement induces very low strain. It can be observed in Figure 4.30.

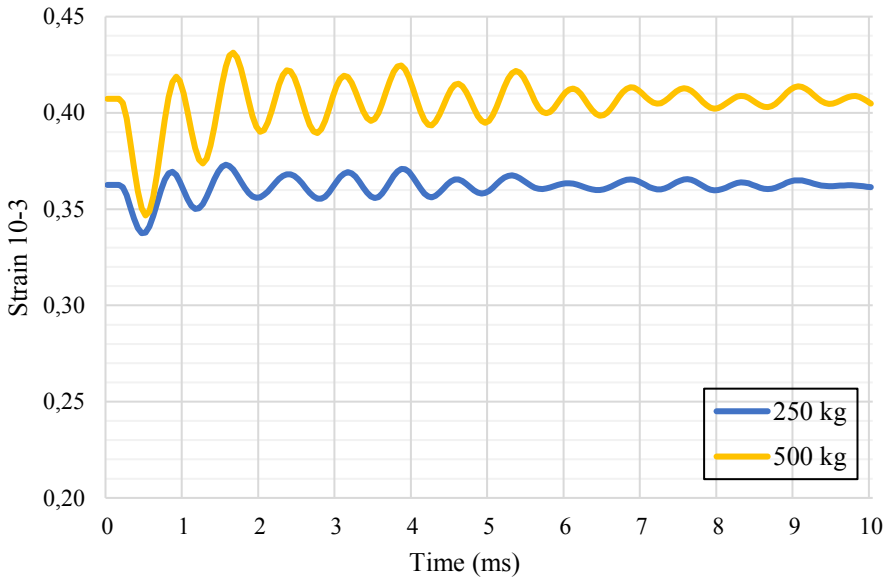

Figure 4.30. Strain variation for blast at x=120m

- Stresses in girder

For blast occurring at tower, stresses in girder (Figure 4.31) are lower than yield limit of steel for both masses. We have a maximum of 387.46 Mpa at t = 0.85 ms for 500 kg of TNT.

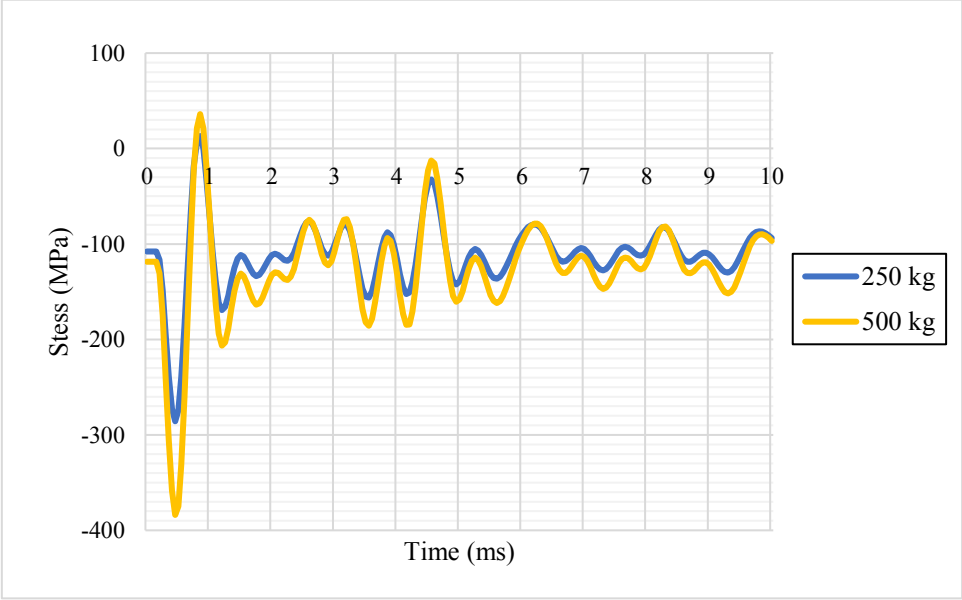

Figure 4.31. Stresses in girder for blast at x=120m

It can be explained by the fact that blast occur supports, thus the solicitations are directly transferred to supports. The structure resists better.

- Stress in cables

For both TNT masses, stress cable stay remains in the good range, below 796.5 MPa.

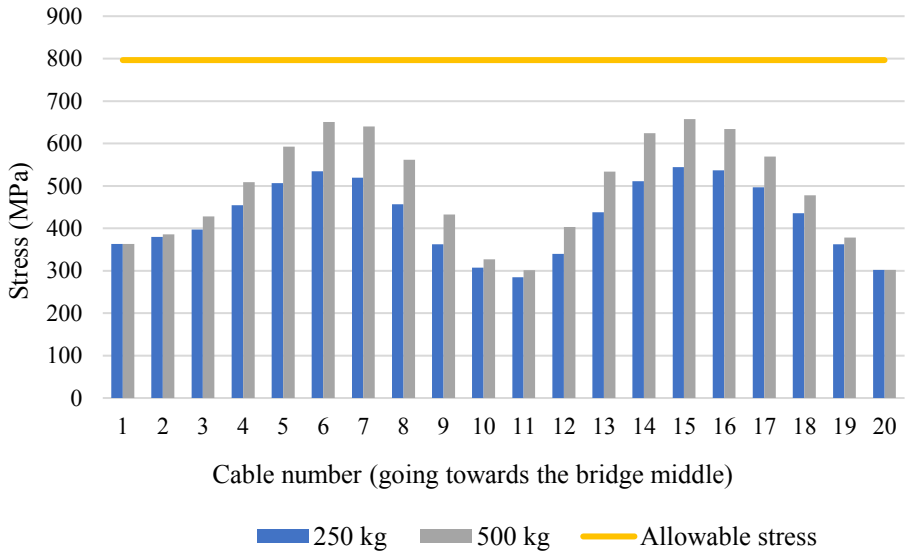

Figure 4.32. Cable stress for blast at x = 120 m

- Blast analysis case 3

All the slab resists to blast load; we can look at figure 4.33 and tell that the concrete yield strength is not reached.

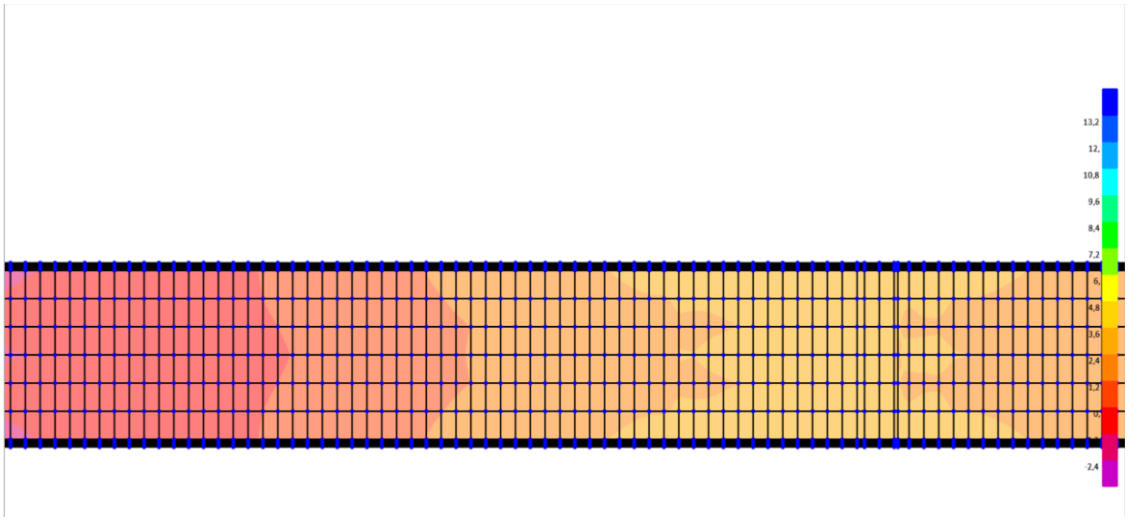

Figure 4.33. Stresses in slab for 250 kg at x=120m

Stresses in girders shown in figure 4.34 are under stress limit.

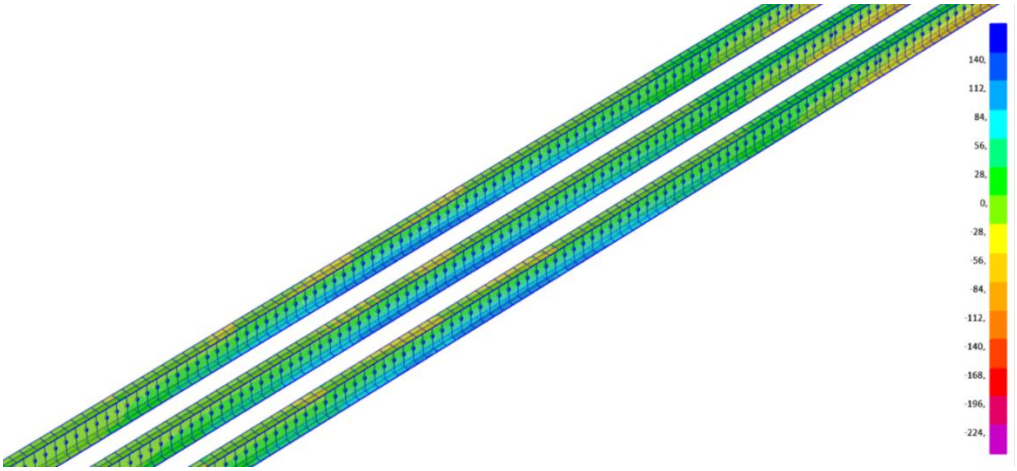

Figure 4.34. Stresses in girder for 250 kg at x=120m

- Blast analysis case 4

Below we have stress contour in slab. The start of bridge is the most improved part of slab.

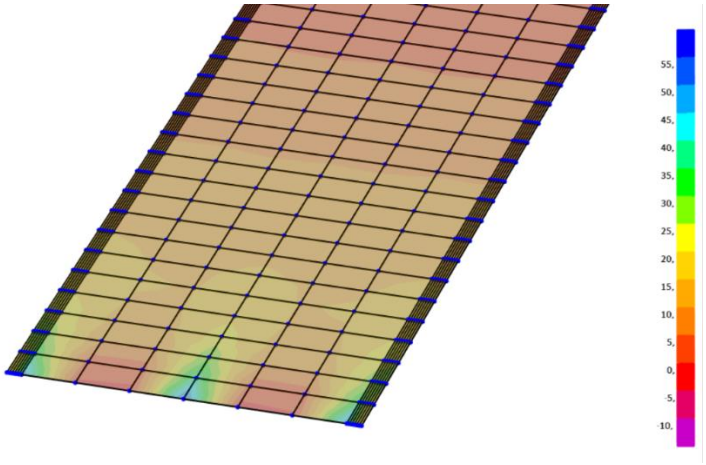

Figure 4.35. Stresses in slab for 500 kg at x=120m

In figure 4.36 the yield strength for S420 material is not reached for stresses in girders.

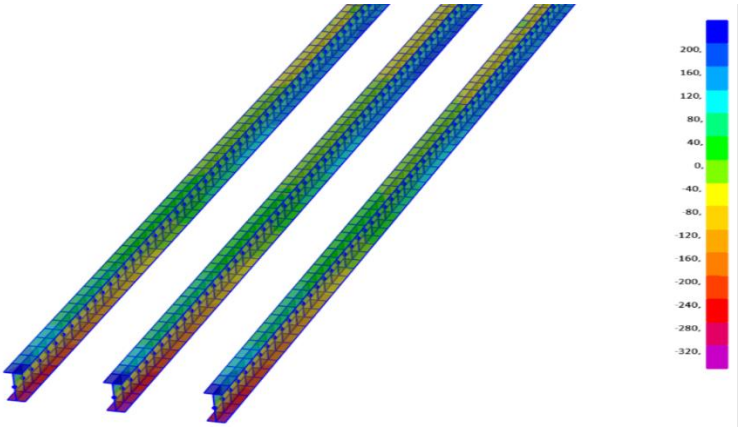

Figure 4.36. Stresses in girders for 500 kg at x=120m

(iii) Blast at mid-span

- Displacement Ux

The maximum displacement found is -682.36 mm at t=0.85 ms.

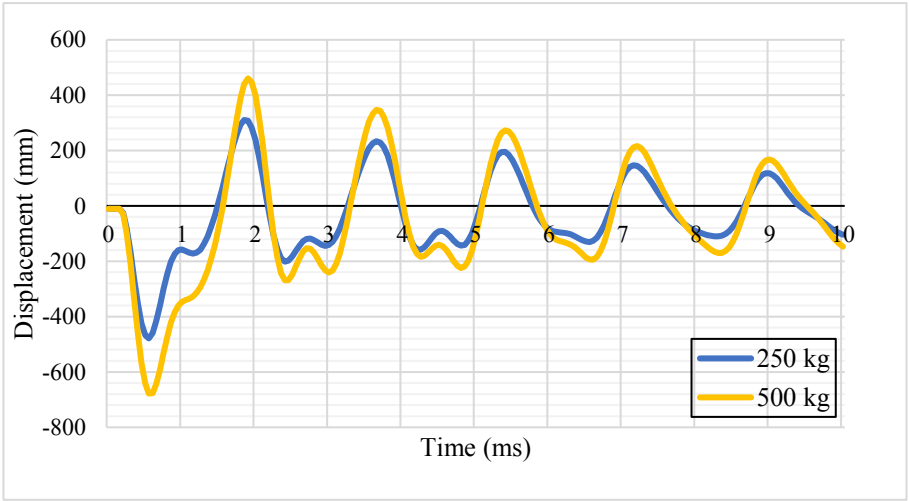

Figure 4.37. Displacement in x direction for blast at x=242.75m

- Strain in girders

The plastic limit is still far from the allowable one in figure 4.38. The section is at mid-span; it is true that it undergoes high stresses but it will not fail because it has not crossed the strain limit.

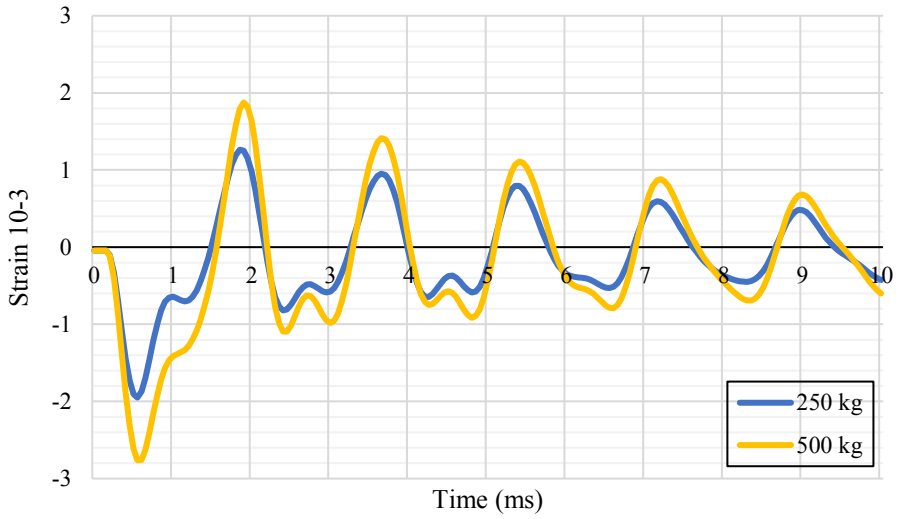

Figure 4.38. Strain variation for blast at x=242.75m

The global displacement of bridge in x direction is displayed in figure 4.39.

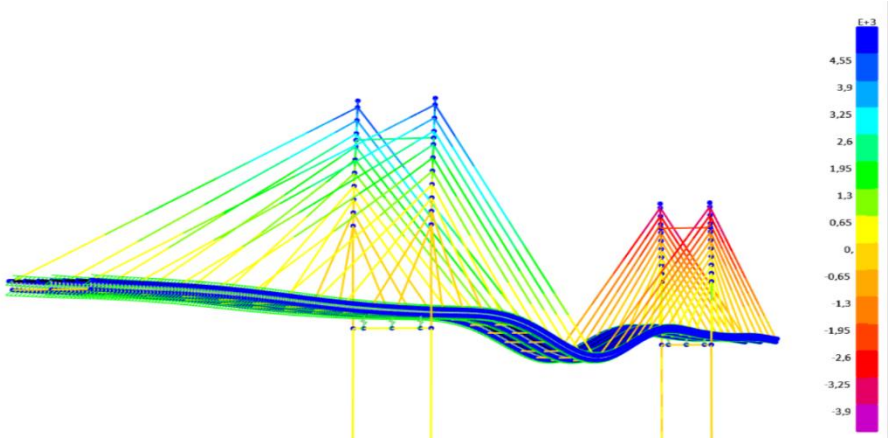

Figure 4.39. Bridge displacement in x direction for blast at x=242.75m

- Stress in cables

We have chosen to show cable stresses for 250 kg of TNT. We can see in figure 4.40 that cables near the blast location experienced the greatest stresses. They can undergo rupture because of high stresses.

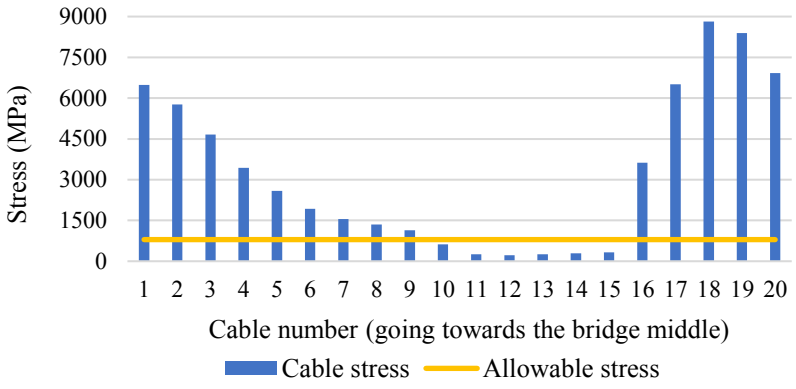

Figure 4.40. Stresses in cables for 250 kg at x=242.75 m

- Strain in cables

Here cables have similar behaviour at right and left sides of the bridge. Cables represented in figure 4.41 are on the left side. The number of cables failed varies with masses. When explosive weight is 250 kg, stress in the eight longest cables have beyond the limit. For 500 kg, first cables around tower remain in good range.

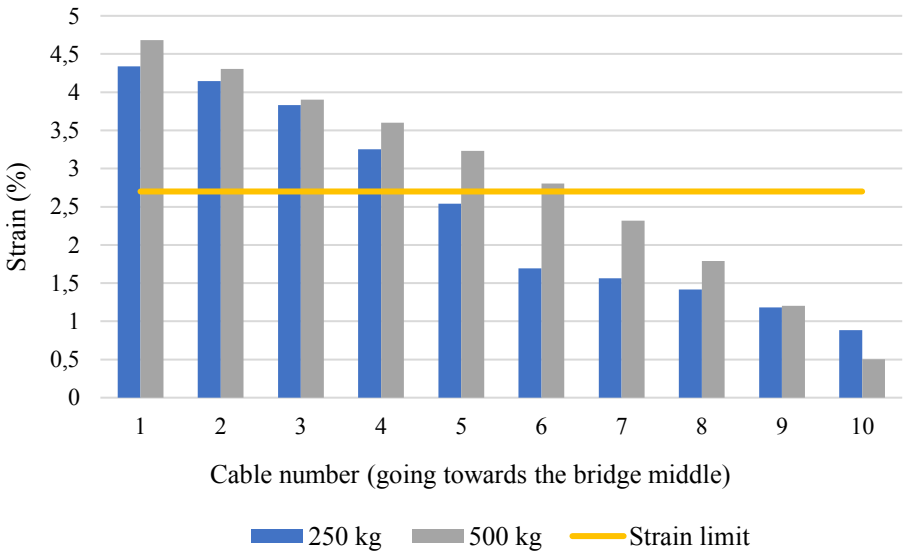

Figure 4.41. Cable strain for blast at x = 242.75 m

b) Variation of stand-off distance

The considered position is at x= 6m; a mass of 250 kg was used for this study.

Figure 4.42 displays the displacement of girder in x direction for three stand-off distances. It can be seen that the stand-off distance influences greatly the response of an element to blast load. For R=3m the curb seems straight, meaning that displacement is near 0mm.

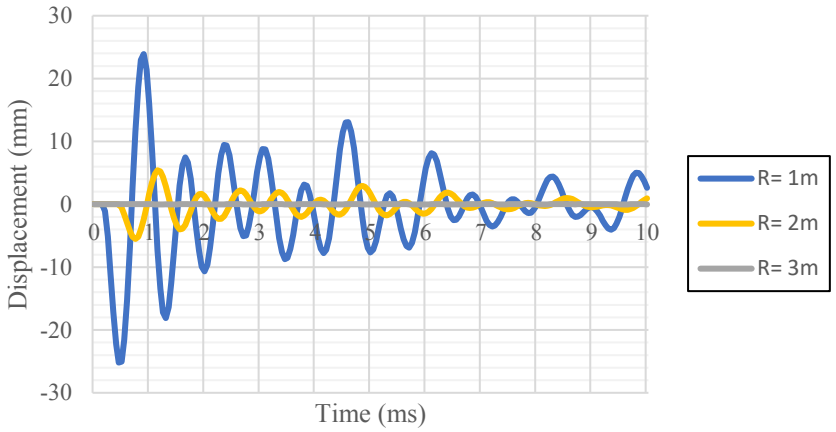

Figure 4.42. Displacement in x direction for 250 kg of TNT varying stand-off distances

For displacement in z direction (Figure 4.43), the same behaviour as before can be described. The displacement increases after a short period and decreases with time.

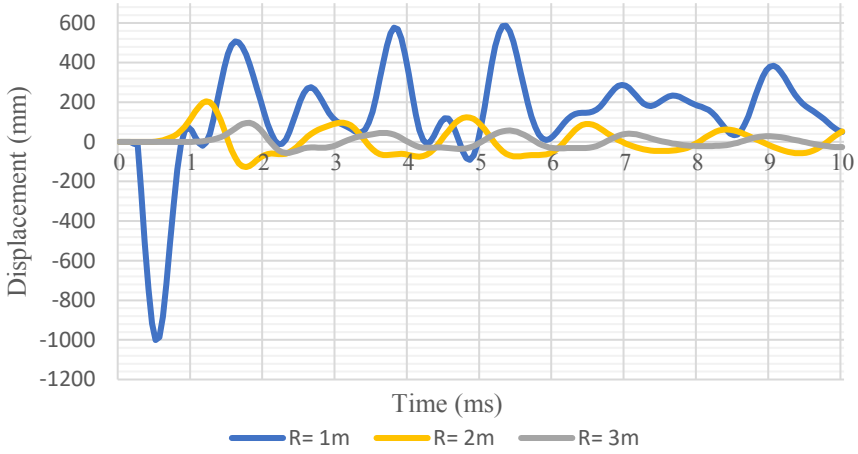

Figure 4.43. Displacement in z direction for 250 kg of TNT varying stand-off distances

The fact that the great is the stand-off distance, the less are the effects on bridge elements can then be concluded.

4.4.3 Interpretation of results

For all the previous cases, structural elements have experienced big stresses due to high impact of blast load. Despite the fact stresses have exceeded yield strength of each element (except cases 3 and 4), in terms of strain it has been observed that strain in girders remains lower than strain failure of 5%.

For cables, when blast of 500 kg occurred at bridge start, the shortest cables undergo large strain while there is no failure for 250 kg of TNT. Blast at mid-span has as consequence failures of longest cables.

Finally, the stress conditions are quite similar in that the blast event, which strongly contributes after the detonation, to the achievement of yielding stress in a short time. A gradual collapse of deck can take place after undergoing such high stresses. In the case of a cable-stayed bridge, progressive collapse can be caused by the loss of two or more cables. For an extreme event such as blast loading, the loss of cables may be due either to the consequences of an air blast or to the reflected pressure near the stays. Other reasons could be the reaching of the excessive tension limit of the cable or finally to the collapse of the deck that would cause the cables near the failure zone to break. In the next part, the loss of anchorage due to air blast was considered.

4.5 Cable loss analyses

Due to front shock of blast wave, cables experienced large strain (greater than 2.7%). Those cables will be removed in order to study the response of bridge elements after their losses. Analysis will be done under permanent loads and pretension in cables. The cases study will be cases 2, 5 and 6.

4.5.1 Case study 2

An increase of bending moment in girders at position where short cables have failed is observed (Figure 4.44). Looking at place on pylon where cables were anchored, a bond in positive moment is remarked.

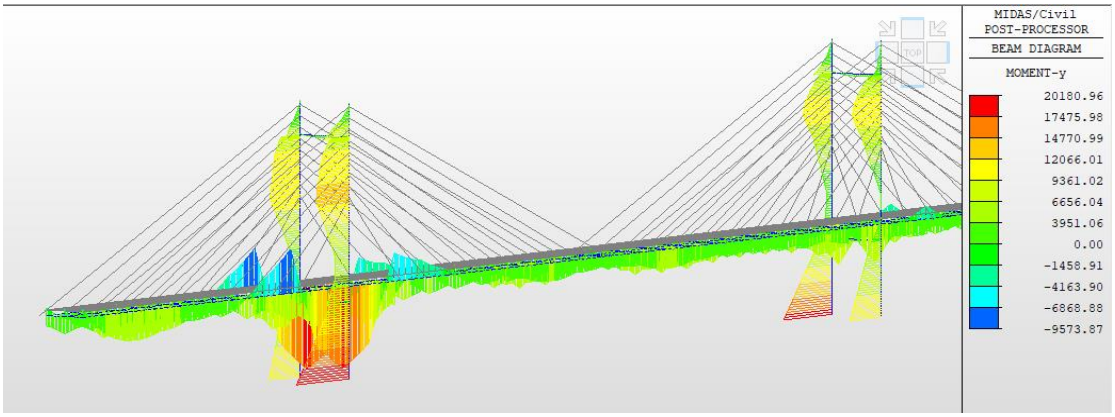

Figure 4.44. Bending diagram after stays failure (case 2)

On the right side of the bridge, an increase of stress in cable plane next stay losses is shown in Figure 4.45. On the left side, there is no remarkable change.

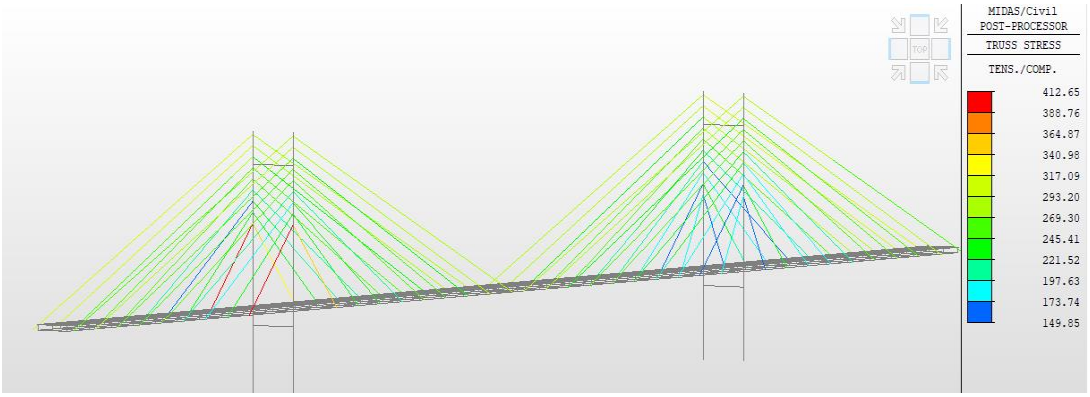

Figure 4.45. Stresses in cables after stays failure (case 2)

4.5.2 Case study 5

Stays in cable plane next cables loss are the most solicitated (Figure 4.46). Stress value is about 862.52 MPa, which is above allowable stress in cables (796.5 MPa). For girders, parts that are not braced show an increase of axial tension while braced girders remain under compression (Figure 4.47).

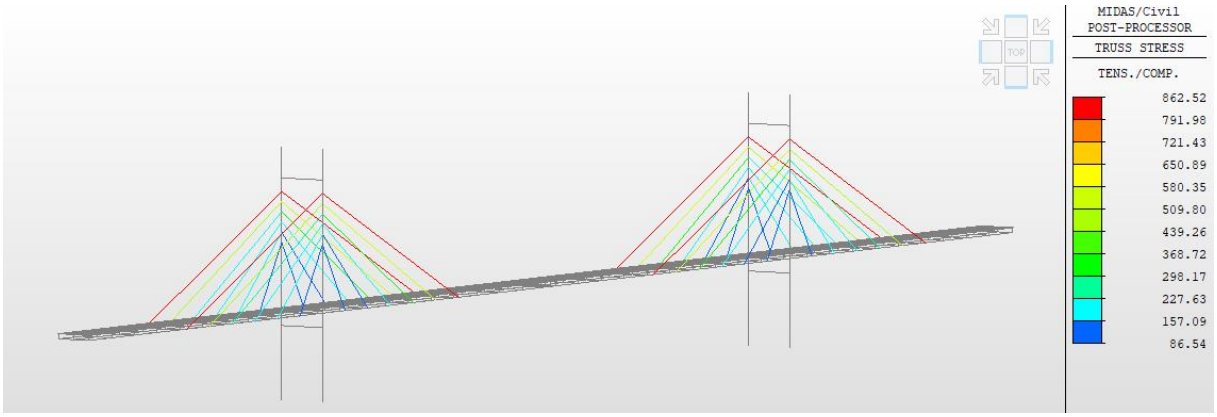

Figure 4.46. Stresses in cables after stays failure (case 5)

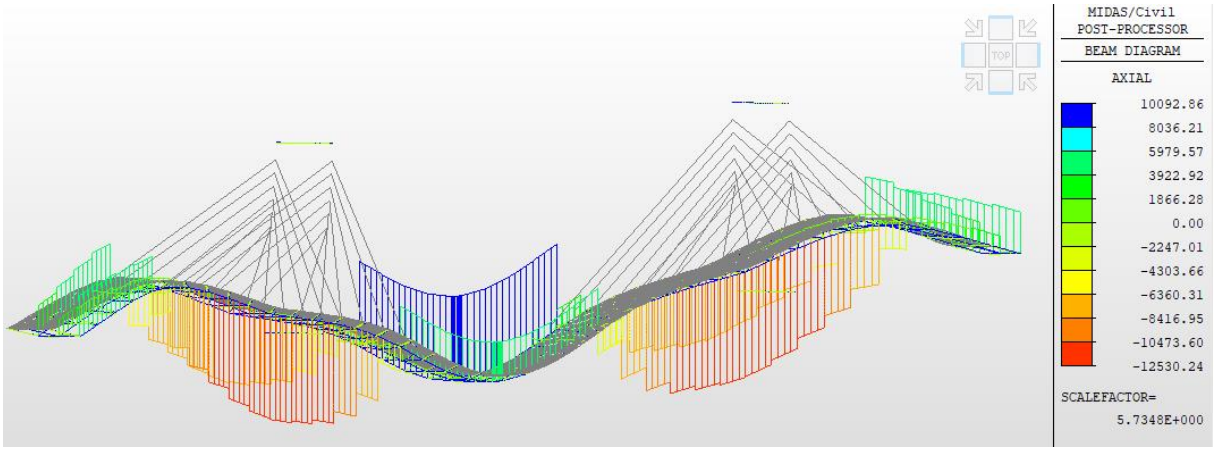

Figure 4.47. Stresses in girders after stays failure (case 5)

Vertical deflections (Figure 4.48) grow strongly and cannot be arrested since the bridge deck is not restrained by fix supports in the longitudinal direction.

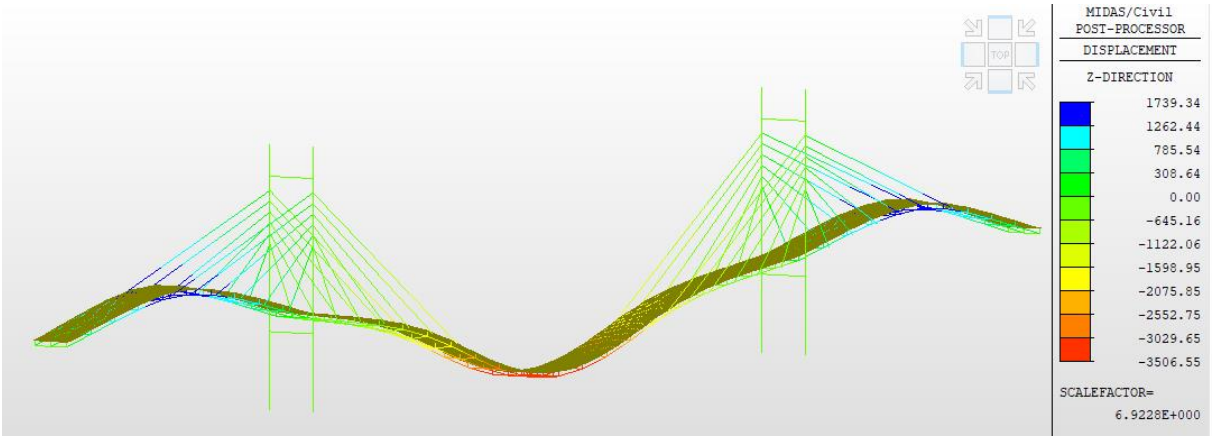

Figure 4.48. Structure displacement in z direction after stays failure (case 5)

4.5.3 Case study 6

More cables are improved because many stays have been loss (Figure 4.49); the shortest cables near tower are in compression, means that they do not work well. It is due to positive displacement of girders observed in Figure 4.50.

Lack of cables creates high bending moment that pulls towers towards the main span (Figure 4.51).

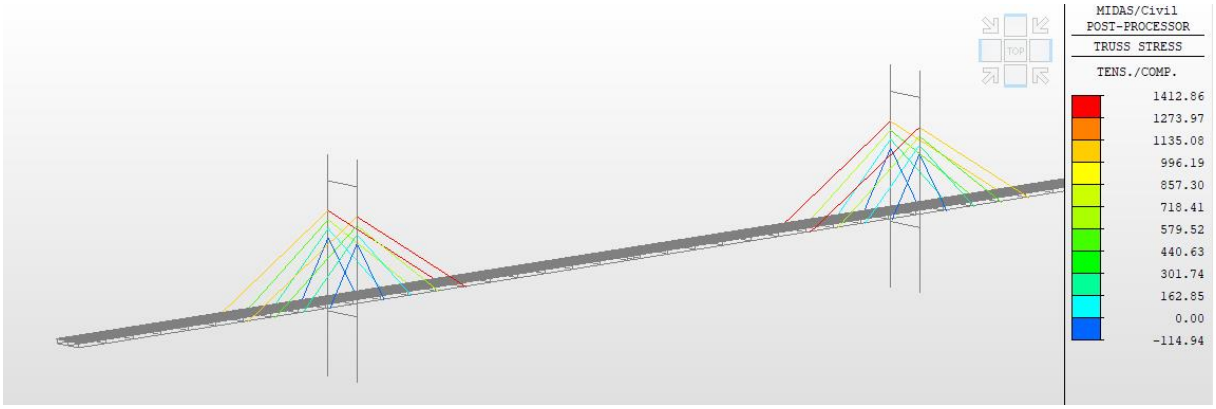

Figure 4.49. Stresses in cables after stays failure (case 6)

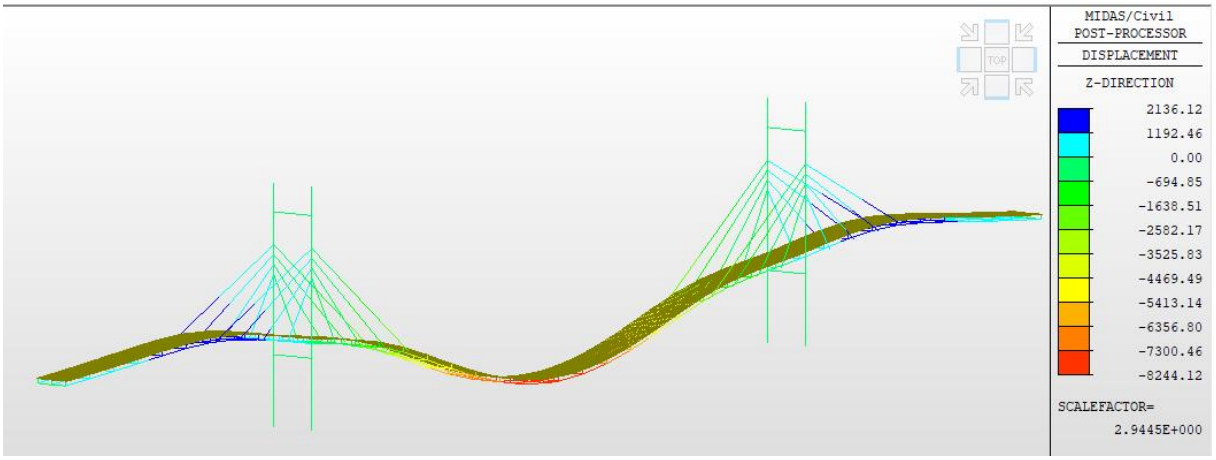

Figure 4.50. Structure displacement in z direction after stays failure (case 6)

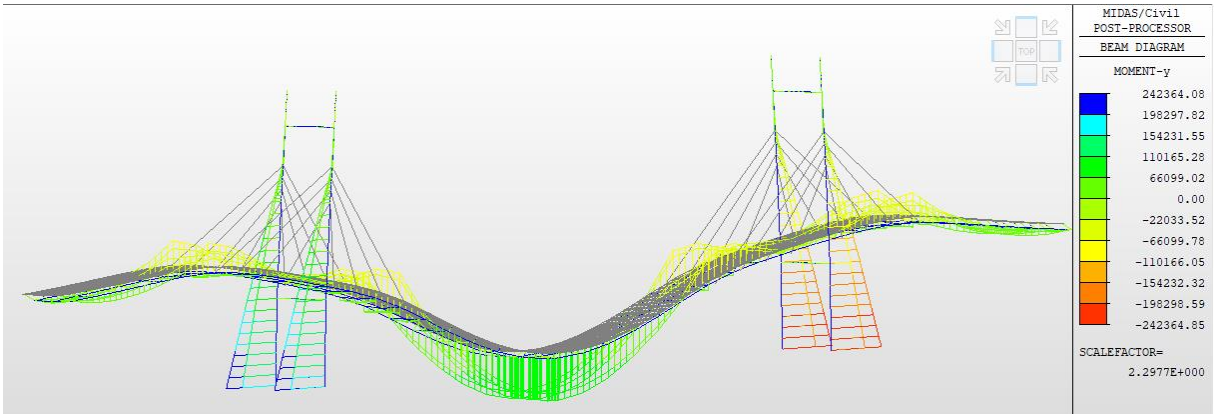

Figure 4.51. Bending diagram after stays failure (case 6)

4.5.4 Collapse prediction

The collapse propagation for the failure of the critical elements, described above, does exhibit features of at least two of the pure collapse types and must therefore be categorized as mixed-type collapse.

At the beginning, there is the initial failure of elements which are responsible – although not primarily - for the stabilization of the bridge girder in compression. Lack of bracing then leads to an increase in vertical deflections and high stresses due to second order effects, firstly in the longitudinal girder of the affected cable plane and then in the second longitudinal girder. These are features of the instability-type collapse although the failure is not a pure buckling.

After above events, the normal forces in the bridge deck, resulting from the horizontal cable forces, are redirected to the bridge part utilizing the deck's tension resistance (Figure 4.47). The forces are transferred to the pylons by the rest of cables. The pylons are pulled towards the main span of the bridge and fail in bending (Figure 4.510). This process exhibits features of the domino-type collapse: the horizontal forces cause an overturning and thus failure of these two individual structures with mainly vertical load bearing capacity.

4.5.5 Robustness of bridge

From the observations made regarding the collapse analysis, conclusions can be drawn for the robustness of the investigated cable-stayed bridge, which has a cable spacing of 12 m. In general, robustness can be defined as insensitivity to local failure. Robustness is therefore always related to the size of the initial failure and to the accepted amount of damage to the remaining structure.

If the design aim is that no or only small plastifications are allowed, the investigated bridge does not act robustly. Here, alternate paths can develop. Loads are transferred through the bridge girder to adjacent cables. Local plastifications develop in the bridge girder and in cables that already undergo blast load.

If only total collapse should be avoided, the bridge can be termed robust regarding the loss of four adjacent cables near tower. The failure of more cables (cases 5 and 6) is not possible without serious damages. The bridge's robustness is therefore limited to the failure of a certain number of cables depending on the predefined design criteria.

Conclusion

The key point of this chapter was to show the results of dynamic analysis investigated on cable-stayed bridge. It has started with presentation of details on the case study. After a static analysis was made to ensure bridge stability. Followed by dynamic analysis, we studied the response of girders and cables elements under high impact loading. The results show that when the blast occurred at tower, stresses remain in a good range. Blast at mid-span is the most prejudicial, enormous stresses developed in both elements. Blast at mid-span causes large displacements of cables thus, strains higher than strain limit of 2.7%. Concerning potential collapse after removal of failed cables, the most possible is mixed-type collapse. It is consequence of instability-type collapse that comes from increase in vertical displacements and high stresses in girders; domino-type collapse which is the result of girders failures that cause damages on pylons. Robustness of this cable-stayed cannot be assessed under previous study cases local plastifications can develop or bridge collapse can happen.

GENERAL CONCLUSION

From the previous analysis, it has been attempted to explore the concept of cable-stayed bridges with focus on dynamic analysis under blast load. In order to reach this goal, the work was divided in four main parts which are presentation of an overview of cable-stayed bridge for the first part; the second was focused on accidental failure mechanisms in cable-stayed bridge; next, we detailed the methodology used in this work and finally we exposed results of our investigation. Following the above, this methodology has been implemented to achieve the principal objective. Design of a cable-stayed bridge was done based on data that we collected from a bridge project in Marsassoum. Using MIDAS/civil, an optimization of cable pretensions and static analysis was performed. Verifications have been done with respect to recommendations in Eurocodes 1, 2, 3 and 4. After ensuring that the structure is stable, we moved on to the blast analysis in SAP2000 software. RC blast software was used in order to obtain the pressure-time function of the blast loads.

Results of analysis revealed that blast at mid-span and bridge start creates high stresses in deck and cable elements. When blast occurs near pylons, stresses do not cross the yield limit for each structural element, the structure resist well the explosion. Moreover, we have seen that the stand-off distance is a great factor in amount of effect caused by blast loading. The great is the stand-off distance, the less will be the effects on an element. Also, when the charge weight increases, the level of damage increases at an increasing rate. Regarding collapse scenario, mixed-type collapse was as the main possibility. It is a combination of instability-type collapse due to high solicitations and domino-type collapse which came from a chain of failures. For robustness, plastic limit will be crossed but loss of four cables will lead to creation of plastic zones; bridge total collapse will not happen. Regarding scenarios where many cables failed after blast at mid-span, progressive collapse of bridge can be concluded as global response of this cable-stayed bridge.

The subject dealt with is very vast and it was necessary to limit the field of research for this work. However, this work cannot be without imperfections due to the failure to carry out certain analyses such as the repercussion of the blast on the substructure during the blast analysis, the importance of pretension in order to resist high impact loads and the effect of

temperature released on bridge structure. In order to improve this work, the following suggestions can be made for future researchs:

- An optimization of cables pretensions in order to resist extreme event such as blast loading;
- Effect of temperature released during blast on cable-stayed bridge;
- A more detailed study on influence of traffic distribution in resistance against blast.

BIBLIOGRAPHY

Aoki, Y., Samali, B., Saleh, A., & Valipour, H. (2011). *Impact of sudden failure of cables on the dynamic performance of a cable-stayed bridge*. 310–321.

Bernardo, S. Di. (1998). *Motion Based Design of Cable-Stayed Bridges by*. *1990*.

Bhatti, M. A., Nasir Raza, S. M., & Rajan, S. D. (1985). Preliminary optimal design of cable-stayed bridges. *Engineering Optimization*, *8*(4), 265–289. https://doi.org/10.1080/03052158508902493

Brockenbrough, R. L., & Merritt, F. S. (2011). *STRUCTURAL STEEL DESIGNER'S HANDBOOK*.

Cable Supported Bridges. (n.d.).

Chen, W., & Duan, L. (2014). *Bridge Engineering Handbook, Second Edition: Superstructure Design*.

EN 1991-1-4. (2011). *1*(2005).

EN 1991-1-5. (2011). *1*(2005).

EN 1991-2. (2003). *1*(2005).

EN 1993-1-1. (2011). *1*(2005).

EN 1993-2. (2011). *1*(2005).

Freire, A. M. S., Negrão, J. H. O., & Lopes, A. V. (2006). Geometrical nonlinearities on the static analysis of highly flexible steel cable-stayed bridges. *Computers and Structures*, *84*(31–32), 2128–2140. https://doi.org/10.1016/j.compstruc.2006.08.047

Garlock, M., Paya-Zaforteza, I., Kodur, V., & Gu, L. (2012). Fire hazard in bridges: Review, assessment and repair strategies. *Engineering Structures*, *35*, 89–98. https://doi.org/10.1016/j.engstruct.2011.11.002

Giovanni Tecchio. (2015). *Cable - stayed bridges*.

Guo, X., Zhang, C., & Chen, Z. (2020). Dynamic performance and damage evaluation of a

scoured double-pylon cable-stayed bridge under ship impact. *Engineering Structures*, *216*(November 2019), 110772. https://doi.org/10.1016/j.engstruct.2020.110772

Hao, H., & Tang, E. K. C. (2010). Numerical simulation of a cable-stayed bridge response to blast loads, Part II: Damage prediction and FRP strengthening. *Engineering Structures*, *32*(10), 3193–3205. https://doi.org/10.1016/j.engstruct.2010.06.006

Hashemi, S. K., Bradford, M. A., & Valipour, H. R. (2016). Dynamic response of cable-stayed bridge under blast load. *Engineering Structures*, *127*, 719–736. https://doi.org/10.1016/j.engstruct.2016.08.038

Hoang, V., Kiyomiya, O., & An, T. (2016). *Experimental and dynamic response analysis of cable-stayed bridge due to sudden cable loss*. *62*(March), 50–60.

Karlos, V., Solomos, G., & Larcher, M. (2016). *Analysis of blast parameters in the near-field for spherical free-air explosions*.

Liu, Y., Ning, B., & Wang, Y. (2012). *Study on Thermal and Structural Behavior of a Cable-Stayed Bridge under Potential Tanker Truck Fires*. *238*, 684–688. https://doi.org/10.4028/www.scientific.net/AMM.238.684

Michaltsos, G. T., Sophianopoulos, D. S., & Avraam, T. P. (2020). Dynamic response of cable-stayed bridges due to sudden failure of stays : the 3D problem. *Archive of Applied Mechanics*, *90*(7), 1431–1456. https://doi.org/10.1007/s00419-020-01676-5

Mishra, R. M. S. S. (2021). Effect of blast loading and resulting progressive failure of a cable - stayed bridge. *SN Applied Sciences*, *January*. https://doi.org/10.1007/s42452-021-04145-y

Mozos, C. M., & Aparicio, A. C. (2010). Parametric study on the dynamic response of cable stayed bridges to the sudden failure of a stay , Part I : Bending moment acting on the deck. *Engineering Structures*, *32*(10), 3288–3300. https://doi.org/10.1016/j.engstruct.2010.07.003

Naji, A., & Reza, M. (2019). Progressive Collapse Analysis of Cable-Stayed Bridges. *Journal of Failure Analysis and Prevention*, *19*(3), 698–708. https://doi.org/10.1007/s11668-019-00649-3

Niels J. Gimsing, C. T. G. (2012). *Cable Supported Bridges: Concept and Design*.

Parke, G., & Hewson, N. (n.d.). *ICE manual of bridge engineering Edited by*.

Podolny, W., & Scalzi, J. B. (1986). *Construction and Design of Cable-Stayed Bridges*.

PTI. (2008). *Recommendations for Stay-Cable Design, Testing and Installation, 5th Edition*.

Son, J., Astaneh-Asl, A., & Rutner, M. (2005). Performance of bridge decks subjected to blast load. *The 6th-Japanese-German-Bridge-Symposium, Munich, Germany*, *29*(1), 9.

Son, J., & Lee, H. J. (2011). Performance of cable-stayed bridge pylons subjected to blast loading. *Engineering Structures*, *33*(4), 1133–1148. https://doi.org/10.1016/j.engstruct.2010.12.031

Starossek, U. (2007). *Typology of progressive collapse*. *29*, 2302–2307. https://doi.org/10.1016/j.engstruct.2006.11.025

Tetougueni, C. D., Zampieri, P., & Pellegrino, C. (2020a). Structural performance of a steel cable-stayed bridge under blast loading considering di ff erent stay patterns. *Engineering Structures*, *219*(August 2019), 110739. https://doi.org/10.1016/j.engstruct.2020.110739

Tetougueni, C. D., Zampieri, P., & Pellegrino, C. (2020b). Structural performance of a steel cable-stayed bridge under blast loading considering different stay patterns. *Engineering Structures*, *219*(August 2019), 110739. https://doi.org/10.1016/j.engstruct.2020.110739

Walther, R., Houriet, B., Isler, W., Moia, P., & Klein, J. F. (1999). *Cable-Stayed-Bridges-2nd-Ed-1999.pdf*.

Wei, D., & Chen, Y. (2018). *Response Analysis for the Tower Model of a Cable-Stayed Bridge under Local Collision*. 1–6.

Weiwei Lin, T. Y. (2017). *BRIDGE ENGINEERING*.

Winget, D. G., Marchand, K. A., & Williamson, E. B. (2005). Analysis and Design of Critical Bridges Subjected to Blast Loads. *Journal of Structural Engineering*, *131*(8), 1243–1255. https://doi.org/10.1061/(asce)0733-9445(2005)131:8(1243)

Wolff, M, & Starossek, U. (2010). *Cable-loss analyses and collapse behavior of cable-stayed bridges*.

Wolff, Maren, & Starossek, U. (2009). Cable loss and progressive collapse in cable-stayed bridges. *Bridge Structures*, *5*(1), 17–28. https://doi.org/10.1080/15732480902775615

Zhou, Y., & Chen, S. (2014). Time-Progressive Dynamic Assessment of Abrupt Cable-Breakage Events on Cable-Stayed Bridges. *Journal of Bridge Engineering*, *19*(2), 159–171. https://doi.org/10.1061/(asce)be.1943-5592.0000517

WEBOGRAPHY

https://www.constrofacilitator.com/cable-stayed-bridge-advantages-types-and-design/

https://fr.slideshare.net/sadekabdelraheem/cable-stayed-bridge-50681292

https://www.meteoblue.com/en/weather/historyclimate/climatemodelled/marsassoum_senegal_2248777

https://fr.slideshare.net/SoumyabrataSaha1/blast-load-and-its-analysis?next_slideshow=1

https://www.civilengineeringx.com/structural-analysis/structural-steel/preliminary-design-of-cable-stayed-bridges/

https://doi.org/10.1016/j.engstruct.2010.12.031

ANNEXES

Annexe A: Tables used in methodology

Terrain category		z_0 m	z_{min} m
0	Sea or coastal area exposed to the open sea	0,003	1
I	Lakes or flat and horizontal area with negligible vegetation and without obstacles	0,01	1
II	Area with low vegetation such as grass and isolated obstacles (trees, buildings) with separations of at least 20 obstacle heights	0,05	2
III	Area with regular cover of vegetation or buildings or with isolated obstacles with separations of maximum 20 obstacle heights (such as villages, suburban terrain, permanent forest)	0,3	5
IV	Area in which at least 15 % of the surface is covered with buildings and their average height exceeds 15 m	1,0	10
NOTE: The terrain categories are illustrated in A.1.			

Table A.1. Terrain categories and terrain parameters

Road restraint system	on one side	on both sides
Open parapet or open safety barrier	d + 0,3 m	d + 0,6 m
Solid parapet or solid safety barrier	$d + d_1$	$d + 2d_1$
Open parapet and open safety barrier	d + 0,6 m	d + 1,2 m

Table A.2. Depth d_{tot} to be used for $A_{ref,x}$

Annexe B: Figures used in methodology

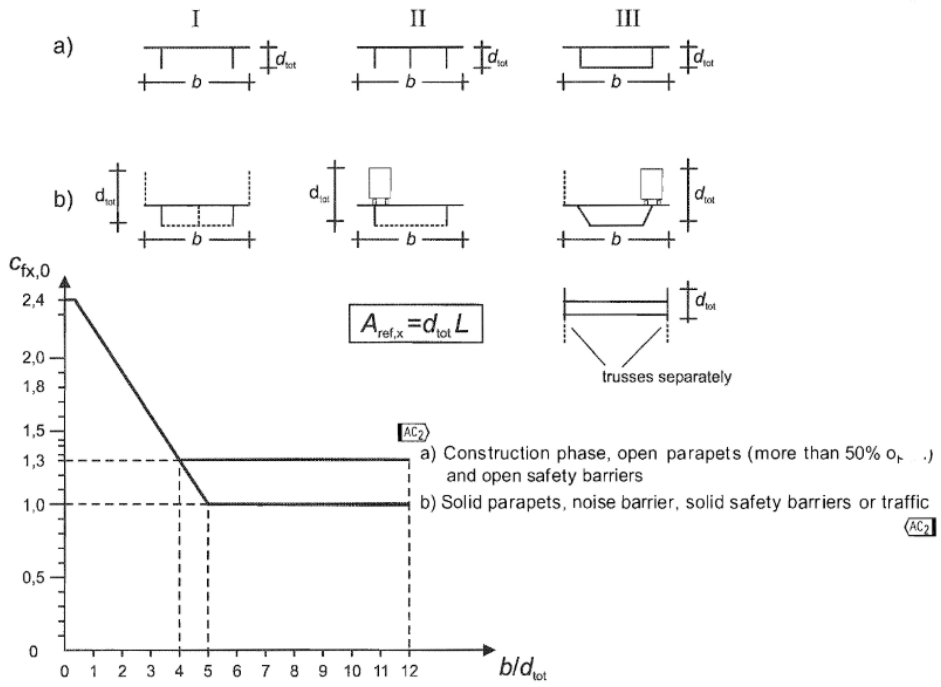

Figure B.1. Force coefficient for bridges, $C_{fx,O}$ (EN 1991-1-4, 2011)

Cross section		Limits		Buckling about axis	Buckling curve S 235 S 275 S 355 S 420	Buckling curve S 460
Rolled sections	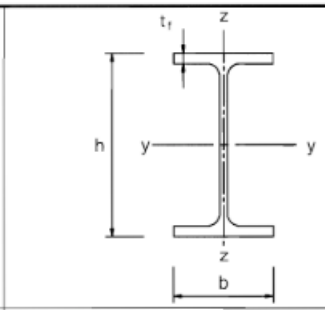	h/b > 1,2	$t_f \leq 40$ mm	y – y z – z	a b	a_0 a_0
			40 mm < $t_f \leq 100$	y – y z – z	b c	a a
		h/b ≤ 1,2	$t_f \leq 100$ mm	y – y z – z	b c	a a
			$t_f > 100$ mm	y – y z – z	d d	c c
Welded I-sections	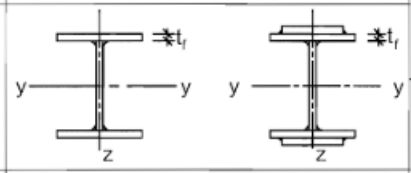		$t_f \leq 40$ mm	y – y z – z	b c	b c
			$t_f > 40$ mm	y – y z – z	c d	c d
Hollow sections			hot finished	any	a	a_0
			cold formed	any	c	c
Welded box sections	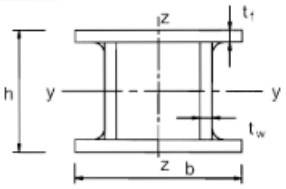		generally (except as below)	any	b	b
			thick welds: a > 0,5t_f b/t_f < 30 h/t_w <30	any	c	c
U-, T- and solid sections	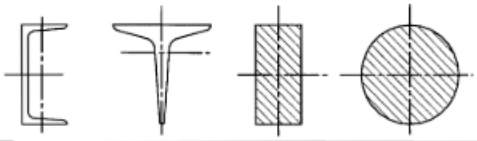			any	c	c
L-sections				any	b	b

Figure B.2. Selection of buckling curve for a cross-section

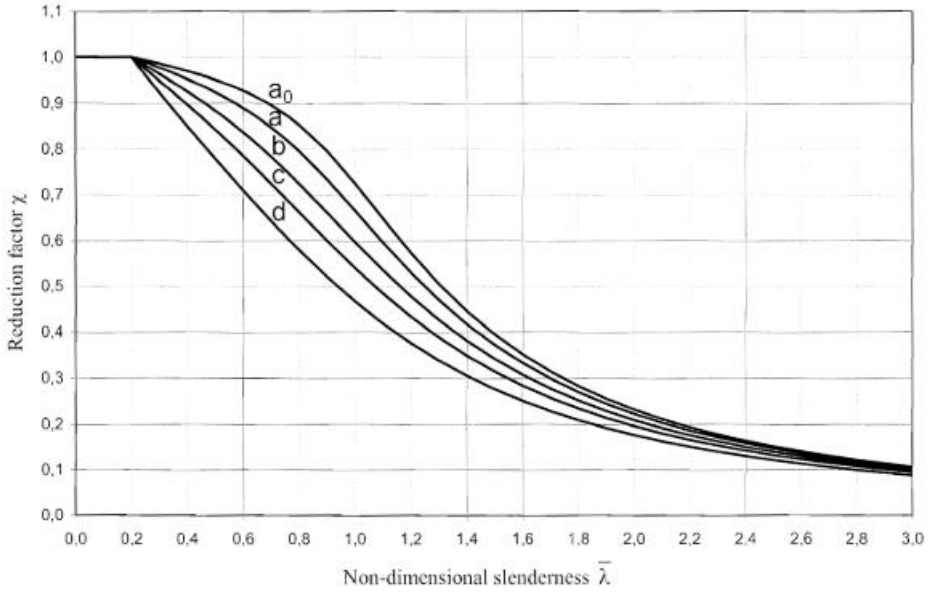

Figure B.3. Buckling curves